TRP channels as sensors of cellular redox status

Nobuaki Takahashi

2010

Preface

This is a thesis submitted by the author of Kyoto University for the degree of Doctor of Engineering. The studies presented in this thesis have been carried out under the direction of Professor Yasuo Mori at the Laboratory of Molecular Biological Chemistry, Department of Synthetic Chemistry and Biological Chemistry, Graduate School of Engineering, Kyoto University during April 2005 to November 2010.

It is the author's great pleasure to express sincere gratitude to Professor Yasuo Mori for his guidance, valuable suggestion and encouragement throughout these studies.

The author also expresses hearty thanks to Professor Tomoyuki Kuwaki, Department of Physiology, Graduate School of Medical and Dental Sciences, Kagoshima University, Associate Professor Shigeki Kiyonaka and Assistant Professor Tomohiro Numata, Department of Synthetic Chemistry and Biological Chemistry, Graduate School of Engineering, Kyoto University, Assistant Professor Takashi Yoshida, Department of Oral Biology, Graduate School of Dentistry, Tohoku University and Assistant Professor Shinichiro Yamamoto, Department of Biological Chemistry, Graduate School of Pharmaceutical Sciences, Kyoto University for their kind support and guidance.

The author is also deeply grateful to Ms. Emiko Mori, Department of Synthetic Chemistry and Biological Chemistry, Graduate School of Engineering, Kyoto University, Professor Shuji Kaneko, Associate Professor Takayuki Nakagawa and Assistant Professor Hisashi Shirakawa, Department of Molecular Pharmacology, Graduate School of Pharmaceutical Sciences, Kyoto University, Professor Koji Uchida and Assistant Professor Takahiro Shibata, Laboratory of Food and Biodynamics, Graduate School of

Bioagricultural Sciences, Nagoya University, Dr. Shinji Naito, Division of Pathology, Research Laboratory, National Ureshino Hospital, Associate Professor Toru Oga, Department of Respiratory Care and Sleep Control Medicine, Graduate School of Medicine, Kyoto University, Professor Seiji Suga, Department of Applied Chemistry, Faculty of Engineering, Graduate School of Natural Science and Technology, Okayama University, Professor Jun-ichi Yoshida and Professor Itaru Hamachi, Department of Synthetic Chemistry and Biological Chemistry, Graduate School of Engineering, Kyoto University, Professor Takashi Morii, Institute of Advanced Energy, Kyoto University, Dr. Yuji Hara, Departments of Physiology and Biophysics, Internal Medicine and Neurology, University of Iowa, Professor Minoru Wakamori, Department of Oral Biology, Graduate School of Dentistry, Tohoku University and Assistant Professor Taketoshi Kajimoto, Department of Synthetic Chemistry and Biological Chemistry, Graduate School of Engineering, Kyoto University.

I would also like to express special thanks to Mr. Yusuke Mizuno, Mr. Satoshi Akiyama, Mr. Daisuke Kozai and all other members of our laboratory. Without their help, it would have been much more difficulty to accomplish this work.

Many thanks to my family and my friends who have been supported me to complete my thesis, for their kind understanding of my career decision and heartwarming assistance.

Nobuaki Takahashi

Laboratory of Molecular Biological Chemistry

Department of Synthetic Chemistry and Biological Chemistry

Graduate School of Engineering

Kyoto University

Contents

General Introduction ····· **2**

Chapter 1 Nitric oxide activates TRP channels by cysteine S-nitrosylation ····· **12**

Chapter 2 Molecular characterization of TRPA1 channel activation by cysteine-reactive inflammatory mediators ····· **53**

Chapter 3 TRPA1 senses O_2 availability in non-carotid body chemoreceptors ····· **81**

General Conclusion ····· **140**

List of Publications ····· **143**

General Introduction

Joseph Priestley, one of the three scientists credited with the discovery of molecular oxygen (O_2), described the death of mice that were deprived of O_2. However, he was also well aware of the toxicity of too much oxygen, stating, "For as a candle burns much faster in dephlogisticated [oxygen-enriched] than in common air, so we might live out too fast, and the animal powers be too soon exhausted in this pure kind of air. A moralist, at least, may say, that the air which nature has provided for us is as good as we deserve."[1].

O_2 constitutes almost 20.95% of the Earth's atmosphere and is the second most abundant element. In the prebiotic environment, O_2 supposedly did not exist in the free form[2]. During the time of the origin of life, the early photosynthetic organisms released O_2 into the atmosphere and facilitated the evolution of aerobic life forms. After many changes, the atmosphere has reached its present gaseous composition, comprising exactly optimal levels of O_2 for sustenance and propagation of life. Although O_2 is essential for aerobic life, it also exerts toxicity through the production of its derivatives such as free radicals, reactive oxygen species (ROS), reactive nitrogen species (RNS) and singlet oxygen. Due to the ambivalent physiological nature of O_2, the control of adequate O_2 provision to the tissues and the capability of generating adaptive responses to changes in *in vivo* O_2 levels are fundamental challenges for aerobic life forms[3].

ROS and RNS have been traditionally considered as nonspecific toxins that cause random damage to cellular components including membrane lipids, DNA and proteins, but recently, they have emerged as signal-transduction molecules (Fig. 1)[4,5]. Tissue damage and inflammation produce an array of these substances that can excite or sensitize nociceptors to elicit pain at the site of injury and that can contribute significantly to the expression of a variety of different inflammatory cytokines, adhesion molecules and enzymes by activating redox-sensitive transcription factors such as nuclear factor-κB

(NF-κB)[4]. In addition, nitric oxide (NO), a kind of RNS, is an important signalling molecule that acts in many tissues to regulate a diverse range of physiological and cellular processes including blood vessel relaxation, neurotransmission, immune defence, the regulation of cell death (apoptosis) and cell motility (Fig. 1)[6].

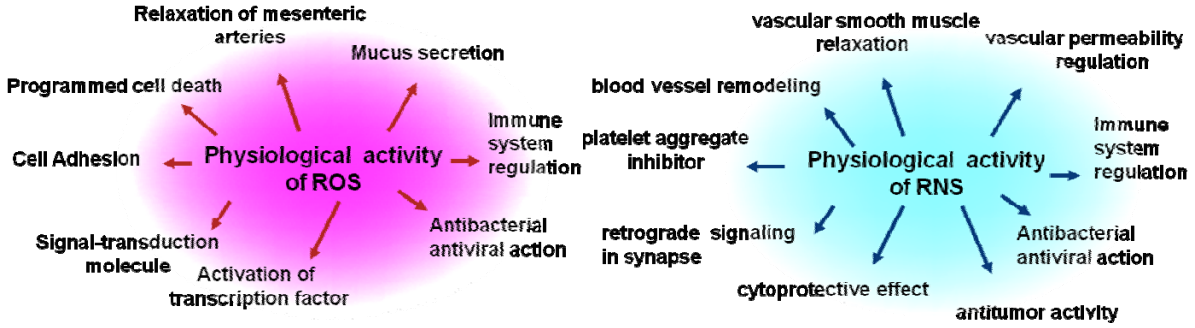

Figure 1. Physiological significance of ROS and RNS

The cellular signals initiated by ROS and RNS are delivered through redox chemistry because these substances are highly reactive electrophiles. This primarily involves the post-translational modification of specific amino acid residues, especially cysteine thiols, on signaling proteins in a similar fashion to the processes that allow kinases to phosphorylate specific amino acids. According to the classical view, the reaction of cysteine thiols had been considered in terms of maintaining protein structure through disulfide bond formation and for regulating catalytic centers through metal binding[7]. However, within the past dozen years, the classical concepts of cysteine thiol reaction have been modified as a result of the discovery of S-nitrosylation in biological systems[5,6], that is the transfer of a NO to a key cysteine thiol, representing a new mode of cysteine oxidation (Fig. 2). Recently, electrophile binding (in chemical biology terms, representing S-alkylation) has come to be regarded as another new mode of cysteine modification (Fig. 2). Thus, the redox reaction involving cysteine thiols can regulate and dramatically control protein function. However, although redox signaling has an

impact on many cellular processes (Fig. 1), precise mechanisms underlying redox sensing are still elusive.

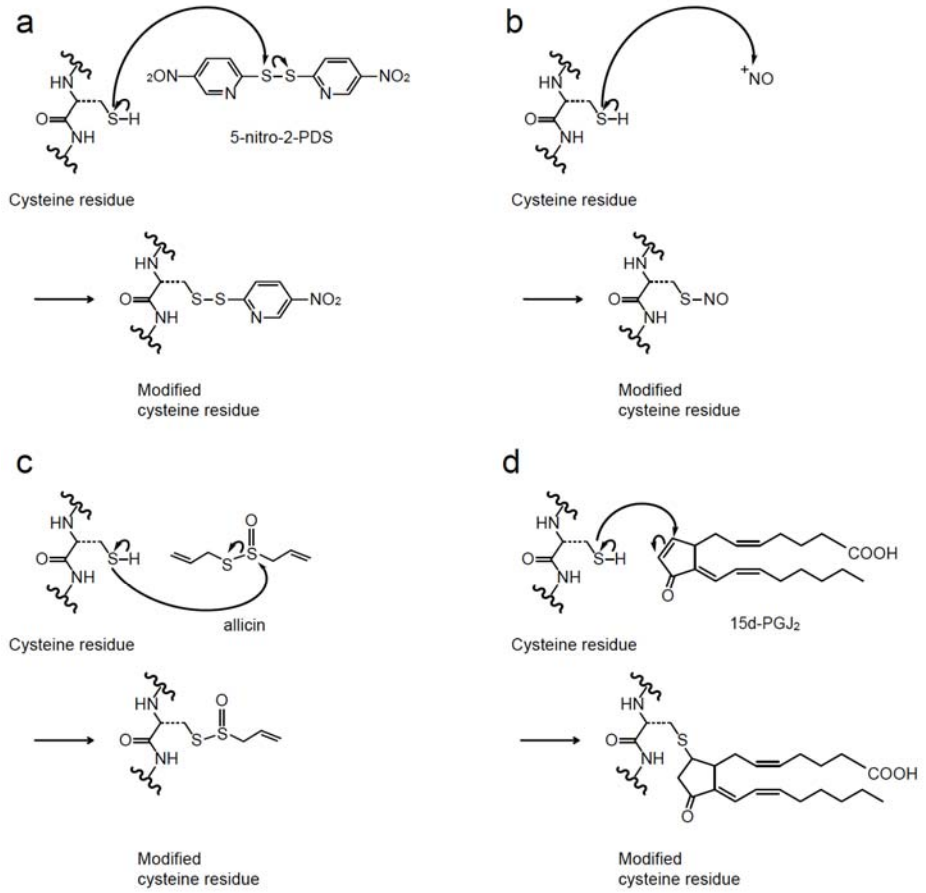

Figure 2. A likely chemical mechanism underlying the action of 5-nitro-2-PDS (a), NO (b), allicin (c) and 15-deoxy-$\Delta^{12,14}$-prostaglandin J_2 (15d-PGJ_2) (d).

The ability to sense and adapt to a wide variety of environmental changes including changes of cellular redox status and O_2 availability is crucial for the survival of all cells. In the last decade, studies of transient receptor potential (TRP) channels, a superfamily of cation-conducting membrane proteins, have significantly extended our knowledge about molecular basis of biology of sensing. Due to their distinct activation mechanisms and biophysical properties, TRP channels are highly suited to function in receptor cells, either as receptors for environmental or endogenous stimuli or as molecular players in signal

transduction cascades downstream of metabotropic receptors. As such, TRP channels play a crucial role in many mammalian senses, including touch, taste and smell.

The *trp* gene was identified through the genetic studies of the *Drosophila* visual transduction mutation[8]. The term "TRP" is derived from "transient receptor potential", because the *trp* gene mutant photoreceptors fail to generate the Ca^{2+}-dependent "sustained" phase of receptor potential and therefore fail to induce subsequent Ca^{2+}-dependent adaptation to light. Approximately 30 TRP homologs in vertebrates have been discovered since the cloning of the *Drosophila trp* gene[8]. They are divided into six subfamilies (canonical (C), vanilloid (V), melastatin (M), polycystic kidney disease (P), mucolipin (ML) and ankyrin (A)) by homology of the protein sequences (Fig. 3). The TRP protein has six putative transmembrane domains and a pore region between the fifth and sixth transmembrane domains, and it assembles into homo- or hetero-tetramers to form channels (Fig. 4)[9,10]. In some TRP subfamilies, there are several ankyrin repeats at N-terminal domain (Fig. 4). The TRPC subfamily contains proteins with the greatest homology to the *Drosophila* TRP protein, and its members are activated in response to phospholipase C activation following receptor stimulation[11–14]. The receptor stimulation eventually induces a biphasic Ca^{2+} signal, which is composed of an initial Ca^{2+} release from the endoplasmic reticulum followed by a sustained and/or oscillatory intracellular Ca^{2+} concentration ($[Ca^{2+}]_i$) increase due to Ca^{2+} influx via TRPC channels. Different modes of receptor-operated Ca^{2+} entry include store operated Ca^{2+} entry or capacitative Ca^{2+} entry, resulting from the depletion of intracellular Ca^{2+} stores, as well as Ca^{2+} entry activated in a Ca^{2+} depletion-independent manner. It has been shown that TRPC1 channel is activated by intracellular Ca^{2+}-store depletion[15], and TRPC3 is also likely to be stimulated, at least in part, by intracellular Ca^{2+}-store depletion[16,17], whereas TRPC5, TRPC6 and TRPC7 channels are distinguishable from store-operated Ca^{2+} channels[13,18,19]. TRPV1 known as a vanilloid receptor and its

homologs are activated by physical or chemical stimuli including heat (TRPV1, TRPV2, TRPV3 and TRPV4)[20–26], protons (TRPV1)[27], osmotic stress (TRPV4)[28,29] and capsaicin (TRPV1)[20]. Electrophysiologic studies showed that current-voltage relationship of these TRPV channels exhibits outward rectification. By contrast, it has been suggested that current-voltage relationship of TRPV5 and TRPV6 exhibit inward rectification[30]. The TRPM subfamily contains eight mammalian members. TRPM1 (melastatin) is a tumor suppressor protein isolated in a screen for genes and its expression level is inversely correlated with the severity of metastatic potential of amelanoma cell line[31]. Recent study has shown that TRPM1 is essential for the light-evoked response of ON retinal bipolar cells and that TRPM1 meets the criteria for the transduction cation channel[32]. TRPM2 is a Ca^{2+}-permeable nonselective cation channel activated by ROS[33]. Recently, our group has demonstrated that Ca^{2+} influx through TRPM2 activated by ROS induces chemokine production in monocytes, which aggravates inflammatory neutrophil infiltration[34]. TRPM8 channels, in contrast to TRPV channels, are activated by cold temperature and menthol[35,36]. The sole member of the TRPA subfamily, TRPA1, has a large N-terminal domain with 17 predicted ankyrin repeats[37]. Pungent compounds, such as allyl isothiocyanate included in mustard oil, and noxiously cold stimuli trigger TRPA1 activation[38,39]. Thus, TRP channels serve as sensors for a variety of environmental factors. Furthermore, Ca^{2+} influx via the TRP channel is involved in the regulation of diverse cellular processes.

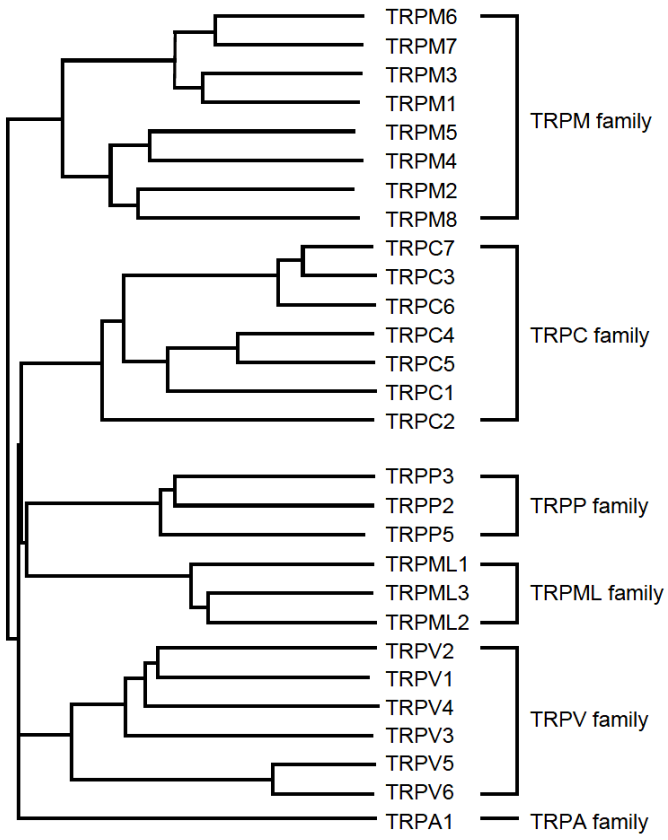

Figure 3. Phylogenetic tree of TRP channels

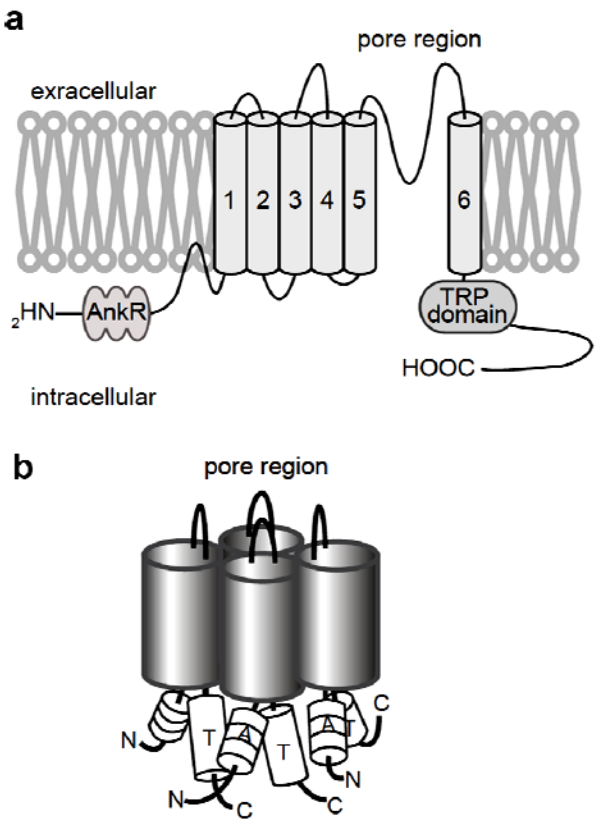

Figure 4. Transmembrane topology of TRP channels. **a,** The TRP protein has six putative transmembrane domains, a pore region between the fifth and sixth transmembrane domains, and a TRP domain in the C-terminal region. Some TRP subfamilies have several ankyrin repeats (AnkR) at N-terminal domain. **b,** The TRP protein assembles into homo-tetramers or hetero-tetramers to form channels. T: TRP domain, A: ankyrin repeats.

This thesis consists of three chapters on functional identification of redox-sensitive TRP channels. The first chapter describes a novel activation mechanism of TRP channels via oxidative cysteine modifications, demonstrating that TRPC and TRPV channels serve as intrinsic cell surface NO sensors. The second chapter shows that TRPA1 channel as well as TRPC and TRPV channels is activated through cysteine modification, and reveals that a variety of inflammatory mediators activate TRPA1 via cysteine modification in heterologous and native systems. The last chapter categorizes the oxidation sensitivity of TRP channels by physicochemical assessment using a congeneric series of reactive disulfides with characteristic redox potentials, and identifies TRPA1 as a novel sensor of O_2.

References

1. Weir, E. K., López-Barneo, J., Buckler, K. J. & Archer, S. L. Acute oxygen-sensing mechanisms. *N. Engl. J. Med.* **353,** 2042–2055 (2005).
2. Forster, R. E. & Estabrook, R. W. Is oxygen an essential nutrient? *Annu. Rev. Nutr.* **13,** 383–403 (1993).
3. Kulkarni, A. C., Kuppusamy, P. & Parinandi, N. Oxygen, the lead actor in the pathophysiologic drama: enactment of the trinity of normoxia, hypoxia, and hyperoxia in disease and therapy. *Antioxid. Redox Signal.* **9,** 1717–1730 (2007).
4. Dröge, W. Free radicals in the physiological control of cell function. *Physiol. Rev.* **82,** 47–95 (2002).
5. Hess, D. T., Matsumoto, A., Kim, S. O., Marshall, H. E. & Stamler, J. S. Protein S-nitrosylation: purview and parameters. *Nat. Rev. Mol. Cell. Biol.* **6,** 150–166 (2005).
6. Stamler, S. J., Lamas, S. & Fang, F. C. Nitrosylation: The Prototypic Redox-Based Signaling Mechanism. *Cell* **106,** 675–683 (2001).
7. Satoh, T. & Lipton, S. A. Redox regulation of neuronal survival mediated by electrophilic compounds. *Trends Neurosci.* **30,** 37–45 (2006).
8. Montell, C. & Rubin, G. M. Molecular characterization of the Drosophila *trp* locus: a putative integral membrane protein required for phototransduction. *Neuron* **2,** 1313–1323 (1989).
9. Goel, M., Sinkins, W. G. & Schilling, W. P. Selective association of TRPC channel subunits in rat brain synaptosomes. *J. Biol. Chem.* **277,** 48303–48310 (2002).
10. Hofmann, T., Schaefer, M., Schultz, G. & Sudermann, T. Subunit composition of mammalian transient receptor potential channels in living cells. *Proc. Natl Acad. Sci. USA* **99,** 7461–7466 (2002).
11. Zhu, X. *et al. trp*, a novel mammalian gene family essential for agonist-activated capacitative Ca^{2+} entry. *Cell* **85,** 661–671 (1996).
12. Hofmann, T. *et al.* Direct activation of human TRPC6 and TRPC3 channels by diacylglycerol. *Nature* **397,** 259–263 (1999).
13. Okada, T. *et al.* Molecular and functional characterization of a novel mouse transient receptor potential protein homologue TRP7. *J. Biol. Chem.* **274,** 27359–27370 (1999).
14. Inoue, R. *et al.* The transient receptor potential protein homologue TRP6 is the essential component of vascular α_1-adrenoceptor-activated Ca^{2+}-permeable cation channel. *Circ. Res.* **88,** 325–332 (2001).
15. Zitt, C. *et al.* Cloning and functional expression of a human Ca^{2+}-permeable cation channel

activated by calcium store depletion. *Neuron* **16,** 1189–1196 (1996).

16. Zitt, C. *et al.* Expression of TRPC3 in Chinese hamster ovary cells results in calcium-activated cation currents not related to store depletion. *J. Cell Biol.* **138,** 1333–1341 (1997).
17. Zhu, X., Jiang, M. & Birnbaumer, L. Receptor-activated Ca^{2+} influx via human Trp3 stably expressed in human embryonic kidney (HEK) 293 cells. *J. Biol. Chem.* **273,** 133–142 (1998).
18. Boulay, G. *et al.* Cloning and expression of a novel mammalian homolog of Drosophila transient receptor potential (Trp) involved in calcium entry secondary to activation of receptors coupled by the G_q class of G protein. *J. Biol. Chem.* **272,** 29672–29680 (1997).
19. Okada, T. *et al.* Molecular cloning and functional characterization of a novel receptor-activated TRP Ca^{2+} channel from mouse brain. *J. Biol. Chem.* **273,** 10279–10287 (1998).
20. Caterina, M. J. *et al.* The capsaicin receptor: a heat-activated ion channel in the pain pathway. *Nature* **389,** 816–824 (1997).
21. Caterina, M. J. *et al.* A capsaicinreceptor homologue with a high threshold for noxious heat. *Nature* **398,** 436–441 (1999).
22. Güler, A. D. *et al.* Heat evoked activation of the ion channel, TRPV4. *J. Neurosci.* **22,** 6408–6414 (2002).
23. Peier, A. M. *et al.* A heat-sensitive TRP channel expressed in keratinocytes. *Science* **296,** 2046–2049 (2002).
24. Smith, G. D. *et al.* TRPV3 is a temperature-sensitive vanilloid receptorlike protein. *Nature* **418,** 186–190 (2002).
25. Watanabe, H. *et al.* Heat-evoked activation of TRPV4 channels in a HEK293 cell expression system and in native mouse aorta endothelial cells. *J. Biol. Chem.* **277,** 47044–47051 (2002).
26. Xu, H. *et al.* TRPV3 is a calcium-permeable temperature-sensitive cation channel. *Nature* **418,** 181–186 (2002).
27. Tominaga, M. *et al.* The cloned capsaicin receptor integrates multiple pain-producing stimuli. *Neuron* **21,** 531–543 (1998).
28. Liedtke,W. *et al.* Vanilloid receptor-related osmotically activated channel (VR-OAC), a candidate vertebrate osmoreceptor. *Cell* **103,** 525–535 (2000).
29. Strotmann, R. *et al.* OTRPC4, a nonselective cation channel that confers sensitivity to extracellular osmolarity. *Nat. Cell Biol.* **2,** 695–702 (2000).
30. Clapham, D. E. TRP channels as cellular sensors. *Nature* **426,** 517–524 (2003).
31. Duncan, L. M. *et al.* Down-regulation of the novel gene melastatin correlates with potential for melanoma metastasis. *Cancer Res.* **58**, 1515–1520 (1998).

32. Koike, C. *et al.* TRPM1 is a component of the retinal ON bipolar cell transduction channel in the mGluR6 cascade. *Proc. Natl Acad. Sci. USA* **107,** 332–337 (2010).
33. Hara, Y. *et al.* LTRPC2 Ca^{2+}-permeable channel activated by changes in redox status confers susceptibility to cell death. *Mol. Cell* **9**, 163–173 (2002).
34. Yamamoto, S. *et al.* TRPM2-mediated Ca^{2+} influx induces chemokine production in monocytes that aggravates inflammatory neutrophil infiltration. *Nat. Med.* **14,** 738–747 (2008).
35. McKemy, D. D., Neuhausser, W. M. & Julius, D. Identification of a cold receptor reveals a general role for TRP channels in thermosensation. *Nature* **416,** 52–58 (2002).
36. Peier, A.M. *et al.* A TRP channel that senses cold stimuli and menthol. *Cell* **108,** 705–715 (2002).
37. Takahashi, N. *et al.* Molecular characterization of TRPA1 channel activation by cysteine-reactive inflammatory mediators. *Channels (Austin)* **2,** 287–298 (2008).
38. Story, G. M. *et al.* ANKTM1, a TRP-like channel expressed in nociceptive neurons, is activated by cold temperatures. *Cell* **112,** 819–829 (2003).
39. Jordt, S. E. *et al.* Mustard oils and cannabinoids excite sensory nerve fibres through the TRP channel ANKTM1. *Nature* **427,** 260–265 (2004).

Chapter 1

Nitric oxide activates TRP channels by cysteine S-nitrosylation

Summary

Transient receptor potential (TRP) proteins form plasma membrane cation channels acting as `sensors` for diverse cellular stimuli. Here, we demonstrate a novel activation mechanism mediated by cysteine S-nitrosylation in TRP channels. Recombinant TRPC1, C4, C5, V1, V3 and V4 of TRPC and TRPV families, commonly classified as receptor-activated channels and thermosensor channels, induce Ca^{2+} entry in response to nitric oxide (NO). Labeling and functional assays using cysteine mutants, together with membrane sidedness in activating action of reactive disulfides, reveal that cytoplasmically accessible Cys553 and nearby Cys558 are nitrosylation sites mediating NO sensitivity in TRPC5. The responsive TRPs harbor conserved cysteines on the same N-terminal side of the pore region. Importantly, native TRPC5 nitrosylated upon G-protein-coupled ATP receptor stimulation elicits Ca^{2+} entry in endothelial cells. These findings identify the structural motif for NO-sensitive activation gate in TRP channels, proposing 'NO sensors' as a new functional category extending over different TRP families.

Introduction

Ionized calcium (Ca^{2+}) is the most common signal transduction molecule in cells ranging from bacteria to brain neurons[1]. Ca^{2+} is derived from two sources. From outside the cells, Ca^{2+} enters by passing through Ca^{2+}-permeable channels across plasma membrane, while it can be released from endoplasmic reticulum (ER) through channels embedded in internal membrane networks. Groups of plasma membrane cation/Ca^{2+}-permeable channels act as 'sensors' by translating cellular stimuli into electrical signals, namely membrane potential changes, or chemical signals such as changes in intracellular Ca^{2+} concentration ($[Ca^{2+}]_i$)[2–4]. *Drosophila transient receptor potential* protein (TRP) and its homologues are putative six-transmembrane polypeptide subunits that assemble into tetramers to form these channels. In mammalian systems, TRP channels comprise six related protein subfamilies: TRPC, TRPV, TRPM, TRPA, TRPP and TRPML[5]. Respective TRP channels are activated by diverse stimuli such as receptor stimulation, heat, osmotic pressure and mechanical and oxidative stress from the extracellular environment as well as from inside the cell[3,4]. The TRPC homologues are receptor-activated Ca^{2+}-permeable cation channels (RACCs), activated upon receptor stimulation that activates phospholipase C (PLC) to hydrolyze phosphatidylinositol-4,5-biphosphate (PIP_2) into inositol 1,4,5-trisphosphate (IP_3) and diacylglycerol (DG)[6,7]. RACCs include store-operated channels (SOCs) activated by IP_3-induced Ca^{2+} release and depletion of ER Ca^{2+} stores. Among seven TRPC homologues (TRPC1-7), TRPC1, C3 and C4 have been reported to form SOCs, while TRPC5, C6, C7 and some TRPC3 channels are distinguishable from SOCs. In contrast to TRPCs, thermosensation can be regarded as a major functional definition of TRPV Ca^{2+}-permeable channels[3,5,8,9]. TRPV1, originally identified as the receptor for the vanilloid compound capsaicin, is responsive to heat (> 43°C), proton (< pH 5.6), the intrinsic ligand anandamide, and to PLC-linked receptor stimulation[5]. Increased

temperature also activates TRPV2 (> 52°C), TRPV3 (> 31 or 39°C) and TRPV4 (> 27°C). TRPV5 and V6 comprise a different subfamily, since they are activated by $[Ca^{2+}]_i$[3,5]. Thus, characteristic activation triggers functionally distinguishes 'sensor' cation channels formed by molecularly distinct TRPC and TRPV families.

Nitric oxide (NO) is another pleiotropic cell signaling molecule that controls diverse biological processes[10,11]. According to the classical view, cGMP is the mediator of NO signaling. However, the importance of cGMP-independent pathway through protein S-nitrosylation is increasingly recognized in NO signal transduction[10,11]. Since nitrosothiols are exceptionally labile due to their reactivity with intracellular reducing reagents such as ascorbic acid, S-nitrosylation functions as reversible post-translational modifications analogous to phosphorylation. Cysteine modifications of proteins are also elicited by other NO-related species, reactive oxygen species (ROS) and glutathione disulfide and free sulfhydryl-specific reactive disulfide[11,12]. However, these modifications are rather pathophysiological, although they can be viewed as a continuum that relates levels of reactive species to the form and consequences of modification. Thus, S-nitrosylation alone conveys physiological redox-based cellular signals[11].

Ca^{2+} and NO signals are precisely coordinated with each other. Among three distinct isoforms of NO synthases (NOS) responsible for NO production, $[Ca^{2+}]_i$ elevation is essential for activation of Ca^{2+}-dependent eNOS and nNOS[13]. Furthermore, IP_3-induced Ca^{2+} release and RACC-mediated Ca^{2+} influx via PLC activation is efficiently evoked upon receptor stimulation by physiological agonists such as vasodilators leading to eNOS activation in endothelial cells and other cell types[14–16]. However, it is still unclear whether activation of eNOS requires specific modes of upstream Ca^{2+} mobilizing mechanism or RACC subtypes formed by particular TRPCs[16–20], while NMDA receptors in neurons and L-type voltage-dependent Ca^{2+} channels in muscles are known to conduct nNOS-activating Ca^{2+} influx[21]. Feedback

regulation of Ca^{2+} signaling by NO remains even more elusive[22]: both positive[23-25] and negative regulation[26,27] by NO of Ca^{2+} mobilization pathways including RACCs was reported. Interestingly, physiological protein targets for cysteine S-nitrosylation include postsynaptic NMDA receptors and skeletal muscle ryanodine receptor Ca^{2+} release channels[11]. However, these channels involved in Ca^{2+} signaling are very restricted in tissue distribution and exert specific physiological functions, compared to the widely recognized generality of NO signaling via protein S-nitrosylation, Ca^{2+} signaling and their crosstalk. Therefore, to understand more general molecular mechanisms that link the two key signals, S-nitrosylation targets ought to be identified among more ubiquitous Ca^{2+} mobilizing ion channels. This study would ultimately provide novel insights into general understanding of activation gating that underlie 'sensor' function in TRP channels.

Here, we describe cysteine modification as a novel mechanism that triggers activation gating of TRPs. Chemical labeling assays using TRPC5 mutants reveal modification of Cys553 and Cys558, whose counterparts are harbored by the NO-responsive TRPC and TRPV members, on the N-terminal side of pore-forming region. Further studies using cultured endothelial cells, in combination with previously reported wide distribution of the NO-responsive TRPC and TRPV channels among diverse tissues[5], suggest that the group of native S-nitrosylation-sensitive TRP channels mediates a ubiquitous mechanism critical for feedback regulation of Ca^{2+} signals by NO.

Results

NO activates TRPC5 channels cysteine via sulfhydryl modifications

Recombinant expression of TRPC5 elicited robust elevation of $[Ca^{2+}]_i$ in response to the NO donor *S*-nitroso-*N*-acetyl-DL-penicillamine (SNAP) in HEK cells (Fig. 1a). Similar $[Ca^{2+}]_i$ increase was induced by another NO donor (±)-(*E*)-4-Ethyl-2-[(*E*)-hydroxyimino]-5-nitro-3-hexenamide (NOR3) but not by peroxynitrite donor 3-(4-Morpholinyl)sydnonimine, hydrochloride (SIN-1) (Fig. 1c). The SNAP-induced Ca^{2+} response is attributable mainly to Ca^{2+} entry through the TRPC5 channel, since SNAP evoked only marginal $[Ca^{2+}]_i$ rises in TRPC5-expressing cells after omission of extracellular Ca^{2+} (Fig. 1d) and in vector-transfected control cells (Fig. 1a). The sensitivity of TRPC5 to SNAP was prominent among TRPC homologues: significant $[Ca^{2+}]_i$ rises distinguishable from control was elicited by TRPC5 in response to SNAP at 10 μM, but by TRPC3 and C7 and by the redox status-sensitive Ca^{2+}-permeable cation channel TRPM2[28] only at much higher concentrations such as 300 μM. TRPM2 mediated pronounced Ca^{2+} responses to H_2O_2 (Fig. 1b). TRPC5 was the only TRPC homologue that elicited robust Ca^{2+} responses to H_2O_2 at 100 μM (Fig. 1b). Furthermore, ATP/Mg^{2+}-sensitive Ca^{2+}-permeable cation channel TRPM7[3], which responds to oxygen/glucose-deprived condition[29], was responsive to H_2O_2 but not to SNAP (Fig. 1a, b). Thus, prominent sensitivity to NO is characteristic of TRPC5 channels.

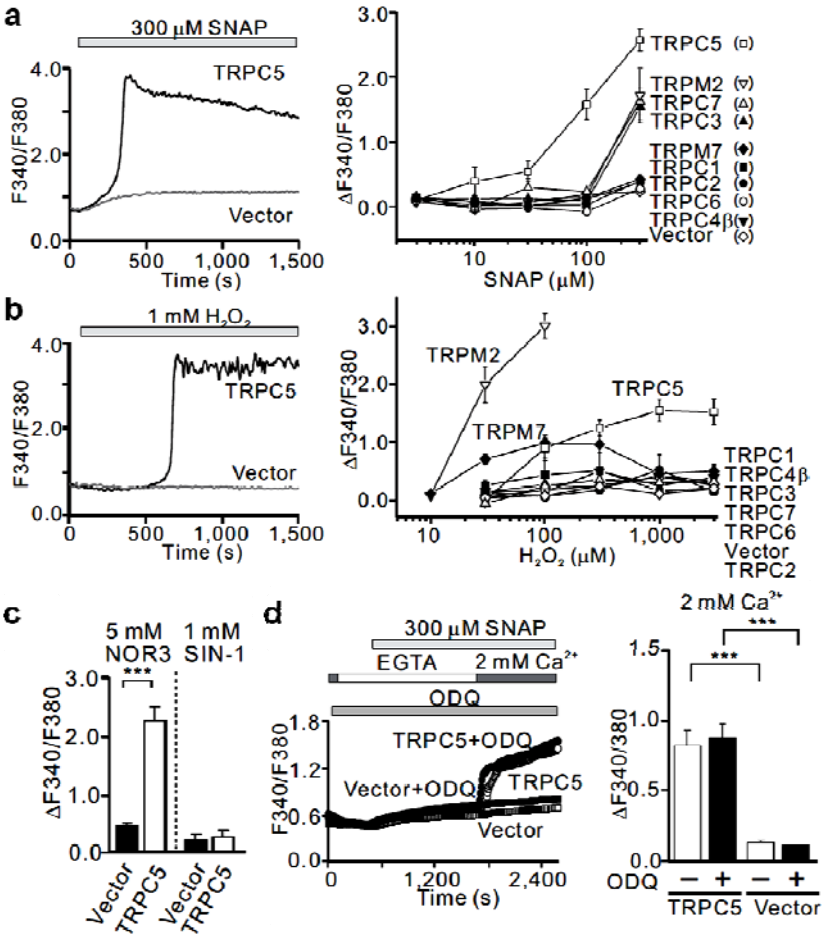

Figure 1. NO activates TRPC5-mediated Ca^{2+} response. **a, b,** $[Ca^{2+}]_i$ rises (F340/F380) evoked by SNAP (**a**) and H_2O_2 (**b**) in the presence of 2 mM extracellular Ca^{2+}. Representative time courses (left) and dose response relationships of maximal $[Ca^{2+}]_i$ rises (ΔF340/F380) (right) in HEK cells transfected with respective TRP homologues or with Vector (n = 6–61). **c,** Maximal $[Ca^{2+}]_i$ rises induced by NOR3 or SIN-1 (n = 19–31). **d,** SNAP (300 μM) was applied to TRPC5- or vector-transfected HEK cells in the presence (TRPC5, closed circles; Vector, closed squares) or absence (TRPC5, open circles; Vector, open squares) of guanylate cyclase inhibitor ODQ (10 μM). Averaged time courses (left). SNAP-induced maximal $[Ca^{2+}]_i$ rises due to Ca^{2+} influx evoked after readmission of extracellular Ca^{2+} (n = 20–38) (right). Data points are the means ± s.e.m.. $^{***}P < 0.001$.

NO-induced Ca^{2+} responses mediated by TRPC5 were resistant to the guanylate cyclase inhibitor 1H-[1,2,4]oxadiazolo[4,3-a]quinoxalin-1-one (ODQ) (Fig. 1d). This suggests the NO action through cGMP-independent pathways such as nitrosylation of free sulfhydryl groups of cysteine residues. Indeed, among reactive disulfides, that selectively detect free sulfhydryl groups of cysteine residues in proteins (Fig. 2a), membrane-permeable pyridyldisulfides (PDS) such as 2,2'-Dithiobis(5-nitropyridine) (5-nitro-2-PDS), 2,2'-Dithiodipyridine (2-PDS) and 4,4'-Dithiodipyridine (4-PDS) induced robust $[Ca^{2+}]_i$ rises in cells expressing TRPC5, whereas membrane-impermeable analogue 5,5'-Dithiobis(2-nitrobenzoic acid) (DTNB) elicited marginal $[Ca^{2+}]_i$ elevation indistinguishable from control (Fig. 2b, c). Expression of other TRPCs, TRPM2 and TRPM7 failed to elicit 5-nitro-2-PDS-induced $[Ca^{2+}]_i$ increases that significantly surpassed control. TRPC5 responses to SNAP as well as those to 5-nitro-2-PDS and H_2O_2 were preceded by time lags after application (time to half peak; 305 ± 14.4 s for 300 μM SNAP (n = 52), 780 ± 50.1 s for 1 mM H_2O_2 (n = 18) and 425 ± 32.7 s for 30 μM 5-nitro-2-PDS (n = 17)). Importantly, robust TRPC5-mediated responses were evoked by co-application of SNAP (30 μM) and 5-nitro-2-PDS (3 μM), which induced slight TRPC5 responses when individually applied (Fig. 2d). Furthermore, maximal responses elicited by 1 mM SNAP were not potentiated by addition of 30 μM 5-nitro-2-PDS, and *vice versa* (Fig. 2e, f). The relationships may imply a common action site(s) for NO and 5-nitro-2-PDS in inducing TRPC5 responses. Thus, reactive disulfides are extremely useful tools for identifying the free sulfhydryl target(s) of NO in TRPC5 activation.

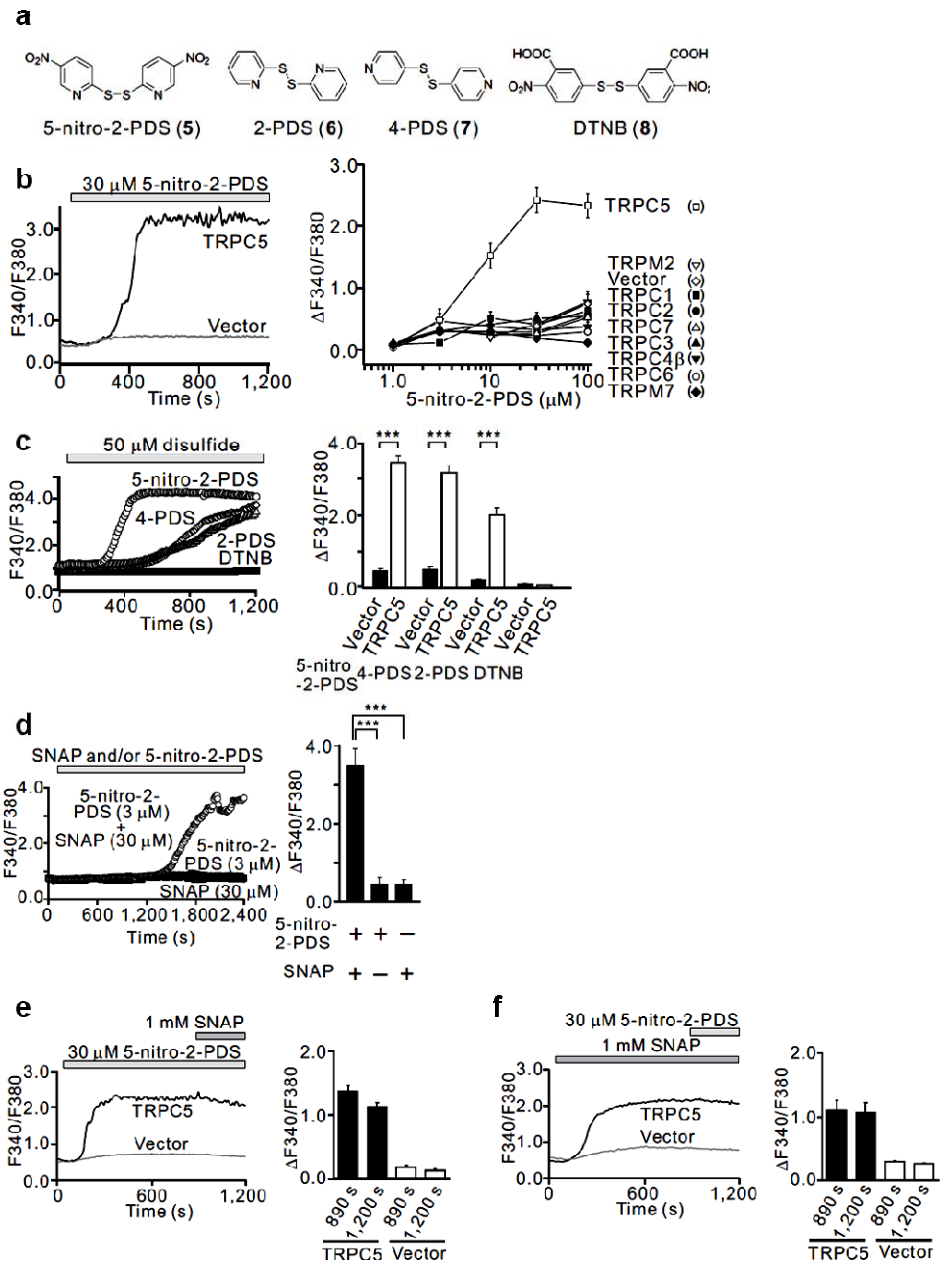

Figure 2. TRPC5-activating action of NO can be probed by reactive disulfides. **a,** Chemical structures of reactive disulfides. **b,** TRPC5-mediated Ca^{2+} responses to 5-nitro-2-PDS. Representative time courses (left) and dose response relationships (right). **c,** TRPC5 responses to various reactive disulfides (50 μM) (n = 9–23). Averaged time courses (left) and maximal $[Ca^{2+}]_i$ rises (right). **d,** 30 μM SNAP and 3 μM 5-nitro-2-PDS induce only marginal Ca^{2+} responses by individual applications (n =25, 26), but in combination trigger robust TRPC5-mediated Ca^{2+} responses (n = 18). Averaged time courses (left) and maximal $[Ca^{2+}]_i$ rises (right). **e, f,** 5-nitro-2-PDS (30 μM) (**e**) or SNAP (1 mM) (**f**) was applied to TRPC5-transfected HEK cells for 14 min prior to co-treatment with SNAP (1 mM) (**e**) or with 5-nitro-2-PDS (30 μM) (**f**), respectively. Representative time courses (left), and $[Ca^{2+}]_i$ rises at 890 s in the treatment with 5-nitro-2-PDS (**e**) or SNAP (**f**) alone and 1,200 s for the co-treatment (n = 11–25). Data points are the means ± s.e.m.. $^{***}P < 0.001$.

The reducing agent ascorbate significantly diminished SNAP-induced TRPC5 responses (Fig. 3a) but not 5-nitro-2-PDS-induced TRPC5 responses (Fig. 3b). Dithiothreitol (DTT) showed a potent suppressive effect on both responses (Fig. 3c, d). Considering the reported selective reduction of nitrosothiol by ascorbate to reform thiol[10], the result supports that NO and reactive disulfides form nitrosothiols and disulfide bonds, respectively, on cysteine residues in eliciting TRPC5-mediated responses. Interestingly, after washout, the TRPC5 response to SNAP was slowly attenuated (Fig. 3a, c) in contrast to the sustained response to 5-nitro-2-PDS (Fig. 3b, d). This suggests that the nitrosylation is reversed by intrinsic antioxidants in HEK cells. The modification stability, the TRPC5 selectivity, and the substitutability for NO prompted us to use reactive disulfides as powerful tools in the following studies on TRPC5 activation.

In TRPC5-expressing cells, 5-nitro-2-PDS-induced Ca^{2+} responses are due to Ca^{2+} entry through the TRPC5 channel, since $[Ca^{2+}]_i$ elevation was evoked predominantly upon readdition of extracellular Ca^{2+} (Fig. 3e). The whole-cell mode of the patch clamp method demonstrated 5-nitro-2-PDS-induced inward currents, which developed gradually in TRPC5-expressing cells (n = 6) but not in control cells (n = 4) at a holding potential (V_h) of –60 mV (Fig. 3f). Current-voltage (I-V) relationships of the 5-nitro-2-PDS-activated currents corresponded well with previously reported receptor-activated TRPC5 currents[30]. 5-nitro-2-PDS-activated TRPC5 currents showed resistance to washout but was slowly reversed by DTT (n = 5), which supports $[Ca^{2+}]_i$ measurements.

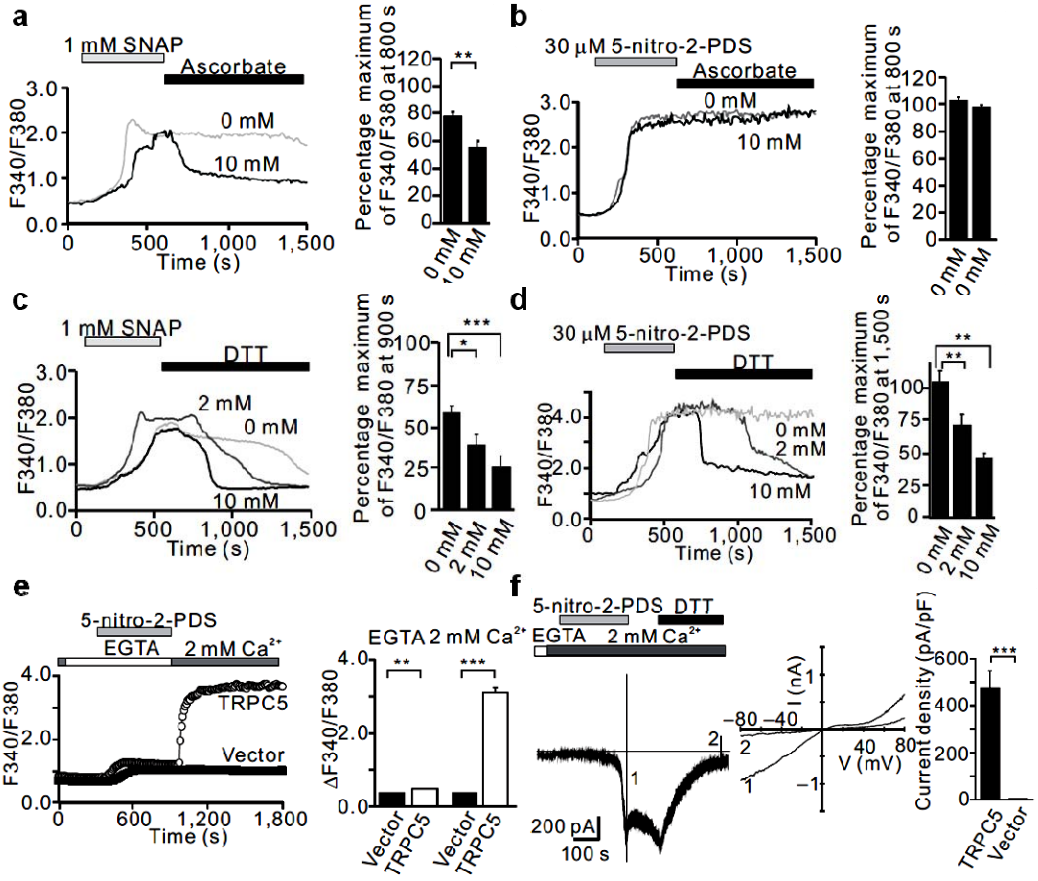

Figure 3. Chemical characterization and membrane sidedness of the action of NO and reactive disulfide in activating TRPC5 channels. **a**, **b,** Ascorbate suppress TRPC5 responses to SNAP (**a**) but not to 5-nitro-2-PDS (**b**). Representative time courses (left), and percentages of $[Ca^{2+}]_i$ rises at 800 s relative to maximal rises (n = 17–42). **c, d,** DTT suppress TRPC5 responses to both SNAP (**c**) and 5-nitro-2-PDS (**d**). Representative time courses (left), and percentages of $[Ca^{2+}]_i$ rises at 1,500 s relative to maximal rises (n = 17–42). **e,** TRPC5-mediated Ca^{2+} entry in response to 5-nitro-2-PDS. 50 μM 5-nitro-2-PDS was applied for 10 min in Ca^{2+}-free HBS containing 0.5 mM EGTA to TRPC5- (open circles) and vector-transfected cells (closed circles). 2 mM Ca^{2+} was then readded to the extracellular solution. Averaged time courses (left). Maximal 5-nitro-2-PDS-induced $[Ca^{2+}]_i$ rises before and after readdition of external Ca^{2+} (n =18–37) (right). **f,** 5-nitro-2-PDS-activated TRPC5 currents. Representative whole-cell current trace measured under voltage clamp conditions (V_h = –60 mV) in TRPC5-expressing cells (left). Extracellular treatment with 5-nitro-2-PDS (3 μM) was followed by wash out (2 min) and subsequent application of DTT (10 mM). *I-V* relationship at the time points indicated in left panel as 1 and 2 (middle). Peak current density induced by 5-nitro-2-PDS (30 μM) in TRPC5- (n = 6) or vector-transfected (n =4) HEK cells (right). Data points are the means ± s.e.m.. $^{*}P < 0.05$, $^{**}P < 0.01$, and $^{***}P < 0.001$.

Membrane sidedness of cysteine modification in TRPC5 activation

The ineffectiveness of extracellular application of the membrane-impermeable DTNB (Fig. 2d) suggests an agonistic modification site(s) accessible from the cytoplasmic side. This was addressed explicitly by the patch clamp method. Intracellular perfusion of DTNB from the patch pipette elicited TRPC5 currents at V_h of –60 mV with a time lag of 1–2 min after the whole-cell mode was established (Fig. 4a). The *I-V* relationship was similar to that activated by 5-nitro-2-PDS (see above). However, extracellular DTNB exerted no significant effects on current levels or *I-V* relationships in TRPC5-expressing cells (Fig. 4b). Methanethiosulfonate derivatives, which directly modify free cysteine thiols by forming a disulfide bond[31], resembled the reactive disulfide action in sidedness: membrane-permeable 2-aminoethylmethanethiosulfonate hydrobromide (MTSEA) but not membrane-impermeable [2-(trimethylammonium)ethyl]methanethiosulfonate bromide (MTSET) induced TRPC5 responses via extracellular administration (Fig. 4c). The results support the cytoplasmic accessibility of the site for cysteine modifications.

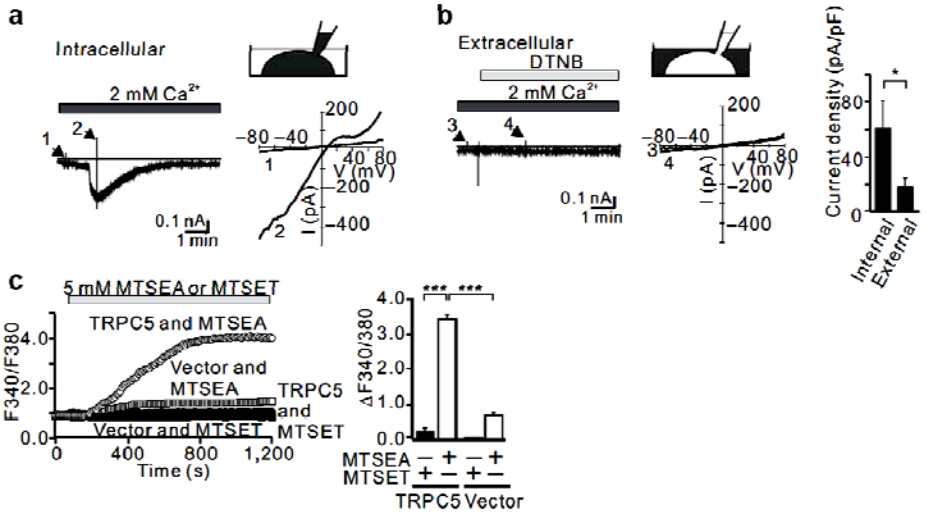

Figure 4. TRPC5 can be activated by modification of intracellular cysteine residues. **a, b,** Whole-cell TRPC5 currents are activated by DTNB via internal dialysis (10 μM) (**a**) but not via external application (30 μM) (**b**). *I-V* relations were determined using 50-ms positive voltage ramps from –80 to +80 mV (middle). Peak current densities (n = 22–27) (right). **c,** Ca^{2+} responses to MTSEA or MTSET. Average time courses (left) and maximal $[Ca^{2+}]_i$ rises (right) (n = 17–33). Data points are the means ± s.e.m.. $^{*}P < 0.05$ and $^{***}P < 0.001$.

Identification of the site of cysteine modification in TRPC5

We have previously demonstrated ATP receptor (P2Y)-mediated activation of TRPC5 channels via Gq/PLCβ in HEK cells[30]. Therefore, the possibility of the P2Y-activated signaling cascade harboring an action site(s) for reactive disulfide in the TRPC5 activation was examined. The quenching of G-protein βγ complexes by the regulator of G-protein signaling 4 (RGS4) and carboxyl terminus of β-adrenergic receptor kinase (βARK-ct) as well as the inhibition of PLCβ by U73122 significantly attenuated TRPC5 responses to P2Y stimulation, but failed to affect those evoked by 5-nitro-2-PDS (Fig. 5a, b). Furthermore, disruption of the three IP_3R subtype genes[32], which suppressed IgM-induced TRPC5 responses via B-cell receptors, significantly promoted 5-nitro-2-PDS-evoked TRPC5 responses in DT40 B lymphocytes (Fig. 5c, d). The results suggest that reactive disulfides activate the TRPC5 channel independently of P2Y-activated signals.

We examined if reactive disulfides directly act on TRPC5 channels using the cell-excised, inside-out mode of patch clamp recording. Single channel currents with unitary conductance of 44.1 pS were induced by 5-nitro-2-PDS applied to the cytoplasmic side of excised patches in TRPC5-expressed cells, but not in control cells (Fig. 5e). From this result, it was deduced that the action site is localized at the plasma membrane and its associated cellular components in TRPC5-expressing cells. Therefore, incorporation of reactive disulfides into TRPC5 channel complexes was investigated using DTNB-2Bio, a DTNB derivative that has two biotin groups attached (Fig. 6a, b). In GFP tagged TRPC5 (TRPC5-GFP)-expressing cells, DTNB-2Bio was incorporated into a ~130 kDa protein band, which corresponds well with the calculated molecular weight of TRPC5-GFP (139 kDa) (Fig. 6c). Importantly, co-application of SNAP inhibited the incorporation of DTNB-2Bio (Fig. 6d), being compatible with the observation in $[Ca^{2+}]_i$ measurements (Fig. 2d). Thus, NO and reactive disulfides share

covalent modification site in TRPC5 channel protein complexes.

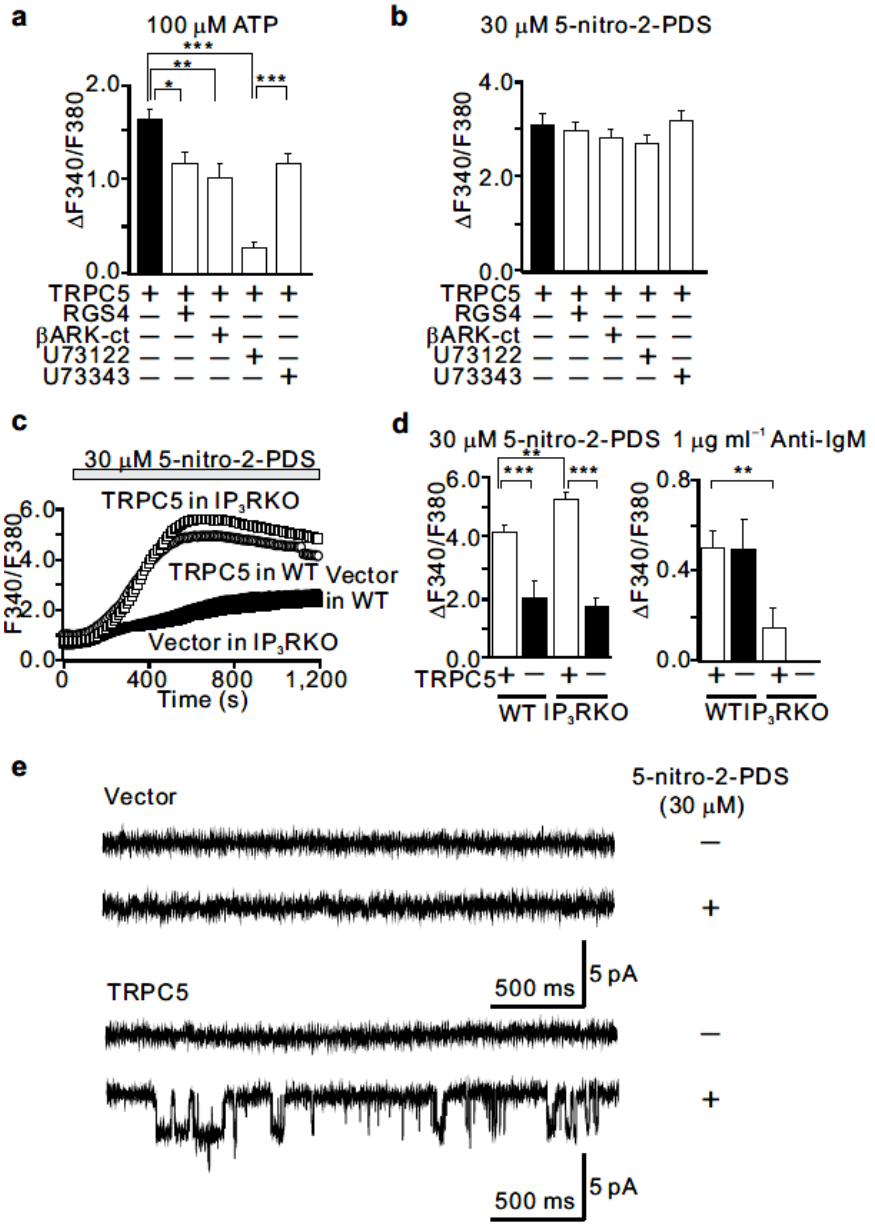

Figure 5. Cysteine modification activates TRPC5 channels via a pathway independent of receptor-activated PLC signaling cascades. **a**, **b,** Effects of βARK-ct, RGS4, U73122 (3 μM) and its inactive analogue U73343 (3 μM) on TRPC5 responses to ATP (n = 35–66) (**a**) and 5-nitro-2-PDS (n = 26–41) (**b**). **c**, **d,** Effects of gene knockout of three IP_3R subtypes on TRPC5 responses to 5-nitro-2-PDS in DT40 lymphocytes. **c,** Average time courses (n = 14–27). **d,** Maximal $[Ca^{2+}]_i$ rises by 5-nitro-2-PDS (left) or by anti-IgM (right) (n = 4–27). **e,** Unitary TRPC5 currents recorded from cell-excised inside-out patches. Consecutive traces before and after application of 30 μM 5-nitro-2-PDS at –60 mV from vector- (top) or TRPC5-transfected HEK cells (bottom). Data points are the means ± s.e.m.. $^{*}P < 0.05$, $^{**}P < 0.01$ and $^{***}P < 0.001$.

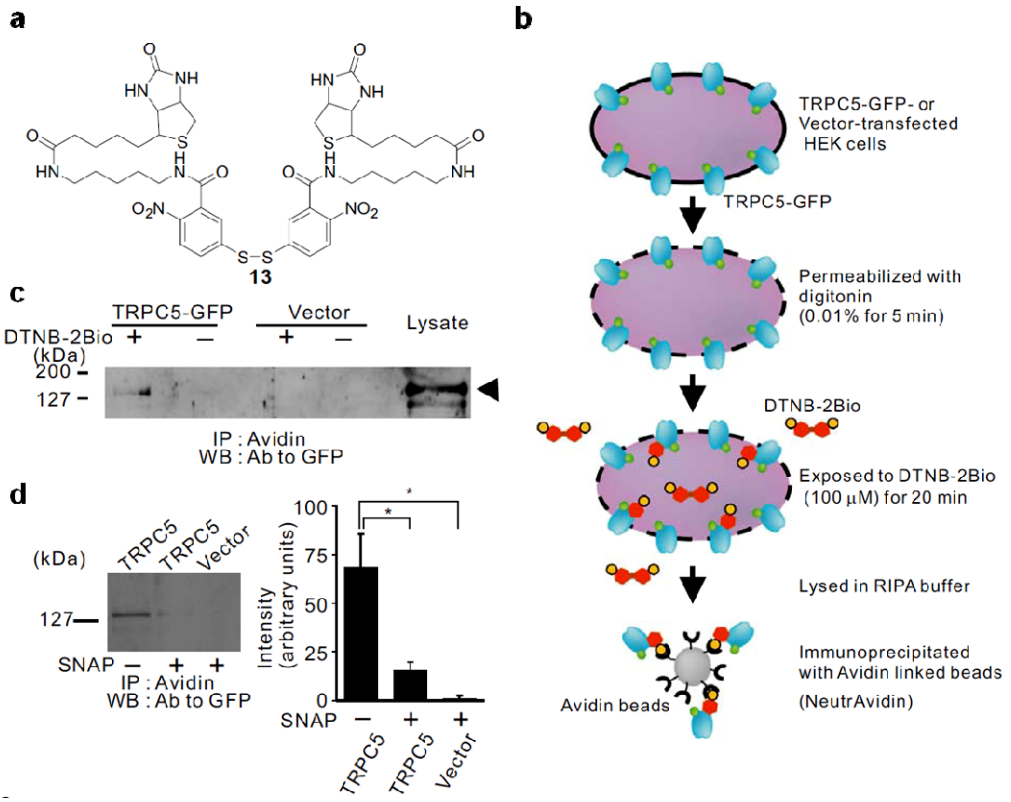

Figure 6. Covalent binding of DTNB-2Bio with TRPC5 channels. **a,** Chemical structure of DTNB-2Bio. **b,** Experimental procedure for labeling with DTNB-2Bio. As described in Methods, TRPC5-GFP-transfected HEK cells were permeabilized with digitonin (0.01%), exposed to 100 μM DTNB-2Bio in HBS, and lysed in RIPA buffer. Proteins absorbed to avidin-linked beads from the prepared cell lysate were subjected to western blot analysis (WB) with anti-GFP antibody to detect TRPC5-GFP in DTNB-2Bio-modified fraction. **c,** Detection of TRPC5-GFP among proteins incorporating DTNB-2Bio (100 μM) by WB using anti-GFP antibody. **d,** Suppression of DTNB-2Bio incorporation by 5 mM SNAP (left). The total band intensity (right). Data points are the means ± s.e.m.. $^{*}P < 0.05$.

Free cysteine sulfhydryls are nitrosylated by NO[11,33], and are modified by reactive disulfides via disulfide exchange reactions in proteins[12]. Hence, cysteine residues are the most likely modification site candidate. Every cysteine residue in TRPC5 was subjected to replacement with serine or to deletion, and the mutants were tested for their responses to 5-nitro-2-PDS and NO (Fig. 7a). Mutations C553S and C558S abrogated TRPC5 responses to NO (5, 16 and 16% of WT for C553S, C558S and Vector, respectively) as well as responses to 5-nitro-2-PDS (13, 15 and 24% of wild-type (WT) for C553S, C558S and Vector, respectively). The resistance of the mutants is not

attributable to localization defects, since the mutants showed intact plasma membrane expression as WT (Fig. 7b, c). TRPC5 responses to receptor stimulations were only partially suppressed by C553S and C558S (Fig. 7d), in contrast to responses to NO. The DTNB-2Bio incorporation was also abolished by C553S, whereas it was unaffected by C558S (Fig. 7e). Cysteine S-nitrosylation detected after selective conversion into biotinylated cysteines[10] was significantly enhanced by SNAP in WT (184 ± 45% of basal level). TRPC5 nitrosylation was significantly suppressed by C553S (38 ± 21% of WT with SNAP), but less extensively by C558S (75 ± 9.7%) (Fig. 7f). The results identify Cys553 as a main nitrosylation site, and as a predominant modification site for reactive disulfides.

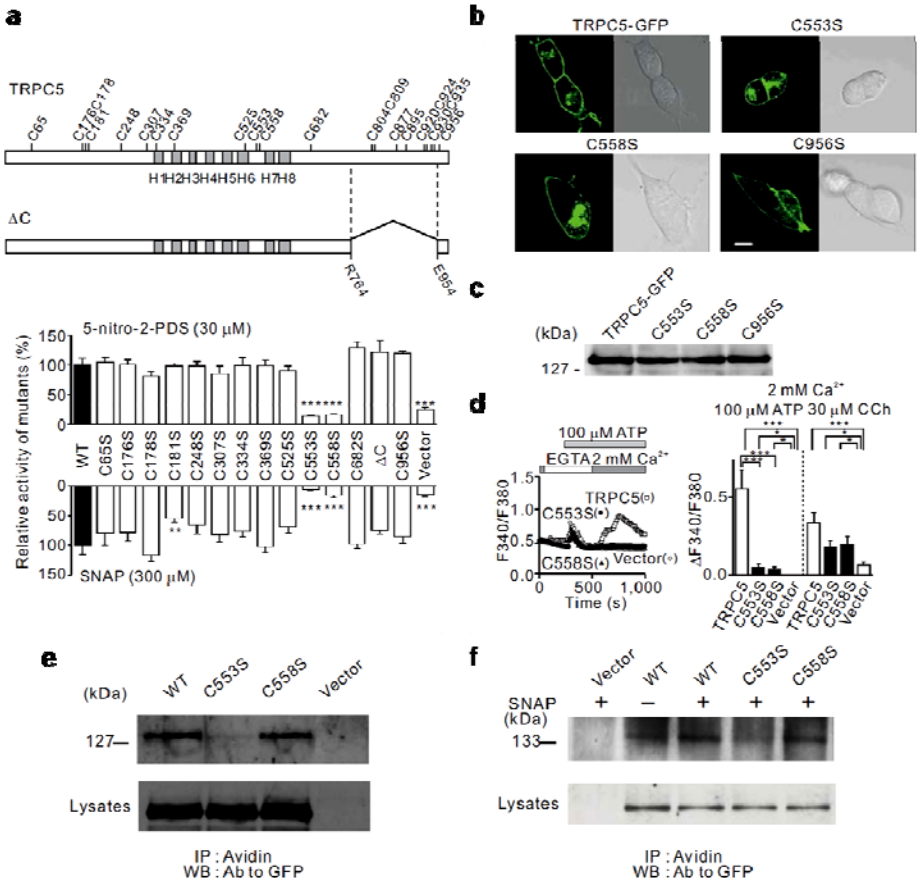

Figure 7. Cysteine residues on the N-terminal side of the pore region contribute to NO- and 5-nitro-2-PDS-induced activity of TRPC5 channel. **a,** Cysteine residues mapped on TRPC5 (top). Cysteines were replaced with serine, or deleted in ΔC mutant (R764 to E954). Relative responses to 5-nitro-2-PDS (n = 15–48) or to SNAP (n = 14–31) of TRPC5 mutants in HEK cells (bottom). $^{**}P < 0.01$

and $^{***}P < 0.001$, compared to WT. **b,** Confocal fluorescence images of TRPC5-GFP, C553S, C558S and C956S. The bar indicates 10 μm. **c,** WB using an anti-GFP antibody demonstrates comparable protein expression levels of recombinant TRPC5 constructs in HEK cells. **d,** TRPC5 mutants show decreased yet significant responses to ATP or CCh stimulation. Average time courses of responses to ATP (left). Maximal $[Ca^{2+}]_i$ rises upon readdition of extracellular Ca^{2+} (right). **e,** Effects of mutations C553S and C558S on DTNB-2Bio incorporation. WB of total cell lysates indicates comparable TRPC5 expression (lysates). **f,** Cysteine S-nitrosylation of WT TRPC5-GFP and mutants C553S and C558S with and without SNAP treatment. Data points are the means ± s.e.m.. $^{*}P < 0.05$ and $^{***}P < 0.001$.

TRP channels with conserved cysteines are responsive to NO

NO-sensitive channel activation was tested for generality in the TRP superfamily. Strikingly, the alignment of amino acid sequences surrounding Cys553 and Cys558 of TRPC5 with counterpart sequences demonstrates that the closest relatives TRPC1 and C4 as well as thermosensor channels TRPV1, V3 and V4 harbor cysteines conserved on the N-terminal side of putative pore-forming regions H7 in the linker region located between the fifth and sixth transmembrane domains S5 and S6 (S5-S6 linker) (Fig. 8a)[30,34]. TRPC1, C4 and V1 contain two cysteines separated by 4 residues as TRPC5, while TRPV3 and V4 carry two and 4 cysteines, respectively, in sequences distantly related to TRPC5. These cysteines predict NO responsiveness of these TRPC and TRPV channels to cysteine modifications.

The recombinants of the above TRP homologues were tested for the susceptibility to SNAP, 5-nitro-2-PDS and H_2O_2 in HEK cells (Fig. 8b–g). As described in Fig. 1, the differences in maximal $[Ca^{2+}]_i$ rises (ΔF340/F380) statistically tested between the total populations of cells expressing TRPC1 or C4 alone and control cells were not significant. However, in response to SNAP (300 μM) and 5-nitro-2-PDS (30 μM), larger fraction (7–9%) of expressing cells showed ΔF340/F380 > 0.5, compared to control cells (2–5%). Strikingly, cells coexpressing TRPC4 and C5 showed SNAP and 5-nitro-2-PDS responses comparable with those in cells expressing TRPC5 alone (Fig. 8b, c), while cells

coexpressing TRPC1 with C5 displayed slightly suppressed and yet robust responses (Fig. 8e, f). Interestingly, in cells coexpressing TRPC5 with C4 (Fig. 8d) or C1 (Fig. 8g), H_2O_2 (1 mM) evoked significantly impaired responses. TRPC5 was coimmunoprecipitated with coexpressed TRPC1 or C4 (Fig. 8h). The results suggest intact NO sensitivity and H_2O_2 resistance of heteromultimeric TRPC5/C1 or C5 /C4 channels in comparison to homomultimetric TRPC5.

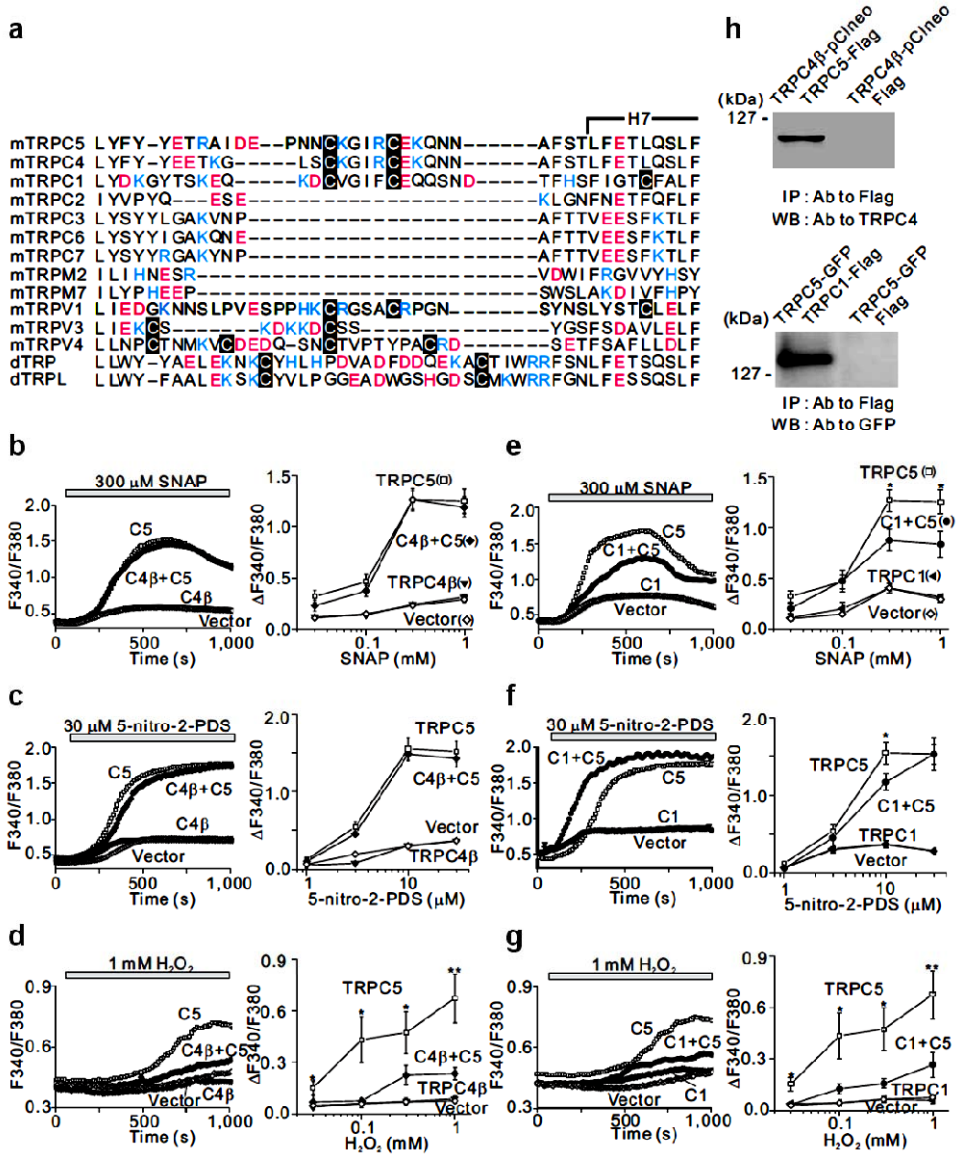

Figure 8. Molecular conservation of NO-induced activation in TRP channels. **a**, Conserved cysteine residues on the N-terminal side of putative pore forming regions in mouse TRPC1–C7, M2, M7, V1, V3, V4 and *Drosophila* TRP and TRPL. **b–g,** Ca^{2+} responses mediated by TRPC4β/TRPC5 (**b–d**) and TRPC1/TRPC5 heteromultimers (**e–g**) in HEK cells. Average time courses of responses to SNAP (**b**, **e**),

5-nitro-2-PDS (**c**, **f**) or H_2O_2 (**d**, **g**) (left). Dose response relationships (n = 21–49) (right). Data points are the means ± s.e.m.. $^{*}P < 0.05$ and $^{**}P < 0.01$ for TRPC5, compared to TRPC5/C4 or C5/C1. **h,** Coimmunoprecipitation of TRPC5 with C4β (top) or C1 (bottom). Immunoprecipitates (IP) with anti-Flag antibody from HEK cells expressing TRPC4β/TRPC5-Flag or TRPC1-Flag/TRPC5-GFP were subjected to WB with antibody to TRPC4 or GFP, respectively.

Activation by NO was observed also for thermosensor TRPV1, V3 and V4 channels as predicted (Fig. 9). The augmentation of $[Ca^{2+}]_i$ rises by extracellular Ca^{2+} revealed NO- and 5-nitro-2-PDS-activated Ca^{2+} entry via TRPV1, V3 and V4 (Fig. 9d, e). To H_2O_2, TRPV1 and V4 were responsive, but TRPV3 was relatively resistant as heteromultimeric TRPC channels (Figs. 8d, g and 9f). The TRPV1 mutant with substitution for Cys615 and Cys620 (V1 mut) showed significantly suppressed responses to NO and other agents (Fig. 9d–f) and nitrosylation (Fig. 9g). Interestingly, H^+ and heat sensitivity of TRPV1 was enhanced by NO (Fig. 9h, i). This enhancement was abolished by the mutation, whereas H^+ and heat responses without SNAP application (Fig. 9h, i). Thus, channel activation regulated by nitrosylation is conserved among multiple TRPs.

Native TRP channels activated by NO in endothelial cells

Native Ca^{2+} influx triggered in response to NO was characterized in vascular endothelial cells. As reported[20,35], cultured bovine aortic endothelial cells (BAEC) showed significant enhancements of TRPC5 protein expression (Fig. 10a) and Ca^{2+} responses (Fig. 10b). To resolve involvements of TRPC5 in native Ca^{2+} influx, $[Ca^{2+}]_i$ rises upon readdition of extracellular Ca^{2+} under agent stimulation were measured after introduction of TRPC5-selective small interference RNA (siTRPC5) and the dominant negative construct of TRPC5 (TRPC5-DN)[36] in BAEC. Ca^{2+} influx evoked by NO and 5-nitro-2-PDS was significantly suppressed by siTRPC5 and

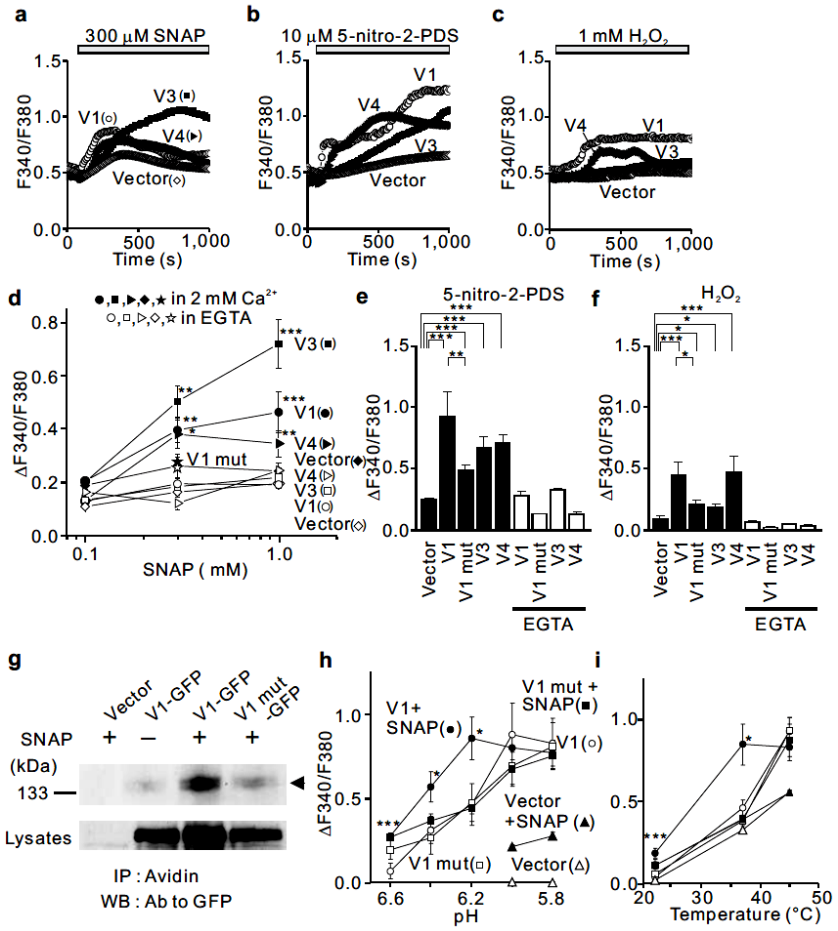

Figure 9. Regulation of TRPV channel activation by nitrosylation. **a–f,** Ca^{2+} responses to SNAP (**a**), 5-nitro-2PDS (**b**) and H_2O_2 (**c**) mediated by rat TRPV1 and its cysteine substitution C616W·C621S mutant (V1 mut), and human TRPV3 and V4. **a–c,** Average time courses. **d,** SNAP dose response relationships. **e, f,** Maximal $[Ca^{2+}]_i$ rises by 5-nitro-2-PDS (**e**) or H_2O_2 (**f**) in the presence and absence (EGTA) of 2mM external Ca^{2+} (n = 12–122). Data points are the means ± s.e.m.. $^{*}P < 0.05$, $^{**}P < 0.01$ and $^{***}P < 0.001$ compared to control (Vector). **g,** S-nitrosylation of TRPV1-GFP and the mutant. **h**, **i,** NO enhances H^+ and temperature sensitivity of TRPV1. Effects of SNAP (300 μM) on pH (**h**) and temperature dependence (**i**) of responses mediated by TRPV1 and the mutant are shown (n = 7–50). $^{*}P < 0.05$ and $^{***}P < 0.001$, compared to TRPV1s in the absence of SNAP.

TRPC5-DN in BAEC (Fig. 10c, d). By contrast, H_2O_2 induced only marginal Ca^{2+} influx insensitive to siTRPC5 and TRPC5-DN (Fig. 10e). The activator sensitivity is reminiscent of recombinant TRPC5/C1 or C5/C4 heteromultimer in HEK cells (Fig. 8b–g), being consistent with the confocal immunoimages showing superimposable distribution of TRPC5 with C1 and C4 at the plasma membrane area (Fig. 10f, g). Thus, heteromultimeric TRPC5/C1 and C5/C4 channels are likely to conduct native NO-activated Ca^{2+} influx in endothelial cells.

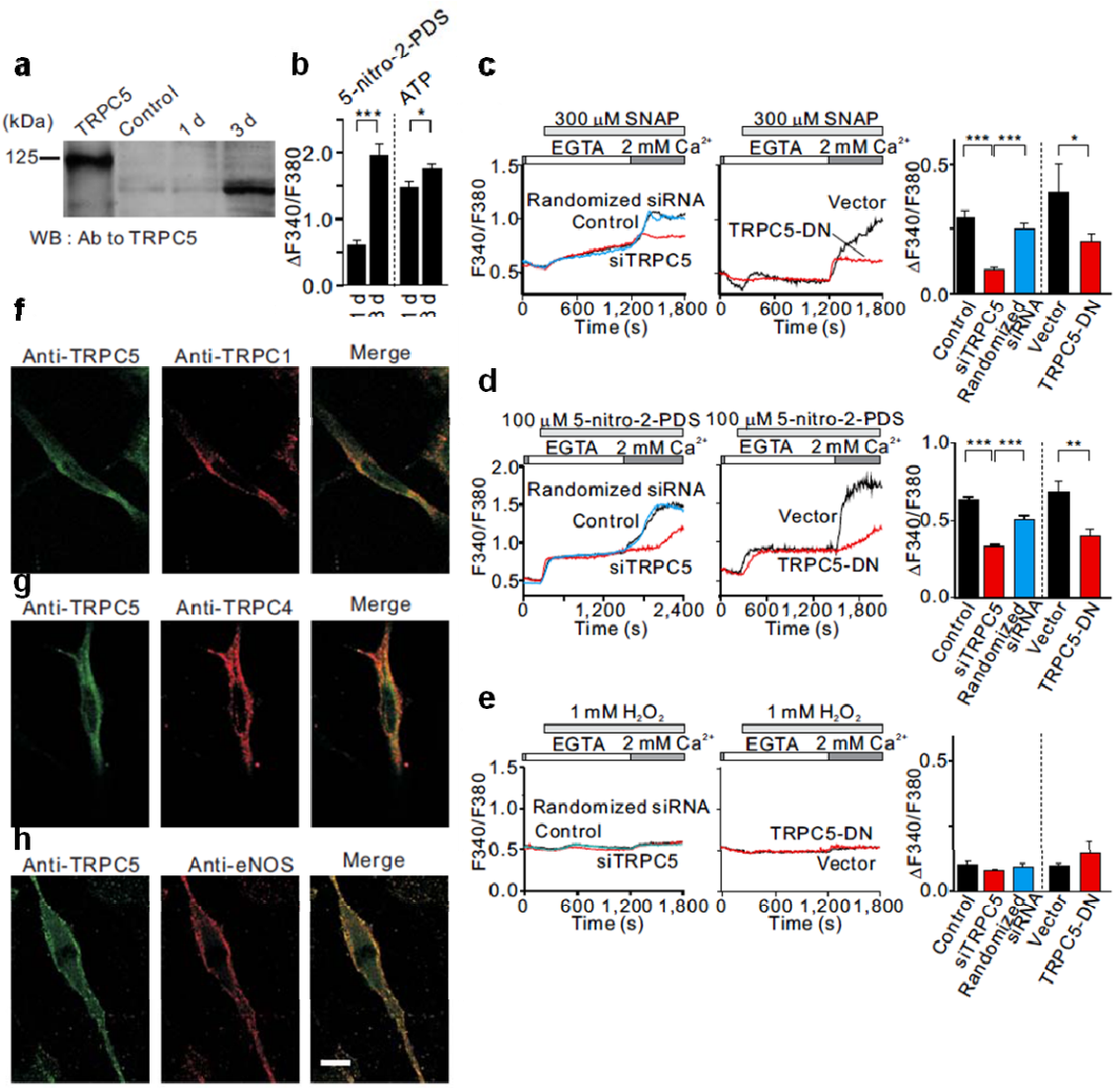

Figure 10. Physiological S-nitrosylation of native TRPC5 proteins in cultured endothelial cells. **a,** WB reveals TRPC5 protein expression enhanced after 3 days culture in BAEC. **b,** Ca^{2+} responses enhanced after 3 days culture in BAEC. Maximal $[Ca^{2+}]_i$ rises in response to 30 μM 5-nitro-2-PDS or 1 μM ATP (n = 30–36). **c–e,** Contribution of TRPC5 to native Ca^{2+} influx induced by SNAP (**c**), 5-nitro-2-PDS (**d**) and H_2O_2 (**e**) in BAEC. Representative Ca^{2+} responses after treatment with TRPC5 specific siRNA (siTRPC5) or with control random siRNA (randomized siRNA), without treatment (Control) (left), and after transfection with TRPC5-DN (middle). Maximal $[Ca^{2+}]_i$ rises attributable to Ca^{2+} influx (n = 17–67) (right). Data points are the means ± s.e.m.. $^{*}P < 0.05$, $^{**}P < 0.01$ and $^{***}P < 0.001$. **f–h,** Confocal fluorescence immunoimages of TRPC5 (green signals), C1 (**f**), C4 (**g**), or eNOS (**h**) (red signals), and overlay of images (yellow signal) in BAEC. The bar indicates 10 μm.

ATP is a vasodilator that activates G protein-coupled receptors resulting in endothelial NO production via eNOS[16]. We tested whether the NO produced by this physiological stimulation activates Ca^{2+} influx in BAEC. ATP induced $[Ca^{2+}]_i$ rises due to Ca^{2+} release in the absence of extracellular Ca^{2+} and Ca^{2+} influx after the readmission of external Ca^{2+} (Fig. 11a, left panel). The NOS inhibitor N^{ω}-nitro-L-arginine methyl ester (L-NAME) failed to affect Ca^{2+} release, but significantly suppressed the Ca^{2+} influx (Fig. 11a, middle panel) and NO production (Fig. 11b). This, together with similar effects elicited by eNOS-targeted siRNA (sieNOS) (Fig. 11c, d) and by NO quencher N-acetyl-L-cysteine (NAC) and ascorbate (Fig. 11e), is indicative of a critical role of endogenous eNOS in inducing ATP receptor-activated Ca^{2+} influx. siTRPC5 more extensively diminished the Ca^{2+} influx, and abolished the L-NAME sensitivity (red bars in Fig. 11a, right panel), suggesting that TRPC5 is essential for Ca^{2+} influx activated by NO via eNOS upon receptor stimulation. TRPC5-DN, which can exert a suppressive effect also on Ca^{2+} influx via nitrosylated TRPC5 (Fig. 11f, g), similarly suppressed the Ca^{2+} influx (Fig. 11c). In BAEC, siTRPC5 has by contrast revealed lack of involvements of TRPC5 in SOC (Fig. 11h). Importantly, native TRPC5 proteins were susceptible to ATP receptor-induced nitrosylation suppressed by ascorbate, L-NAME, NAC, and sieNOS (Fig. 12a, b). Furthermore, confocal immunoimages indicate colocalization of TRPC5 with eNOS (Fig. 10h). The results provide evidence for native TRPC5 channels activated by nitrosylation via eNOS upon ATP receptor stimulation in endothelial cells.

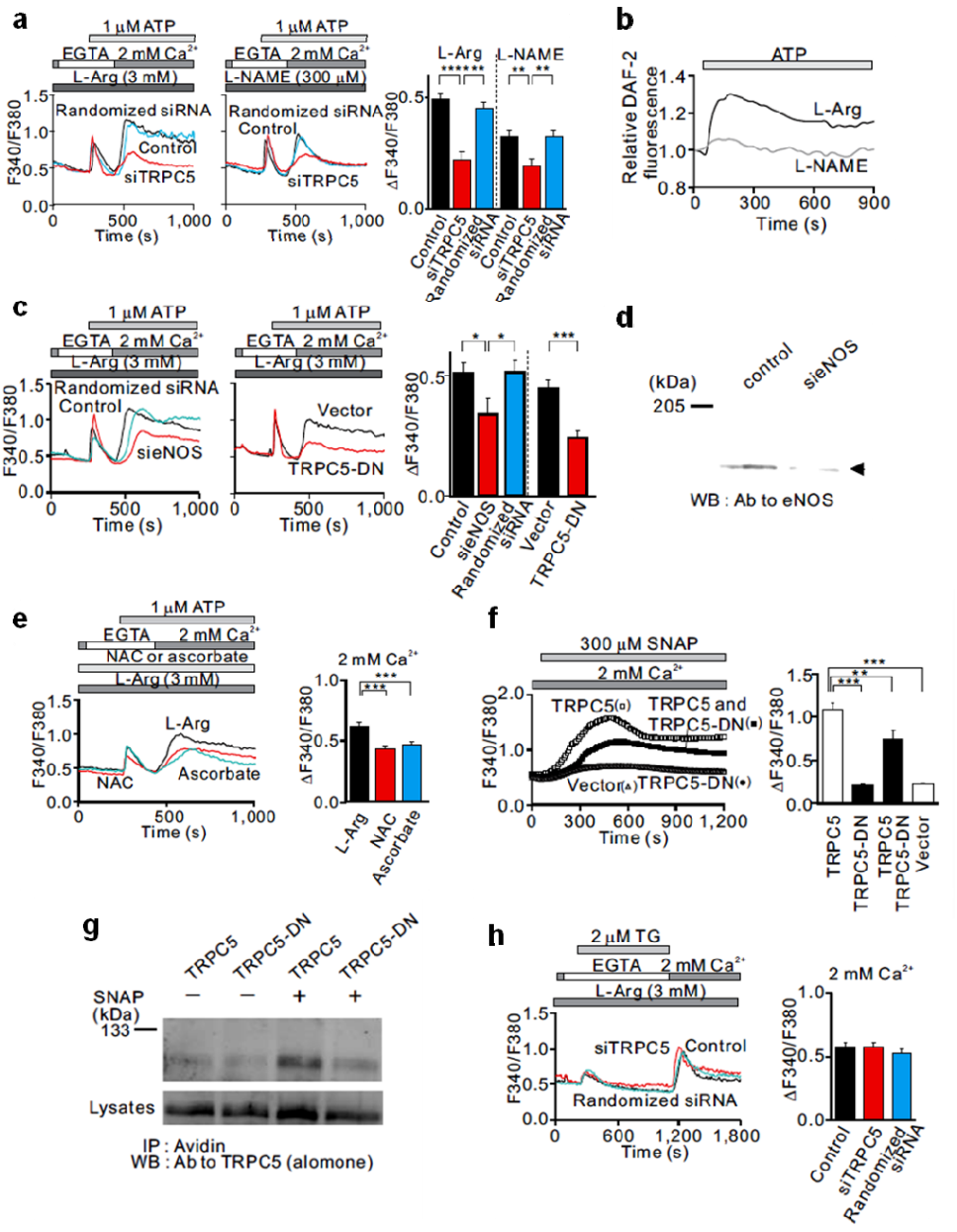

Figure 11. Native TRPC5 channels are essential for NO-induced Ca^{2+} influx in endothelial cells. **a,** Representative Ca^{2+} responses after treatment with siTRPC5 plus L-Arginine (left) or L-NAME (middle). Maximal Ca^{2+} rises attributable to Ca^{2+} influx (n = 50–94) (right). **b,** Representative time-courses of increment of DAF-2 fluorescence in response to 1 μM ATP in the presence of L-Arginine (3 mM) or of eNOS inhibitor L-NAME (300 μM). **c,** Representative Ca^{2+} responses after suppression by sieNOS (left) and TRPC5-DN (middle). Maximal Ca^{2+} rises attributable to Ca^{2+} influx (n = 21–38) (right). **d,** eNOS expression suppressed by eNOS specific siRNA (sieNOS). **e,** Contribution of S-nitrosylation by NO to native ATP receptor-activated Ca^{2+} influx in BAEC. Representative Ca^{2+} responses after treatment with L-Arginine (3 mM) plus N-acetyl-L-cysteine (NAC, 10 mM) or ascorbate (1 mM). Maximal $[Ca^{2+}]_i$ rises attributable to Ca^{2+} influx (right). **f, g,** TRPC5-DN exerts dominant negative suppression effect on Ca^{2+} influx induced by SNAP. **f,** Ca^{2+} responses mediated by TRPC5/TRPC5-DN heteromultimers in HEK cells. Average time courses of responses to SNAP (left). Maximal $[Ca^{2+}]_i$ rises in the presence of external Ca^{2+} (right). **g,** S-nitrosylation of TRPC5-DN comparable to that of WT TRPC5 with and without

SNAP treatment. **h,** Store-operated Ca^{2+} entry is independent of TRPC5 in BAEC. Representative Ca^{2+} responses after treatment with TRPC5 specific siRNA (siTRPC5) or with control random siRNA (Randomized siRNA), without treatment (Control) (left). Maximal $[Ca^{2+}]_i$ rises due to Ca^{2+} entry (right). Data points are the means ± s.e.m.. $^{*}P < 0.05$, $^{**}P < 0.01$ and $^{***}P < 0.001$.

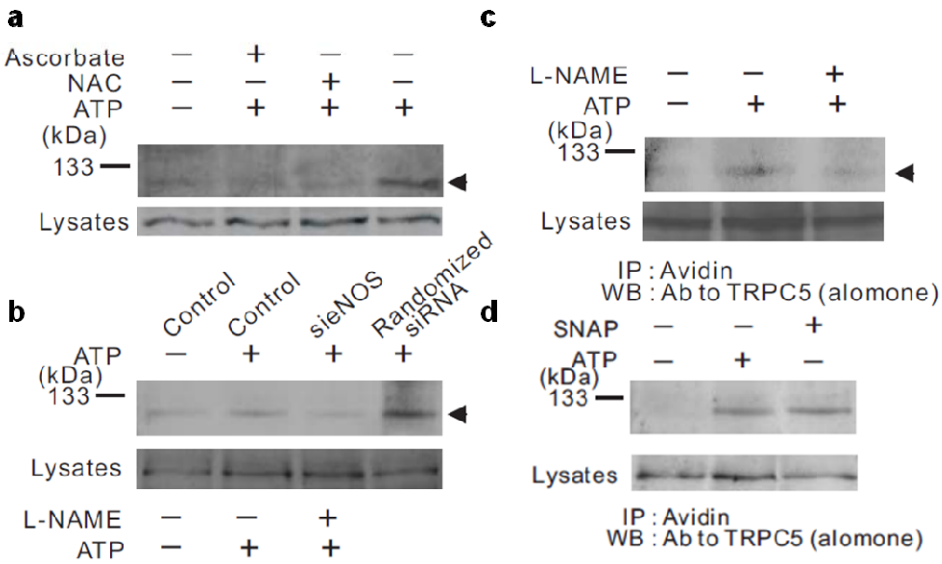

Figure 12. S-nitrosylation of native TRPC5 by ATP receptor stimulation. **a–c,** Inhibition of S-nitrosylation of TRPC5 by NAC and ascorbate (**a**), sieNOS (**b**) and L-NAME (**c**) in BAEC. **d,** S-nitrosylation of native TRPC5 by physiological ATP receptor stimulation occurs at a level comparable to that by SNAP treatment (5 mM) in BAEC.

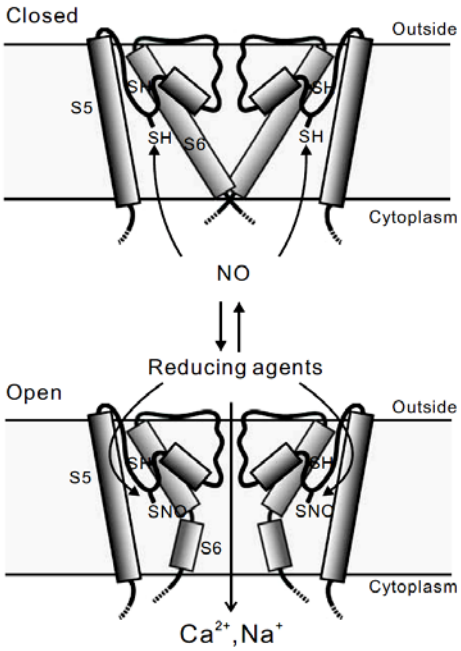

Figure 13. Model for TRP channel activation by NO and reactive disulfides. Possible protein conformation change during activation of TRPC5 channels by NO is shown. The activation trigger NO modifies the free sulfhydryl group of Cys553 accessible from the cytoplasmic side. This direct thiol S-nitrosylation induce a bend of S6 that opens the intracellular activation gate. The cysteine modification is reversed by the hydrophilic reducing-agents DTT and ascorbate applied externally.

Discussion

The present study describes a novel activation mechanism of TRP channels via cysteine S-nitrosylation, as well as a structural motif essential for the activation gating. Among TRPCs coupled to phospholipase C-linked receptors, TRPC5 showed prominent sensitivity to NO. Nitrosylated Cys553 and Cys558 mediated the responsiveness in TRPC5. Critical contribution of native nitrosylated TRPC5 to Ca^{2+} entry was revealed by siRNA and dominant negative suppression in endothelial cells. Strikingly, TRPC1 and C4 associated with TRPC5, and thermosensors TRPV1, V3 and V4, which harbored cysteines nearby the same putative pore-forming region, responded well to NO. These TRPC and TRPV channels may comprise a new TRP category that serves as ubiquitous cell surface NO sensors essential for integration of NO and Ca^{2+} signals.

The data (Fig. 5) suggests that NO and reactive disulfides exert their action independently of receptor-induced cascade or Ca^{2+} store depletion in activating TRPC5. In fact, SNAP at low concentrations and reactive disulfides failed to activate TRPC2, C3, C6 and C7 that are activated by receptor stimulation[2–7]. SNAP also failed to significantly affect endogenous SOCs in HEK cells. The abolishment of DTNB-2Bio incorporation by SNAP co-application and by C553S, and the suppression of nitrosylation by C553S (Figs. 6 and 7) further that both NO and reactive disulfides directly modify Cys553 in the TRPC5 protein. Compared to C553S, C558S weakly reduces nitrosothiol levels. This, together with the partial resistance of NO-induced TRPC5 response to ascorbate (Fig. 3a) may suggest that the free sulfhydryl group of Cys558 nucleophilically attacks nitrosylated Cys553 to form a disulfide bond that stabilizes open state. S-nitrosylation has been demonstrated to activate the ryanodine receptor channel[37] and cyclic nucleotide-gated cation channels[38]. S-nitrosylation modulates NMDA receptors[33]. Ryanodine receptors are also activated by reactive disulfides[12]. In proteins with high

NO sensitivity, basic and acidic amino acids surrounding S-nitrosylated cysteines[11] have been proposed to enhance nucleophilicity of sulfhydryl and its S-nitrosylation, as reported in acid-base catalysis of hemoglobin nitrosylation. In this context, charged residues flanking Cys553 and Cys558 (Fig. 8a) might confer modification susceptibility to their free sulfhydryls of and the counterpart cysteines in TRPC and TRPV channels, commonly distinguished on the basis of their characteristic activation triggers, receptor activation and heat. Interestingly, so-called "thermoTRPs" are comprised of members of multiple TRP families (V, M and A)[3–5]. Therefore, together with NO-activated TRPs, thermoTRPs[3–5] can be considered as those few functional categories extended over multiple TRP families. Our findings may provide the first clear chemical biological basis for TRP categorization of this hierarchy.

The obtained results suggest that NO and reactive disulfides selectively modify Cys553 and Cys558 coupled to gating apparatus among functionally critical domains in the TRPC5 protein. Since C553S and C558S only partially suppressed receptor-induced TRPC5 responses (Fig. 7d), the cysteines are not absolute necessities but should play an important regulatory role in the TRPC5 activation. Intact receptor-induced responses after DTT treatment (unpublished results) further suggest that the oxidative cysteine modifications are not required for receptor stimulation to activate TRPC5. In TRPV1, the cysteine mutation that impaired NO sensitivity failed to affect H^+ and temperature sensitivities under the control condition in the absence of NO. Hence, it is presumed that the role played by the nitrosylation target cysteines in H^+- or heat-induced activation of TRPV1 is qualitatively comparable to the regulatory role played by the counterpart cysteines in receptor-induced activation of TRPC5, although quantitative differences should be considered in impacts attributable to structural changes between mutations. Surprisingly, despite the location of Cys553 and Cys558 in the extracellularly disposed S5-S6 linker according to previous studies[34], the modifications are unlikely to affect the

structure of ion conducting pore, since similar single channel conductances were observed for the spontaneously activated TRPC5 channel (47.6 pS)[39] and the 5-nitro-2-PDS-activated TRPC5 channel (44.1 pS). Moreover, the sidedness of action of DTNB as well as the time lags preceding the responses after the agent application supports the hypothesis that modification agents access from the cytoplasmic side to open the intracellular activation gate of TRPC5 channels (Fig. 13). In Shaker voltage-gated K^+ channels, the activation gate formed by S6 residues near the intracellular entrance of pore cavity has been identified[31]. Considering the longer S5–S6 linkers of TRPC5/C1/C4 comprised of approximately 60 residues in comparison with 50 and 40 of TRPC2/C3/C6/C7 and Shaker K^+ channel, respectively, the TRPC5 S5–S6 linker with modified Cys553 may be invaginated toward the cytoplasm to reach the S6 activation gate (Fig. 13). However, external DTT and ascorbate reversed the TRPC5 activation (Fig. 3a–d), and in TRPV1 the cysteine counterparts have been suggested as sites for blockade by externally applied oxidizing agents[40,41], while the antibody raised against a peptide containing Cys553 at the C-terminus inhibited TRPC5 activity[42]. Therefore, Cys553 is very likely located at the interface between the inside and outside of the cell.

The plasma membrane expression of TRPC5 unaffected by C553S and C558S (Fig. 7b, c) may suggest minimal contribution of the protein trafficking to the NO-induced activation in HEK cells. However, involvements of protein recruitments through the fusion of vesicles with the plasma membrane and lateral movements within plasma membrane cannot be excluded. Interestingly, Ca^{2+}-dependent BK-type K^+ channels are modulated by multiple mechanisms such as redox-sensitive extracellular gates containing cysteine residues in the auxiliary β subunit[43] and haem bound to the pore-forming α subunit[44]. Therefore, conformational changes elicited by the cysteine modification in an unidentified associated protein can be transmitted to TRPC5 via Cys553, if the protein association is maintained during the labeling assays. Thus, cysteine modifications may

exert their action via multiple pathways on the pore-forming TRPC5 protein, in consistency with the previously reported multiplicity of signals responsible for channel activation of TRPC5[45].

Ca^{2+} influx via nitrosylated TRP channels may mediate the positive feedback regulation of Ca^{2+}-dependent NO production. In support of our view, native NO-activated Ca^{2+} channels have been reported in different systems including endothelial cells[24,25,46,47], where cation currents are activated by glutathione disulfide[48]. In endothelial cells, however, suppressive effects of NO on Ca^{2+} entry was also demonstrated[26,27]. This discrepancy is at least in part attributable to diversity in NO susceptibility of ion channels and signaling pathways that regulate Ca^{2+} influx. In fact, Ca^{2+} entry via SOCs is potentiated indirectly by NO through the enhancement of Ca^{2+} release[23]. In those endothelial cells, where cGMP mediates NO signals as in smooth muscle[26,27], suppression of Ca^{2+} entry by NO is described. Moreover, inhibition of NOS by NO is known[11]. Thus, ensembles of multiple NO-regulated mechanisms may determine net Ca^{2+} entry. Interestingly, in the NMDA receptor Ca^{2+}-permeable channel NR1/NR2A, nNOS physically coupled to NR1 through PSD95 nitrosylates NR2A to elicit feedback inhibition of channel activity[33]. To resolve the complexity in crosstalk between NO and Ca^{2+} signals, precise identification of physiological protein interaction between nitrosylated TRP channels and NOSs is necessary.

Our immunolocalization studies have revealed TRPC5 distribution on both the apical and basal membrane in the endothelial cell layer of vascular tissue (unpublished results). Given that vasodilator receptors are distributed at the apical luminal surface of endothelial cell layer, NO initially produced there may diffuse across the cytoplasm and activate TRPC5 located at the basolateral membrane. This may lead to an efficient propagation of Ca^{2+} signals vectorized toward basal membrane. The feedback mechanism may further contribute to global $[Ca^{2+}]_i$ rises/oscillations and full activation of

eNOS at Golgi in endothelial cells, leading to synchronization of neighboring smooth muscle cells in vascular relaxation. Interestingly, Greka *et al*. demonstrated the importance of TRPC5 in neurite extension[36]. Since NO signals are reported to regulate neurite extension[49], the feedback mechanism may be important also in growth cone morphology. In terms of TRPVs, obtained results may raise a possibility for nitrosylation-induced Ca^{2+} entry involved in heat or pain sensation. Thus, the positive feedback regulation of Ca^{2+} signals by NO-activated TRP channels can be involved in diverse biological systems.

Impaired aortic vasorelaxation and reduced endothelial $[Ca^{2+}]_i$ increase upon agonist stimulation was demonstrated in TRPC4-defecient mice[50]. The report is intriguing in the context of present study, considering Cys553 and Cys558 counterparts harboured by TRPC4. TRPC5/C4 and C5/C1 channels displayed intact NO sensitivity and significant H_2O_2 resistance. These observations together with immunohistochemistry and coimmunoprecipitation experiments (Figs. 8, 10 and 12) suggest that the heteromultimerization with TRPC1 or C4 may enable TRPC5 to maintain NO sensing function along with resistance to the pathological ROS action[11,28] in endothelial cells. To understand the underlying mechanism, detailed studies of the binding pocket for the activation triggers using cysteine modification agents of different sizes as well as three-dimensional structural analysis is critical.

Methods

Molecular cloning. Mouse TRPC4β (GenBank accession No. AF019663) was cloned from mouse brain cDNA library[51] by applying a PCR-based approach, and was subcloned into the expression vector pCI-neo (Promega). Rat TRPV1 (GenBank accession No. NM_031982)[8] and human TRPV3 (GenBank accession No. NM_145068)[52] cDNAs were isolated from Rat Brain or Human Brain, whole Marathon-Ready cDNA (BD Biosciences) by using a similar strategy. Human TRPV4 (GenBank accession No. AF258465) cDNA was cloned according to Strotmann *et al*.[54] by RT-PCR from the Human Brain, whole Marathon-Ready cDNA (BD Biosciences) and was subcloned into the expression vector pcDNA3.1 (Invitrogen).

Cell culture and cDNA expression. The TRPC5 mutants were constructed using PCR techniques. TRPC1-Flag and TRPC5-Flag were first established in pCMV-Tag4 (Stratagene). The culture of HEK (American Type Culture Collection) cells and chicken DT40 B lymphocytes as well as cDNA expression were performed as described previously[28,32]. Bovine aortic endothelial cells were cultured in phenol red-free Dulbecco's modified Eagle's medium (DMEM) (GIBCO) containing 10% fetal bovine serum (FBS), 30 units ml^{-1} penicillin, 1 μM all-*trans*-retinoic acid (RA), and 30 μg ml^{-1} streptomycin at 37°C under 5% CO_2. To remove retinoid hormones, FBS was incubated with 0.5% dextran-coated charcoal (Sigma) at 4°C overnight. TRPC5-DN was transfected using Lipofectamine 2000 (Invitrogen). Cells were trypsinized and diluted by DMEM and plated onto glass coverslips 24 h after transfection. The cells were subjected to measurements 8–24 h after the plating. The WT TRPC5 was fused at the C terminus with GFP (TRPC5-GFP) using an EGFP-N1 vector (BD Biosciences). GFP-tagged single amino acid substitution mutants and deletion mutant were constructed using QuikChange Site-Directed Mutagenesis Kit (Stratagene). Primers used for the mutagenesis were as follows: 5'-GTCAACATCAACTCCATGGATCCTTTGGGC-3' and

5’-GCCCAAAGGATCCATGGAGTTGATGTTGAC-3’ for C65S;

5’-CCCCACCAGATCCGCTCCAACTGTGTGGAG-3’ and

5’-CTCCACACAGTTGGAGCGGATCTGGTGGGG-3’ for C176S;

5’-GATCCGCTGCAACTCTGTGGAGTGTGTATC-3’ and

5’-GATACACACTCCACAGAGTTGCAGCGGATC-3’ for C178S;

5’-GCAACTGTGTGGAGTCTGTATCCAGTTCGG-3’ and

5’-CCGAACTGGATACAGACTCCACACAGTTGC-3’ for C181S;

5’-GAACTTTCCCAGCAATCTAAGCTCTTTGCC-3’ and

5’-GGCAAAGAGCTTAGATTGCTGGGAAAGTTC-3’ for C248S;

5’-CGTTCAGCCAAACTCCCAACAATTGCTAGC-3’ and

5’-GCTAGCAATTGTTGGGAGTTTGGCTGAACG-3’ for C307S;

5’-GTCAAGCTTCTGACCTCCATGACCATTGG-3’ and

5’-CCAATGGTCATGGAGGTCAGAAGCTTGAC-3’ for C334S;

5’-CTTTATTAAGTTCATCTCCCACACAGCATC-3’ and

5’-GATGCTGTGTGGGAGATGAACTTAATAAAG-3’ for C369S;

5’-CTCTTTATCTACTCCCTAGTACTACTGG-3’ and

5’-CCAGTAGTACTAGGGAGTAGATAAAGAG-3’ for C525S;

5’-CCTAACAACTCCAAGGGGATCCGATGTG-3’ and

5’-CCCCTTGGAGTTGTTAGGTTCATCAATAGC-3’ for C553S;

5’-GCAAGGGGATCCGATCTGAAAAACAG-3’ and

5’-GTTCTGTTTTTCAGATCGGATCCCCTTGC-3’ for C558S;

5’-CAACAACACCTTCTCTCCCAAAAGAGACCC-3’ and

5’-GGGTCTCTTTTGGGAGAGAAGGTGTTGTTG-3’ for C682S;

5’-CTTGGGGAGAGGCTTCTGACTTGCTCATGC-3’ and

5’-GCATGAGCAAGTCAGAAGCCTCTCCCCAAG-3’ for C956S;

5’-GAAGTGCTTGACCTCTTGGGAAACGCTTCTGACTTGCTCA-3’ and

5’-TTTGTGCATGAGCAAGTCAGAAGCGTTTCCCAAGAGGTCA-3’ for ΔC. The TRPV1 was fused at the C terminus with GFP using EGFP-N1 (BD Biosciences). TRPV1 mutant was constructed using QuikChange Site-Directed Mutagenesis Kit (Stratagene). Primers used for the mutagenesis were as follows: 5’-CACACCACACAAGTGGCGGGGGTCTGCC-3’, 5’-GGCAGACCCCCGCCACTTGTGTGGTGTG-3’, 5’-CGGGGGTCTGCCTCCAAGCCAGGTAACTC-3’ and 5’-GAGTTACCTGGCTTGGAGGCAGACCCCCG-3’ for TRPV1 mut. TRPC5-expressing cells were selected through detection of fluorescence from pEGFP-F or TRPC5-GFP. For co-expression of TRPC1/TRPC5 or TRPC4β/TRPC5, equal amount of each expression plasmid was co-transfected to HEK cells. βARK-ct[54] and TRPC5-DN[55] are as described previously.

Fluorescent $[Ca^{2+}]_i$ measurements and electrophysiology. The fura-2 fluorescence was measured in HBS contained (in mM): NaCl 107, KCl 6, $MgSO_4$ 1.2, $CaCl_2$ 2, glucose 11.5, HEPES 20 adjusted to pH 7.4 with NaOH. The 340:380 nm ratio images were obtained on a pixel-by-pixel basis. Fura-2 measurements were carried out at 22 ± 1°C using HBS adjusted to pH 7.4, otherwise stated. Whole-cell currents were recorded at RT using the conventional whole-cell mode of patch clamp technique with EPC9 amplifier (HEKA) as described previously[28]. The standard pipette-filling solution contained (in mM): CsOH 105, L-aspartate 105, CsCl 40, $CaCl_2$ 1.33, $MgCl_2$ 2, Ethyleneglycol-*bis*(β-aminoethyl)-*N*,*N*,*N’*,*N’*-tetraacetic acid (EGTA) 5, HEPES 5, Na_2ATP 2 adjusted to pH 7.25 with CsOH (50 nM calculated free Ca^{2+}). The ‘2 mM Ca^{2+}-NaCl solution’ contained (in mM): NaCl 125, $MgCl_2$ 1.2, $CaCl_2$ 2, glucose 10, HEPES 11.5, mannitol 49, adjusted to pH 7.4 with NaOH. The osmolarity of external solutions was adjusted to about 325 mOsm. For the inside-out patch recording, the recording pipette contained the ‘2 mM Ca^{2+}-NaCl solution’, and the bathing solution had

the same composition as standard pipette-filling solution. Recordings were filtered at 1 kHz. Linear regression was employed to yield a single-channel conductance from *I*-*V* relationship.

Synthesis of DTNB-2Bio. DTNB（146.6 mg, 0.370 mmol Dojindo） was treated with WSC hydrochloride (*N*-(3-Dimethylaminopropyl)-*N*'-ethylcarbodiimide hydrochloride) (156.4 mg, 0.816 mmol, SIGMA) and *N*-hydroxysuccinimide (102.8 mg, 0.0893 mmol, WAKO) under nitrogen atmosphere at room temperature (RT) in dry *N*,*N*-dimethylformamide (20 ml). After 2 h stirring, the solvent was partially distilled off *in vacuo*. The residual reaction mixture was poured into ethyl acetate and extracted with 0.1N HCl aq. The combined organic layers were washed with aqueous sodium carbonate solution, dried with $MgSO_4$, and evaporated to give crude succinimidyl DTNB. EZ-linkTM 5-(Biotinamido) pentylamine (50.0 mg, 0.152 mmol PIERCE) in 5 H_2O (1.5 mL) was added to the yielded crude succinimidyl DTNB (44.1 mg, 0.075 mmol) in dried dioxane (6 mL) under the nitrogen atmosphere, and the biotinylation reaction was carried out overnight at RT. The biotinylated DTNB (DTNB-2Bio) precipitated as a white powder in dioxane and purified using filtration. The recovery of DTNB-2Bio was estimated 45.7% for two steps. DTNB-2Bio was dried *in vacuo*, and dissolved in DMSO for further use. 1H NMR and 13C NMR spectra was recorded in deuterated solvents on JEOL JNM-A400 spectrometer and calibrated to the residual solvent peak. Multiplicities are abbreviated as follows: s = singlet, d = doublet, t = triplet, m = multiplet, q = quartet. Data for DTNB-2Bio: 1H-NMR (400 MHz, DMSO-*d*6) δ 8.67 (t, *J* = 5.2 Hz, 2H), 8.09 (d, *J* = 8.8 Hz, 2H), 7.78-7.75 (m, 4H), 7.73 (s, 2H), 6.43 (s, 2H), 6.36 (s, 2H), 4.32–4.30 (m, 2H), 4.13-4.11 (m, 2H), 3.18 (q, *J* = 6.0 Hz, 4H), 3.09–3.06 (m, 2H), 3.03–3.02 (m, 4H), 2.81 (dd, *J* = 12.4, 5.2 Hz, 2H), 2.58–2.59 (m, 2H), 2.04 (t, *J* = 7.2 Hz, 4H), 1.53-1.28 (m, 24H); 13C NMR (100 MHz, DMSO-*d*6) δ 23.69, 25.31, 26.65, 28.03, 28.22, 28.26, 28.78, 35.23, 59.21, 61.06, 125.50, 133.82, 161.21, 162.71, 164.53, 171.89;

HRMS (FAB) m/z : Calculated for C44H61N10O10S4 (M+H)+: 1017.3455. Found 1017.3458.

Immunoprecipitation and western blot analysis. HEK Cells (~3 × 10^6) transfected with TRPC4β with TRPC5-Flag, TRPC5-GFP with TRPC1-Flag, TRPC4β with pCMV-Tag4, or TRPC5-GFP with pCMV-Tag4 were lysed in 200 μL of RIPA buffer (pH 8.0) containing 150 mM NaCl, 1% NP-40, 0.5% sodium deoxycholate, 0.1% SDS, 50 mM Tris, 1 mM PMSF and 10 μg ml^{-1} leupeptin. TRPC5-Flag or TRPC1-Flag was immunoprecipitated with anti-Flag M2 monoclonal antibody (SIGMA) in the presence of sepharose A-agarose beads (Amersham Pharmacia) rocked overnight at 4°C. The immune complexes were washed eight times with RIPA buffer for 5 min at RT, and resuspended in SDS sample buffer. The protein samples were fractionated by 7.5% SDS-PAGE and electrotransferred onto a nitrocellulose membrane. The blots were incubated with anti-GFP antibody (BD Biosciences) or anti-TRPC4 antibody (SIGMA) and stained using the ECL system (Amersham Pharmacia). Cultured bovine aortic endothelial cells were subjected to western blot analysis (WB) using anti-mouse TRPC5 rabbit antiserum (H8C1) directed against the C-terminus (CPKRDPDGRRRRHNLRS).

DTNB-2Bio labeling assay. DTNB-2Bio was synthesized by biotinylation of the two carboxyl groups of DTNB (Dojindo) using EZ-link^{TM} 5-(Biotinamido) pentylamine (50 mg, PIERCE) after converting DTNB to succinimidyl DTNB. TRPC5-GFP- or vector-transfected HEK cells (~5 × 10^6) were washed by phosphate-buffered saline (PBS) three times. The surface membrane was permeabilized by exposure to HEPES-buffered saline (HBS) containing 0.01% digitonin for 5 min. The cells were collected and exposed to HBS containing 100 μM DTNB-2Bio for 20 min at RT. The cells were washed with PBS three times, harvested, and lysed in RIPA buffer. Cell lysates were incubated batch-wise with NeutrAvidin-Plus beads (PIERCE) overnight at 4°C with constant shaking. The beads were rinsed six times with RIPA buffer by centrifugation at

14,000 rpm for 30 s. The proteins were eluted in sample buffer containing DTT (50 mM) at RT for 20 min and analyzed by 10% SDS-PAGE and WB detection using anti-GFP antibody (BD Biosciences).

S-nitrosylation assay. S-nitrosylation assay (biotin switch assay) was performed as described previously[10] with a few modifications. HEK cells expressing TRPC5-GFP constructs were incubated with SNAP (5 mM) or with control DMSO in the dark at RT for 10 min, and BAECs were pretreated with ascorbate (10 mM), NAC (1 mM) for 15 min, or L-NAME (10 mM) for 32 h, then exposed to ATP (1 μM) in the dark at RT for 5 min. The cells were washed with PBS two times, harvested and lysed in RIPA buffer. The extracts were incubated with 100 mM methyl methanethiosulfonate (MMTS) and 2.5% SDS at 50°C for 30 min, and MMTS was removed by precipitation with an equal volume of –30°C acetone. After resuspending the proteins in HEN buffer (250 mM HEPES pH 7.7, 1 mM EDTA and 0.1 mM neocuproine) containing 1% SDS, sodium ascorbate (1 mM final concentration) and biotin-HPDP (1 mM final concentration, PIERCE) were added. The mixtures were incubated for 1 h at 25°C in the dark with intermittent vortexing. Biotinylated nitrosothiols were then acetone-precipitated with 2 volumes of –30°C acetone to remove residual biotin-HPDP. After centrifugation, the pellet was resuspended in 0.1 mL HEN buffer containing 1% SDS. Two volumes of Neutralization buffer (20 mM HEPES, pH 7.7, 100 mM NaCl, 1 mM EDTA, 0.5% Triton X-100) were added, and biotinylated proteins were incubated with 20 μL of NeutrAvidin-Plus beads (PIERCE) for 1 h at RT. The resin was extensively washed in 10 volumes of Neutralization buffer containing 600 mM NaCl. The proteins were eluted in sample buffer containing DTT (50 mM) at RT for 30 min and analyzed by 7.5% SDS-PAGE and WB with anti-GFP antibody (BD Biosciences) to detect TRPC5-GFP or anti-TRPC5 antibody (alomone) to detect native bovine TRPC5.

siRNA experiment. Sense siRNA sequence was

5’-AATGCCTTCTCCACGCTCTTT-3’ for bovine TRPC5 (GenBank accession No. XM_617015) and 5’-AATATCCTGGAGGATGTGGCC-3’ for bovine eNOS (GenBank accession No. NM_181037). Randomized siRNA target sequence was 5’-AATCGCCTCTTACGCTCCTTT-3’ and 5’-AATGCGTGTTGCTAGACGCAG-3’, respectively. Computer analysis confirmed this sequence to be a good and specific target without homology to other bovine genes. Silencer^{TM} siRNA Construction Kit (Ambion) was used for construction of siRNA oligomers. The siRNAs were transfected to cultured endothelial cells using Lipofectamine 2000.

Confocal immunovisualization in cultured bovine aortic endothelial cells. Cultured bovine endothelial cells on coverslips were fixed with 4% (v/v) formaldehyde in PBS for 20 min at RT, washed with PBS three times and then permeabilized with 0.2% (v/v) Triton X-100 in PBS for 10 min at RT. Followed by washing with PBS three times, the coverslips were incubated with 5% bovine serum albumin (BSA) for 1 h at RT. The cells were then incubated for 1 h at RT with anti-TRPC5 goat polyclonal antibody (1:100) (Santa Cruz Biotech) and anti-TRPC1 (1:100) (SIGMA), anti-TRPC4 (1:100) (Alomone) rabbit polyclonal antibodies or anti-eNOS mouse monoclonal antibody (1:500) (CALBIOCHEM) containing 5% BSA in PBS, and incubated for 1 h with the fluorescein isothiocyanate (FITC)-conjugated anti-goat IgG for TRPC5, Cy3-conjugated anti-mouse IgG to detect eNOS, and Cy3-conjugated anti-rabbit IgG to detect TRPC1 or C4. Followed by washing with PBS three times, the coverslips were sealed with PermaFluor Aqueous (IMMUNONTM, SHANDON) to prevent evaporation and stored at 4°C before imaging. The fluorescence images were acquired with a confocal laser-scanning microscope using the 488-nm line of an argon laser for 7 excitation and a 505–525 nm band-pass filter for emission and 543-nm line of a He-Ne laser for excitation and a 560-nm long-pass filter for emission. The specimens were viewed at high magnification using plan oil objectives (60×, 1.40 NA, Olympus).

Confocal visualization of TRPC5-GFP and cysteine mutant proteins. For TRPC5-GFP and Cysteine mutant proteins, TRPC5-GFP-expressing cells were plated onto poly-L-lysine coated glass coverslips after 50 h of transfection. Fluorescence images were acquired with a confocal laser-scanning microscope (FV500, Olympus) using the 488-nm line of an argon laser for excitation and a 505-nm long-pass filter for emission. The specimens were viewed at high magnification using plan oil objectives (60×, 1.40 NA, Olympus).

Intracellular NO measurements. NO production was measured by esterase-sensitive NO-sensitive fluorescent dye DAF-2 DA (Daiichi Pure Chemicals). Cells were loaded with 10 μM DAF-2 DA for 15 min at 37°C. The DAF-2 fluorescence was measured by using the same equipment as $[Ca^{2+}]_i$ measurements with a different filter set, i.e., excitation at 490 nm and emission at 515 nm. To decrease quenching of DAF-2 fluorescence, we applied the excitation at 30 s intervals. Since it has been reported that DAF-2 fluorescence increases almost linearly with the NO concentration, we expressed the intracellular NO production as the net increment of DAF-2 fluorescence in 15 min relative to its basal value. Because NOS produces O_2 instead of NO in the absence of a sufficient concentration of L-arginine, 3 mM L-arginine was added in solutions for NO measurement, except for the experiment with N^{ω}-nitro-L-arginine methyl ester (L-NAME)-treated cells.

Statistical analysis. All data were expressed as means ± s.e.m.. The data were accumulated under each condition from at least three independent experiments. The statistical analyses were performed using Student's *t*-test.

References

1. Berridge, M. J., Bootman, M. D. & Lipp, P. Calcium—a life and death signal. *Nature* **395**, 645–648 (1998).

2. Montell, C., Birnbaumer, L. & Flockerzi, V. The TRP channels, a remarkably functional family. *Cell* **108**, 595–598 (2002).

3. Clapham, D. E. TRP channels as cellular sensors. *Nature* **426**, 517–524 (2003).

4. Voets, T., Talavera, K., Owsianik, G. & Nilius, B. Sensing with TRP channels. *Nat. Chem. Biol.* **1**, 85–92 (2005).

5. Clapham, D. E., Julius, D., Montell, C. & Schultz, G. International Union of Pharmacology. XLIX. Nomenclature and structure-function relationships of transient receptor potential channels. *Pharmacol. Rev.* **57**, 427–450 (2005).

6. Zhu, X. *et al. trp*, a novel mammalian gene family essential for agonist-activated capacitative Ca^{2+} entry. *Cell* **85**, 661–671 (1996).

7. Vazquez, G., Wedel, B. J., Aziz, O., Trebak, M. & Putney, J. W., Jr. The mammalian TRPC cation channels. *Biochim. Biophys. Acta.* **1742**, 21–36 (2004).

8. Caterina, M. J. *et al.* The capsaicin receptor: a heat-activated ion channel in the pain pathway. *Nature* **389**, 816–824 (1997).

9. Patapoutian, A., Peier, A. M., Story, G. M. & Viswanath, V. Thermo TRP channels and beyond: mechanisms of temperature sensation. *Nat. Rev. Neurosci.* **4**, 529–539 (2003).

10. Jaffrey, S. R., Erdjument-Bromage, H., Ferris, C. D., Tempst, P. & Snyder, S. H. Protein *S*-nitrosylation: a physiological signal for neuronal nitric oxide. *Nat. Cell Biol.* **3**, 193–197 (2001).

11. Hess, D. T., Matsumoto, A., Kim, S. O., Marshall, H. E. & Stamler, J.S. Protein S-nitrosylation: purview and parameters. *Nat. Rev. Mol. Cell. Biol.* **6**, 150–166 (2005).

12. Zaidi, N. F., Lagenaur, C. F., Abramson, J. J., Pessah, I. & Salama, G. Reactive disulfides trigger Ca^{2+} release from sarcoplasmic reticulum via an oxidation reaction. *J. Biol. Chem.* **264**, 21725–21736 (1989).

13. Moncada, S., Higgs, A. & Furchgott, R. International Union of Pharmacology Nomenclature in Nitric Oxide Research. *Pharmacol. Rev.* **49**, 137–142 (1997).

14. Venema, V. J. *et al.* Bradykinin stimulates the tyrosine phosphorylation and bradykinin B2 receptor association of phospholipase Cγ1 in vascular endothelial cells. *Biochem. Biophys. Res. Commun.* **246**, 70–75 (1998).

15. Zachary, I. & Gliki, G. Signaling transduction mechanisms mediating biological actions of the vascular endothelial growth factor family. *Cardiovasc. Res.* **49**, 568–581 (2001).

16. Koyama, T., Kimura, C., Park, S. J., Oike, M. & Ito, Y. Functional implications of Ca^{2+} mobilizing properties for nitric oxide production in aortic endothelium. *Life Sci.* **72**, 511–520 (2002).

17. Hutcheson, I. R. & Griffith, T. M. Central role of intracellular calcium stores in acute flow- and agonist-evoked endothelial nitric oxide release. *Br. J. Pharmacol.* **122**, 117–125 (1997).

18. Lantoine, F., Iouzalen, L., Devynck, M. A., Millanvoye-Van Brussel, E. & David-Dufilho, M. Nitric oxide production in human endothelial cells stimulated by histamine requires Ca^{2+} influx. *Biochem. J.* **330**, 695–699 (1998).

19. Lin, S. *et al.* Sustained endothelial nitric-oxide synthase activation requires capacitative Ca^{2+} entry. *J. Biol. Chem.* **275**, 17979–17985 (2000).

20. Yao, X. & Garland, C.J. Recent developments in vascular endothelial cell transient receptor potential channels. *Circ. Res.* **97**, 853–863 (2005).

21. Mungrue, I. N. & Bredt, D. S. nNOS at a glance: implications for brain and brawn. *J. Cell Sci.* **117**, 2627–2629 (2004).

22. Khan, S. A. & Hare, J. M. The role of nitric oxide in the physiological regulation of Ca^{2+} cycling. *Curr.opin. Drug. Discov. Devel.* **6**, 658–666 (2003).

23. Volk, T., Mäding, K., Hensel, M. & Kox, W. J. Nitric oxide induces transient Ca^{2+} changes in endothelial cells independent of cGMP. *J. Cell. Physiol.* **172**, 296–305 (1997).

24. Chen, J. *et al.* Autocrine action and its underlying mechanism of nitric oxide on intracellular Ca^{2+} homeostasis in vascular endothelial cells. *J. Biol. Chem.* **275**, 28739–28749 (2000).

25. Li, N., Sul, J. Y. & Haydon, P. G. A calcium-induced calcium influx factor, nitric oxide, modulates the refilling of calcium stores in astrocytes. *J. Neurosci.* **23**, 10302–10310 (2003).

26. Kwan, H. Y., Huang, Y. & Yao, X. Store-operated calcium entry in vascular endothelial cells is inhibited by cGMP via a protein kinase G-dependent mechanism. *J. Biol. Chem.* **275**, 6758–6763 (2000).

27. Dedkova, E. N. & Blatter, L. A. Nitric oxide inhibits capacitative Ca^{2+} entry and enhances endoplasmic reticulum Ca^{2+} uptake in bovine vascular endothelial cells. *J. Physiol.* **539**, 77–91 (2002).

28. Hara, Y. *et al.* LTRPC2 Ca^{2+}-permeable channel activated by changes in redox status confers susceptibility to cell death. *Mol. Cell* **9**, 163–173 (2002).

29. Aarts, M. *et al.* A key role for TRPM7 channels in anoxic neuronal death. *Cell* **115**, 863–877 (2003).

30. Okada, T. *et al.* Molecular cloning and functional characterization of a novel receptor-activated TRP Ca^{2+} channel from mouse brain. *J. Biol. Chem.* **273**, 10279–10287 (1998).

31. del Camino, D. & Yellen, G. Tight steric closure at the intracellular activation gate of a voltage-gated K^+ channel. *Neuron* **32**, 649–656 (2001).

32. Sugawara, H., Kurosaki, M., Takata, M. & Kurosaki, T. Genetic evidence for involvement of type 1, type 2 and type 3 inositol 1,4,5-trisphosphate receptors in signal transduction through the B-cell antigen receptor. *EMBO. J.* **16**, 3078–3088 (1997).

33. Choi, Y. B. *et al.* Molecular basis of NMDA receptor-coupled ion channel modulation by *S*-nitrosylation. *Nat. Neurosci.* **3**, 15–21 (2000).

34. Vannier, B., Zhu, X., Brown, D. & Birnbaumer, L. The membrane topology of human transient receptor potential 3 as inferred from glycosylation-scanning mutagenesis and epitope immunocytochemistry. *J. Biol. Chem.* **273**, 8675–8679 (1998).

35. Chang, A. S., Chang, S. M., Garcia, R. L. & Schilling, W. P. Concomitant and hormonally regulated expression of trp genes in bovine aortic endothelial cells. *FEBS Lett.* **415**, 335–340 (1997).

36. Greka, A., Navarro, B., Oancea, E., Duggan, A. & Clapham, D. E. TRPC5 is a regulator of hippocampal neurite length and growth cone morphology. *Nat. Neurosci.* **6**, 837–845 (2003).

37. Xu, L., Eu, J. P., Meissner, G. & Stamler, J. S. Activation of the cardiac calcium release channel (ryanodine receptor) by poly-S-nitrosylation. *Science* **279**, 234–237 (1998).

38. Broillet, M. C. & Firestein, S. Direct activation of the olfactory cyclic nucleotide-gated channel through modification of sulfhydryl groups by NO compounds. *Neuron* **16**, 377–385 (1996).

39. Yamada, H. *et al.* Spontaneous single-channel activity of neuronal TRP5 channel recombinantly expressed in HEK293 cells. *Neurosci. Lett.* **285**, 111–114 (2000).

40. Jin, Y. *et al.* Thimerosal decreases TRPV1 activity by oxidation of extracellular sulfhydryl residues. *Neurosci. Lett.* **369**, 250–255 (2004).

41. Tousova, K., Susankova, K., Teisinger, J., Vyklicky, L. & Vlachova, V. Oxidizing reagent copper-*o*-phenanthroline is an open channel blocker of the vanilloid receptor TRPV1. *Neuropharmacology* **47**, 273–285 (2004).

42. Xu, S. Z. *et al.* Generation of functional ion-channel tools by E3 targeting. *Nat. Biotechnol*. **23**, 1289–1293 (2005).

43. Zeng, X. H., Xia, X. M. & Lingle, C. J. Redox-sensitive extracellular gates formed by auxiliary β subunits of calcium-activated potassium channels. *Nat. Struct. Biol.* **10**, 448–454 (2003).

44. Tang, X. D. *et al.* Haem can bind to and inhibit mammalian calcium-dependent Slo1 BK channels. *Nature* **425**, 531–535 (2003).

45. Zeng, F. *et al.* Human TRPC5 channel activated by a multiplicity of signals in a single cell. *J. Physiol.* **559**, 739–750 (2004).

46. van Rossum, D. B., Patterson, R. L., Ma, H. T. & Gill, D. L. Ca^{2+} entry mediated by store depletion, S-nitrosylation, and TRPC3 channels. *J. Biol. Chem.* **275**, 28562–28568 (2000).

47. Thyagarajan, B. *et al*. Expression of Trp3 determines sensitivity of capacitative Ca^{2+} entry to nitric oxide and mitochondrial Ca^{2+} handling: evidence for a role of Trp3 as a subunit of capacitative Ca^{2+} entry channels. *J. Biol. Chem.* **276**, 48149–48158 (2001).

48. Koliwad, S. K., Kunze, D. L. & Elliott, S. J. Oxidant stress activates a non-selective cation channel responsible for membrane depolarization in calf vascular endothelial cells. *J. Physiol.* **491 (Pt 1)**, 1–12 (1996).

49. Zhang, N., Beuve, A. & Townes-Anderson, E. The nitric oxide-cGMP signaling pathway differentially regulates presynaptic structural plasticity in cone and rod cells. *J. Neurosci.* **25**, 2761–2770 (2005).

50. Freichel, M. *et al.* Lack of an endothelial store-operated Ca^{2+} current impairs agonist-dependent vasorelaxation in TRP4-/- mice. *Nat. Cell. Biol.* **3**, 121–127 (2001).

51. Okada, T. *et al.* Molecular and functional characterization of a novel mouse transient receptor potential protein homologue TRP7. Ca^{2+}-permeable cation channel that is constitutively activated and enhanced by stimulation of G protein-coupled receptor. *J. Biol. Chem.* **274**, 27359–27370 (1999).

52. Peier, A. M. *et al.* A heat-sensitive TRP channel expressed in keratinocytes. *Science* **296**, 2046–2049 (2002).

53. Strotmann, R., Harteneck, C., Nunnenmacher, K., Schultz, G. & Plant, T. D. OTRPC4, a nonselective cation channel that confers sensitivity to extracellular osmolarity. *Nat. Cell Biol.* **2**, 695–702 (2000).

54. Koch, W. J., Hawes, B. E., Inglese, J., Luttrell, L. M. & Lefkowitz, R. J. Cellular expression of the carboxyl terminus of a G protein-coupled receptor kinase attenuates $G_{\beta\gamma}$-mediated signaling. *J. Biol. Chem.* **269** 6193–6197 (1994).

55. Strübing, C., Krapivinsky, G., Krapivinsky, L., & Clapham, D. E. Formation of novel TRPC channels by complex subunit interactions in embryonic brain. *J. Biol. Chem.* **278** 39014–39019 (2003).

Chapter 2

Molecular characterization of TRPA1 channel activation by cysteine-reactive inflammatory mediators

Summary

TRPA1 is a member of the transient receptor potential (TRP) cation channel family, and is predominantly expressed in nociceptive neurons of dorsal root ganglia (DRG) and trigeminal ganglia. Activation of TRPA1 by environmental irritants such as mustard oil, allicin and acrolein causes acute pain. However, the endogenous ligands that directly activate TRPA1 remain elusive in inflammation. Here, we show that a variety of inflammatory mediators (15-deoxy-$\Delta^{12,14}$-prostaglandin J_2 (15d-PGJ_2), nitric oxide (NO), hydrogen peroxide (H_2O_2) and proton (H^+)) activate human TRPA1 heterologously expressed in HEK cells. These inflammatory mediators induced robust Ca^{2+} influx in a subset of mouse DRG neurons. The TRP channel blocker ruthenium red almost completely inhibited neuronal responses by 15d-PGJ_2 and NO, but partially suppressed responses to H_2O_2 and H^+. Functional characterization of site-directed cysteine mutants of TRPA1 in combination with labeling experiments using biotinylated 15d-PGJ_2 demonstrated that modifications of cytoplasmic N-terminal cysteines (Cys421 and Cys621) were responsible for the activation of TRPA1 by 15d-PGJ_2. In TRPA1 responses to other cysteine-reactive inflammatory mediators, such as NO and H_2O_2, the extents of impairment by respective cysteine mutations differed from those in TRPA1 responses to 15d-PGJ_2. Interestingly, the Cys421 mutation critically impaired the TRPA1 response to H^+ as well. Our findings suggest that TRPA1 channels are targeted by an array of inflammatory mediators to elicit inflammatory pain in the nervous system.

Introduction

Pain is initiated when noxious thermal, mechanical or chemical stimuli excite the peripheral terminals of specialized primary afferent neurons called nociceptors[1]. The activation of nociceptors generates depolarizing currents, which are conducted to the spinal cord along unmyelinated, slow conducting C fibers and more rapidly conducting Aδ primary sensory fibers. Through synaptic transfer, this sensory inflow then activates secondary sensory neurons in the dorsal horn of the spinal cord, which project into the cortex via a relay in the thalamus[1]. In this pain-sensing process, plasma membrane cation channels are responsible for Na^+ influx to induce depolarizing currents in the nociceptors. The influx of Ca^{2+} from the extracellular space is also mediated by plasma membrane Ca^{2+}-permeable cation channels, which act as sensors by translating cellular stimuli into electrical signals, namely membrane potential depolarization or chemical signals such as changes in intracellular Ca^{2+} concentration ($[Ca^{2+}]_i$)[2]. Increases in $[Ca^{2+}]_i$ play an important role in plastic changes in peripheral nociceptive terminals[3].

The *Drosophila melanogaster* transient receptor potential (TRP) protein and its homologs are putative six-transmembrane polypeptide subunits that assemble into tetramers to form cation-permeable ion channels. In mammalian systems, TRP channels comprise six related protein subfamilies[2]. They are activated by diverse stimuli, including receptor stimulation, heat, osmotic pressure and mechanical stress from the extracellular environment and from inside the cell[2]. Recently, we described activation of the TRPC and TRPV subfamilies by nitric oxide (NO)-mediated reversible covalent modification (nitrosylation) of cysteine residues[4]. More recently, channel activation by pungent compounds such as allyl isothiocyanate (AITC) and allicin via covalent modification of cysteine residues has been demonstrated for TRPA1, which is a member of the TRP ankyrin subfamily[5,6]. Thus, a group of TRP channels acts as sensors for thiol reactive compounds with diverse chemical structure via covalent modification of cysteine

residues.

TRPA1 plays an important role in modulating nociceptor excitability and neurogenic inflammation in the setting of tissue injury[7,8]. This channel is highly expressed by a subset of C-fiber nociceptors[9–11] and is activated by a number of environmental irritants that cause pain, including α,β-unsaturated aldehydes such as acrolein, as well as AITC[11] and allicin as described above[12]. Sensory neurons from TRPA1-deficient mice show greatly diminished responses to each of these compounds, demonstrating that TRPA1 is the primary molecular site through which they activate the pain pathway[7,8]. TRPA1 mediates neurogenic inflammatory responses of bradykinin that gates the channel indirectly through intracellular Ca^{2+} release or other consequences of phospholipase C activation[7,11,13]. However, the direct action of various endogenous substances produced during inflammatory processes on TRPA1 is poorly understood.

Prostaglandins (PGs) are a subfamily of eicosanoids that act as important inflammatory mediators and reproduce the major signs of inflammation, including augmented pain[14]. Among the PGs, the cyclopentenone PG 15-deoxy-$\Delta^{12,14}$-prostaglandin J_2 (15d-PGJ_2), a product of the cyclooxygenase pathway, is formed through the spontaneous dehydration of PGD_2 (ref. 15). It has been shown that 15d-PGJ_2 is produced in carrageenan-induced pleurisy in rats[16] and is detected in the anterior horn cells of sporadic amyotrophic lateral sclerosis patients[17]. As 15d-PGJ_2 has highly reactive structures that contain α,β-unsaturated aldehyde moieties, it can covalently bind to cysteine sulfhydryl groups via a Michael addition reaction[18]. These moieties covalently modify critical proteins in multiple pathways, such as IκB kinase (IKK) in inhibition of IKK activity, and thioredoxin in potentiation of apoptosis in neuronal cells[18–20].

In addition to 15d-PGJ_2, tissue damage and inflammation produce an array of inflammatory mediators, such as ATP, bradykinin, proton (H^+), NO, hydrogen peroxide

(H_2O_2) and cytokines that can excite or sensitize nociceptors to elicit pain at the site of injury. NO and H_2O_2 can also modify cysteine sulfhydryl groups via nitrosylation and oxidation, respectively[21,22]. NO is a short-lived mediator whose release is strongly potentiated mainly by inducible NO synthase (NOS) in inflammation[23,24]. The non-selective NOS inhibitor, N^{ω}-nitro-L-arginine methyl ester, reduces thermal hyperalgesia in inflammatory pain models[25], and intracutaneous injections of NO precursors evoke pain in humans[26], indicating a role of NO in inflammatory pain. Likewise, it is known that a large amount of H_2O_2 exist at inflamed sites[27]. The activation of inflammatory cells, such as macrophages, neutrophils and eosinophils that are recruited to inflamed sites, generates reactive oxygen species (ROS) in response to a sufficient level of secretagogue stimulus. $O_2^{\bullet-}$ released from inflammatory cells is rapidly converted to H_2O_2 by superoxide dismutase[27,28]. Moreover, $O_2^{\bullet-}$ is known to activate a group of cardiac sympathetic Aδ and C-fiber afferents during myocardial ischemia and reperfusion, and may play an important role in mediating cardiovascular sympathetic reflex responses and/or pain transmission[29]. Notably, involvements of H_2O_2 and/or NO in inflammatory pain are consistent with our previous finding that TRPV channels are susceptible to activation by either of these substances[4].

Here, we provide evidence that 15d-PGJ_2 and inflammatory mediators activate TRPA1 via cysteine modification in heterologous and native systems. Site-directed cysteine mutagenesis combined with biochemical and physiological assays indicates that covalent binding of 15d-PGJ_2 to cytoplasmic N-terminal cysteines of the TRPA1 channel is involved in TRPA1 activation. In TRPA1 activation by other inflammatory mediators, NO, H_2O_2 and H^+, N-terminus cysteines also play important roles, but relative criticality of each cysteine is different from that in 15d-PGJ_2-induced TRPA1 activation. These findings suggest that TRPA1 channels are targeted by an array of cysteine-reactive inflammatory mediators to elicit inflammatory pain in the nervous system.

Results

The inflammatory mediator 15d-PGJ_2 activates the TRPA1 channel.

To examine whether 15d-PGJ_2 (Fig. 1a) serves as a TRPA1 activator, we used live-cell $[Ca^{2+}]_i$ imaging to measure the effect of 15d-PGJ_2 on HEK cells transfected with human TRPA1 cDNA. Functional expression of TRPA1 was confirmed by $[Ca^{2+}]_i$ increases and ionic currents in response to AITC, and by western blotting analysis (data not shown)[11]. Indeed, the 15d-PGJ_2-elicited $[Ca^{2+}]_i$ increases involved an initial rapid phase, followed by a sustained phase, in a concentration-dependent manner (half-maximal effective concentration (EC_{50}) value was 1.2 μM) (Fig. 1b). The 15d-PGJ_2-evoked $[Ca^{2+}]_i$ responses were mainly attributable to Ca^{2+} entry through the TRPA1 channel, as 15d-PGJ_2 evoked only marginal $[Ca^{2+}]_i$ increases in TRPA1-expressing HEK cells when extracellular Ca^{2+} was omitted, and in vector-transfected control cells (Fig. 1c).

We next used the whole-cell mode of patch clamp recording methods to measure 15d-PGJ_2-evoked ionic currents in TRPA1-expressing HEK cells. Consistent with our hypothesis that 15d-PGJ_2 activates TRPA1, we observed that 30 μM 15d-PGJ_2 evoked inward currents in TRPA1-expressing HEK cells with peak current densities of 22.5 ± 3.7 pA/pF, but failed to detect any significant effects on current levels or the current-voltage (*I-V*) relationship in vector-transfected control cells, at a holding potential of –60 mV (Fig. 1d). The *I-V* relationship of the 15d-PGJ_2-activated TRPA1 currents corresponded well to those activated by 100 μM AITC (Fig. 1e). In contrast to TRPA1-mediated $[Ca^{2+}]_i$ responses in $[Ca^{2+}]_i$ imaging, TRPA1 currents showed rapid run-down. The previous report by Karashima et al demonstrates that desensitization of AITC-activated TRPA1 currents is delayed by phosphatidylinositol 4,5-biphosphate (PIP_2)[30]. Therefore, it is possible that PIP_2 is diluted by intracellular dialysis of patch pipette solution in whole-cell mode in contrast to $[Ca^{2+}]_i$ imaging carried out in intact cell configuration that retains intracellular PIP_2 levels.

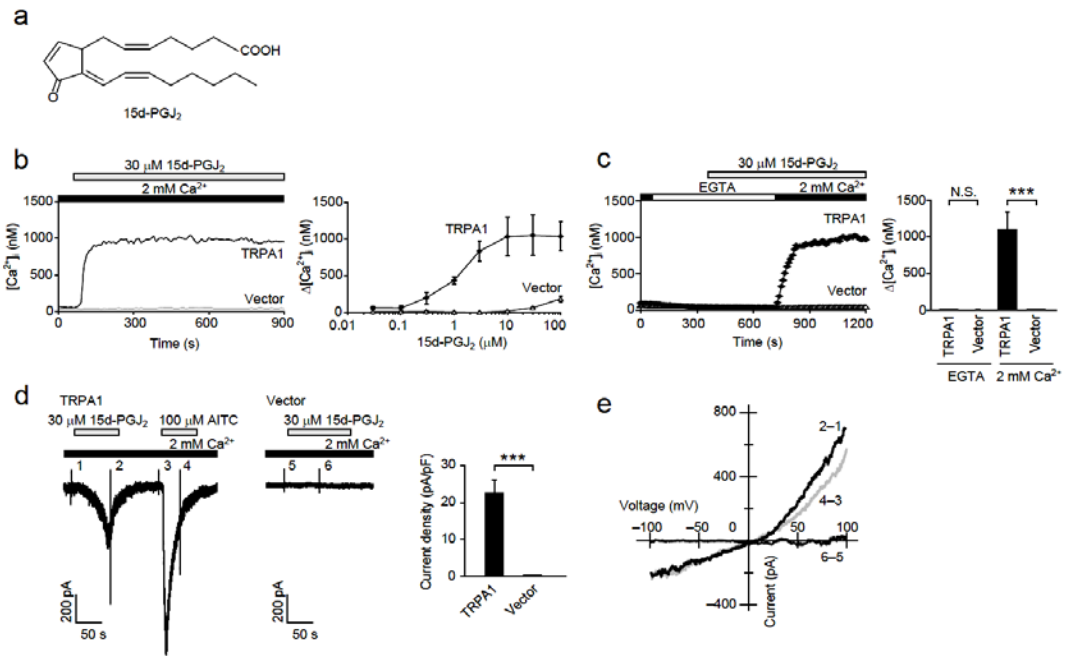

Figure 1. 15d-PGJ$_2$ activates TRPA1 channel. **a,** Chemical structure of 15d-PGJ$_2$. **b, c,** Ca^{2+} entry induced by 15d-PGJ$_2$ in TRPA1-expressing HEK cells. In **b**, representative time courses (left panel) and dose response relationships of maximal $[Ca^{2+}]_i$ increases (right panel) in HEK cells transfected with TRPA1 or vector are shown. In **c**, averaged time courses of $[Ca^{2+}]_i$ changes (left panel) and maximum $[Ca^{2+}]_i$ rises induced by 30 μM 15d-PGJ$_2$ in Ca^{2+}-free, 0.5 mM EGTA- or 2 mM Ca^{2+}-containing solution (right panel) are shown. **d,** Representative current traces in HEK cells transfected with TRPA1 or control vector (left and middle panels). TRPA1 channel currents activated by 30 μM 15d-PGJ$_2$ and subsequently by 100 μM AITC at holding potential –60 mV are shown. Peak current density induced by 30 μM 15d-PGJ$_2$ in HEK cells transfected with TRPA1 or control vector (right panel) (n = 11–15). **e,** *I-V* relationships assessed by 180 ms voltage ramps of ionic currents induced by 15d-PGJ$_2$ (2–1 in **d**) and AITC (4–3) in TRPA1-expressing cells, and of ionic currents induced by 15d-PGJ$_2$ (6–5) in control cells. Data points are mean ± s.e.m. $^{***}P < 0.001$ and N.S., not significant ($P > 0.05$).

Covalent modification of TRPA1-channels by 15d-PGJ$_2$.

The α,β-unsaturated carbonyl group in the cyclopentenone ring of 15d-PGJ$_2$ is susceptible to nucleophilic addition reaction (Michael addition) with thiols[31,32]. Moreover, recent studies have shown that environmental irritants, such as AITC and acrolein, activate TRPA1 through covalent modification of key cysteines within the N-terminal cytoplasmic domain of the channel[5,6]. Therefore, it is likely that 15d-PGJ$_2$-induced activation of TRPA1 is due to the covalent modification of TRPA1-channel protein by 15d-PGJ$_2$. In

support of this idea, formation of the 15d-PGJ_2-TRPA1 adduct was identified using a biotinylated derivative of 15d-PGJ_2 (Fig. 2a)[18]. After exposure of HEK cells expressing green fluorescent protein-tagged TRPA1 (TRPA1-GFP) to biotinylated 15d-PGJ_2 (5 μM), the cell lysate was incubated with avidin-conjugated beads. Proteins bound to the beads were subjected to western blotting analysis with anti-GFP antibody. As demonstrated in Figure 2b, TRPA1-GFP was detected in the proteins incorporating biotinylated 15d-PGJ_2. These results suggest that 15d-PGJ_2 is covalently attached to TRPA1 channel.

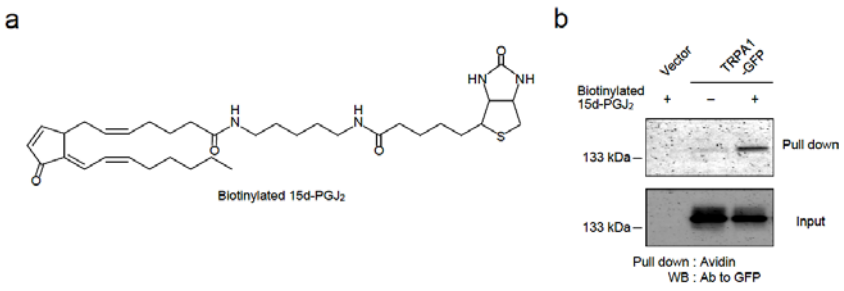

Figure 2. Covalent binding of biotinylated 15d-PGJ_2 with TRPA1 channels. a, Chemical structure of biotinylated 15d-PGJ_2. **b,** Detection of TRPA1-GFP among proteins in TRPA1-GFP-expressing HEK cells after incorporation of 5 μM biotinylated 15d-PGJ_2 by western blotting analysis (WB) using antibody to GFP. WB of total cell lysates indicates comparable protein expression of TRPA1 constructs (Input).

Inflammatory mediators NO, H_2O_2 and H^+ activate the TRPA1 channel.

In addition to 15d-PGJ_2, NO and H_2O_2 are also known to act as potent inflammatory mediators[23,28], and to modify free sulfhydryl cysteine residues through nitrosylation and oxidization, respectively[21,22]. As demonstrated in Figure 3, the NO donor *S*-nitroso-*N*-acetyl-DL-penicillamine (SNAP) and H_2O_2 elicited sustained $[Ca^{2+}]_i$ increases with time-lag after application in TRPA1-expressing cells in a concentration-dependent manner (the EC_{50} values were 8.6 μM and 23 μM, respectively) (Fig. 3a, b). NO- and H_2O_2-evoked $[Ca^{2+}]_i$ responses were attributable mainly to Ca^{2+} entry through the TRPA1 channel, as NO and H_2O_2 evoked only marginal $[Ca^{2+}]_i$ increase in TRPA1-expressing HEK cells when extracellular Ca^{2+} was omitted, and in vector-transfected control cells (Fig. 3d, e).

During inflammation, extracellular pH reaches 6 (ref. 33), and acidosis is an

important source of pain[34,35]. It is also known that native TRPA1 is expressed in small-diameter neurons of the trigeminal and dorsal root ganglia (DRG)[9,36], which integrate multiple pain-inducing stimuli, including acidic extracellular pH[37–39]. Notably, we found that H^+ elicited sustained $[Ca^{2+}]_i$ increases with time-lag after application in TRPA1-expressing cells in a dose-dependent manner (the EC_{50} value was pH 6.5) (Fig. 3c). The H^+-evoked $[Ca^{2+}]_i$ responses were attributable mainly to Ca^{2+} entry through the TRPA1 channel, as H^+ evoked only marginal $[Ca^{2+}]_i$ increases in TRPA1-expressing HEK cells when extracellular Ca^{2+} was omitted, and in vector-transfected control cells (Fig. 3f); indicating that H^+ also activates the TRPA1 channel. Therefore, our comprehensive examination of inflammatory mediators suggests that TRPA1 is activated in inflammatory conditions.

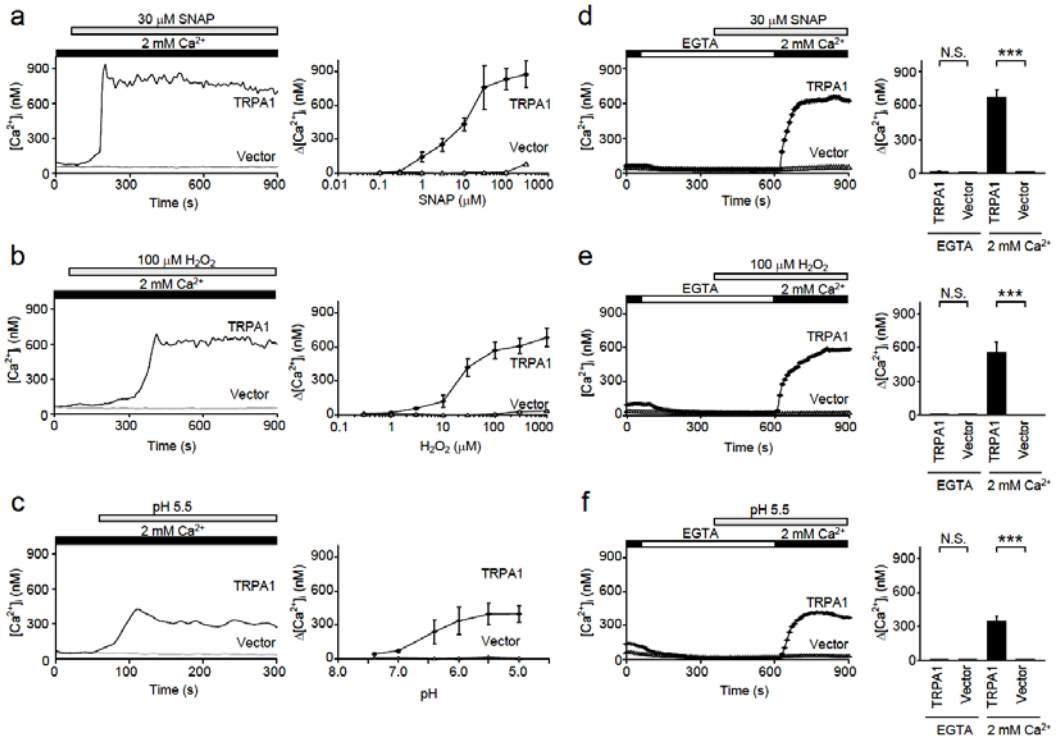

Figure 3. NO, H_2O_2 and H^+ activate TRPA1 channels. **a–c,** $[Ca^{2+}]_i$ increases induced by SNAP (**a**), H_2O_2 (**b**) and H^+ (**c**) in the presence of 2 mM extracellular Ca^{2+}. Representative time courses (left panels) and dose response relationships of maximal $[Ca^{2+}]_i$ increases (right panels) are shown. **d–f,** Averaged time courses of $[Ca^{2+}]_i$ changes (left panels) and maximum $[Ca^{2+}]_i$ increases induced by SNAP (**d**), H_2O_2 (**e**) and H^+ (**f**) in Ca^{2+}-free or 2 mM Ca^{2+}-containing external solution (right panels). Data points are mean ± s.e.m. $^{***}P < 0.001$ and N.S., not significant ($P > 0.05$).

15d-PGJ_2, NO and H_2O_2 activate the TRPA1 channel via oxidative cysteine modification.

We next examined whether 15d-PGJ_2, NO, H_2O_2 and H^+ activate the TRPA1 channel via oxidative sulfhydryl modification, using the cell-permeable reducing agent dithiothreitol (DTT), which reverses cysteine disulfide formation and nitrosylation or oxidization of cysteine sulfhydryls but not alkylation via Michael addition[4,6,40]. Recent study has shown that disulphide-forming activator (2-aminoethyl)methanethiosulphonate (MTSEA)- and Michael addition activator supercinnamaldehyde (SC)-induced TRPA1 responses are not significantly diminished by wash out, whereas MTSEA-induced TRPA1 responses but not SC-induced TRPA1 responses were significantly diminished by DTT[6]. 15d-PGJ_2-, SNAP- or H_2O_2-induced TRPA1 responses were not significantly diminished by wash out, whereas SNAP- or H_2O_2-induced TRPA1 responses but not 15d-PGJ_2-induced TRPA1 responses were significantly diminished by DTT (5 mM) (Fig. 4a–c). This result supports the notion that NO, H_2O_2 and 15d-PGJ_2 form nitrosylated, oxidized, and alkylated thiols, respectively, on cysteine residues in eliciting TRPA1-mediated responses. In contrast, H^+-induced TRPA1 responses were significantly diminished by wash out but not by addition of DTT to H^+-containing solution (Fig. 4d, e). This result may suggest that H^+ activates TRPA1 through a mechanism independent of oxidative cysteine modification. TRPA1 responses evoked by inflammatory mediators were sensitive to suppression by ruthenium red, a blocker of TRP channels including TRPA1 (Fig. 4f–i).

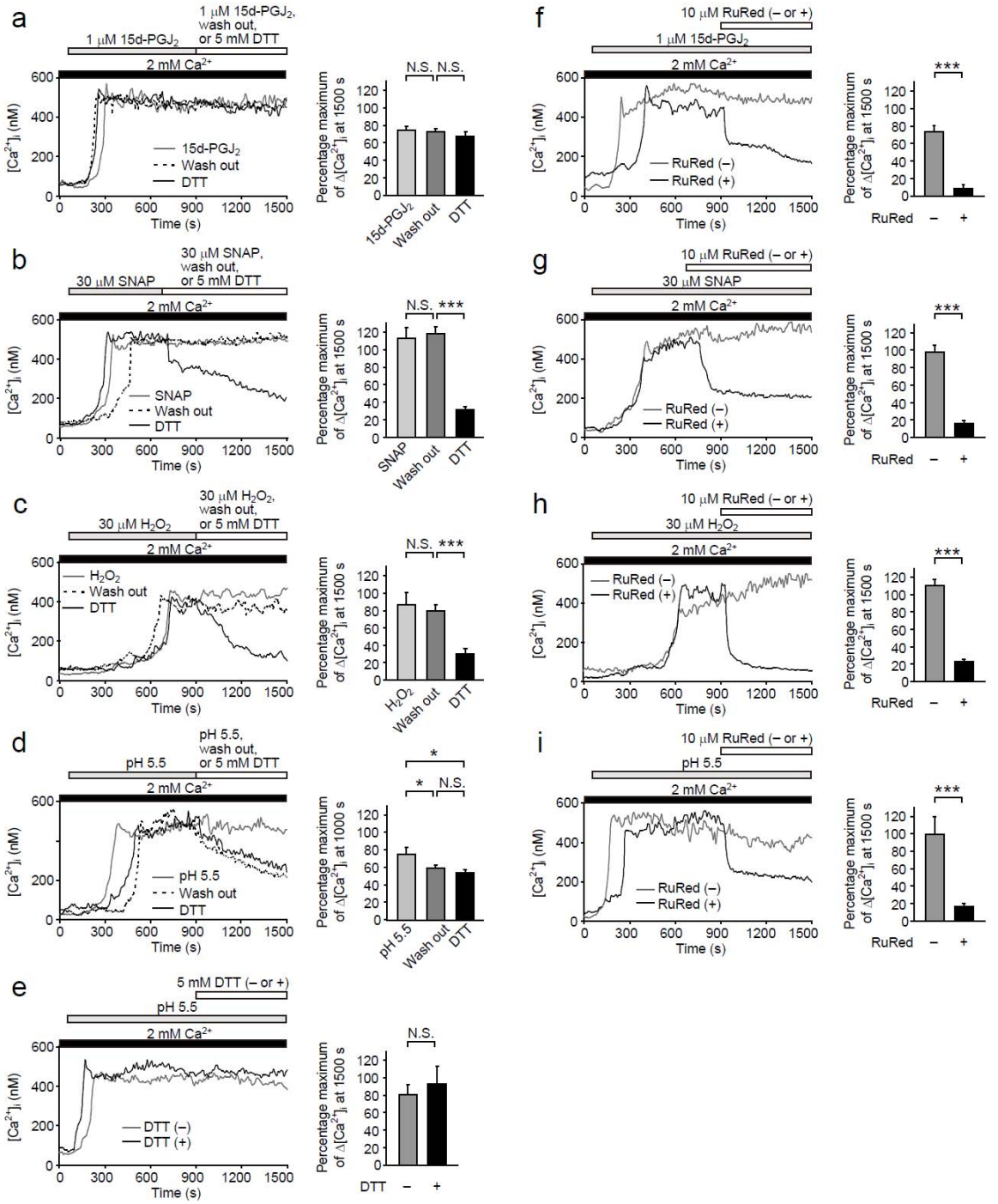

Figure 4. Reducing agent DTT reverses activation of TRPA1 by NO and H_2O_2. **a–e,** DTT inhibits TRPA1 responses to SNAP (**b**) and H_2O_2 (**c**), but not that to 15d-PGJ_2 (**a**) and H^+ (**d, e**) in HEK cells. **f–i,** 15d-PGJ_2-, NO-, H_2O_2- or H^+-induced $[Ca^{2+}]_i$ increases are blocked by the TRP channel blocker ruthenium red (RuRed). Representative time courses (left panels) and percentages of $[Ca^{2+}]_i$ increases (right panels) at 1500 s (**a–c, e–i**) or 1000 s (**d**) relative to maximal rises are shown. Data points are mean ± s.e.m. $^{*}P < 0.05$, $^{***}P < 0.001$, and N.S., not significant ($P > 0.05$).

15d-PGJ_2, NO, H_2O_2 and H^+ activate a subset of mouse DRG neurons.

We next examined whether 15d-PGJ_2, NO, H_2O_2 and H^+ induce responses in a subset of primary sensory neurons and tested whether TRPA1 contributes these responses. We used $[Ca^{2+}]_i$ imaging to measure the effect of 15d-PGJ_2, NO, H_2O_2 and H^+ on cultured neurons prepared from DRG of mice. Identification of neurons was confirmed by $[Ca^{2+}]_i$ responses to 60 mM potassium chloride (KCl) that activates voltage-gated Ca^{2+} channels. Indeed, we observed robust $[Ca^{2+}]_i$ increases after application of 1 μM 15d-PGJ_2, 30 μM SNAP, 30 μM H_2O_2 or H^+ (pH 5.5) in 33.8%, 32.4%, 58.9% or 16.9% of KCl-responsive cells, respectively (Fig. 5). Ruthenium red (10 μM) almost completely blocked $[Ca^{2+}]_i$ responses to 1 μM 15d-PGJ_2 and 30 μM SNAP (Fig. 5a, b). $[Ca^{2+}]_i$ responses to 30 μM H_2O_2 were not diminished by ruthenium red in 37.5% of H_2O_2-responsive neurons, the rest of which only showed partial blockade by the agent (Fig. 5c). Since protons (pH below 6) are known to activate TRPV1 expressed by primary afferent nociceptors[41], we tested the effect of 10 μM capsazepine, a blocker of TRPV1, on responses to H^+ (Fig. 5d). We observed two types of $[Ca^{2+}]_i$ responses to H^+ (pH 5.5) in cultured neurons: sustained $[Ca^{2+}]_i$ increases and transient $[Ca^{2+}]_i$ increases (75.0 and 25.0%, respectively, of H^+-responsive neurons). Although H^+-induced sustained $[Ca^{2+}]_i$ increases were partially diminished by capsazepine, and that the residual capsazepine-insensitive $[Ca^{2+}]_i$ responses was further diminished by ruthenium red (Fig. 5d, upper panel), transient $[Ca^{2+}]_i$ increases were insensitive to the agents (Fig. 5d, lower panel). Only 67.4% and 66.7% of total H^+-responsive neurons were sensitive to capsazepine and ruthenium red, respectively. These results may suggest that 15d-PGJ_2, NO, H_2O_2 and H^+ activate native TRPA1 in sensory neurons of DRG, and that these inflammatory mediators, especially H^+, additionally activate TRPV1 and other ion channels and receptors in DRG neurons.

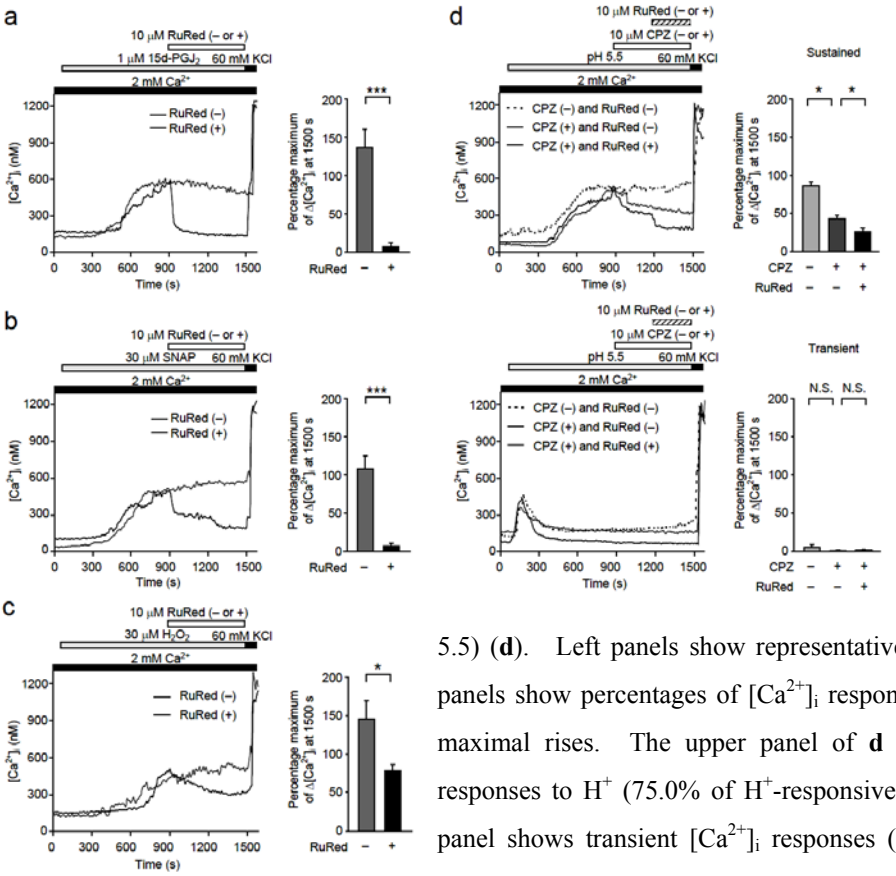

Figure 5. 15d-PGJ$_2$, NO, H_2O_2 and H^+ induce $[Ca^{2+}]_i$ responses in mouse DRG neurons. a–d, RuRed almost completely blocks responses by 1 μM 15d-PGJ$_2$ (**a**) and 30 μM SNAP (**b**), whereas it partially blocks responses to 30 μM H_2O_2 (**c**) and H^+ (pH 5.5) (**d**). Left panels show representative time courses and right panels show percentages of $[Ca^{2+}]_i$ responses at 1500 s relative to maximal rises. The upper panel of **d** shows sustained $[Ca^{2+}]_i$ responses to H^+ (75.0% of H^+-responsive neurons) and the lower panel shows transient $[Ca^{2+}]_i$ responses (25.0% of H^+-responsive neurons). Data points are mean ± s.e.m. $^*P < 0.05$, $^{***}P < 0.001$, and N.S., not significant ($P > 0.05$).

Identification of the modification site-cysteines in TRPA1.

Recently, the sites for covalent cysteine modification of TRPA1 were determined[5,6]. Using site-directed mutagenesis, Hinman et al identified three neighboring cysteines within the cytoplasmic N-terminus on human TRPA1 (Cys621, Cys641 and Cys665) whose simultaneous mutation negates the channel-activating effects of several cysteine-modifying reagents[5]. Using mass spectrometry, Macpherson et al revealed three cysteines on mouse TRPA1 (Cys415, Cys422 and Cys622), which are conserved in the human homolog (Cys414, Cys421 and Cys621), as the target sites for electrophilic agonists[6]. We therefore subjected these cysteine residues (Fig. 6a; Cys414, Cys421, Cys621, Cys641 and Cys665) in human TRPA1 for replacement of serine, and examined the mutants for their responses to 15d-PGJ$_2$, NO, H_2O_2 and H^+ using $[Ca^{2+}]_i$ imaging (Fig.

6). Mutations C414S, C421S and C621S elicited significant suppression in TRPA1 responses to 15d-PGJ_2 (1 and 30 μM) (Fig. 6b). Interestingly, mutations C414S, C421S, C641S and C665S induced significant suppression in responses to 3 μM SNAP, while only C414S and C421S induced significant suppression in responses to 100 μM SNAP (Fig. 6c). The $[Ca^{2+}]_i$ responses evoked by 30 μM H_2O_2 were also significantly suppressed by C414S, C421S, C641S and C665S, while only C414S and C421S induced significant suppression in responses to 100 μM H_2O_2 (Fig. 6d). The $[Ca^{2+}]_i$ responses evoked by H^+ (pH 5.5) were significantly suppressed by C414S and C421S (Fig. 6e). Constructs with these mutations, except for C414S, retained sensitivity to 2-aminoethyl diphenylborinate (2-APB), which activates TRPA1 through a mechanism distinct from cysteine modification[5]. The mutation C414S abolished responses to all tested stimuli (Fig. 6f) including icilin (data not shown), suggesting that this substitution had deleterious effects on channel function at large. Thus, Cys421 is likely a common site for oxidative covalent modifications of TRPA1 and also an important site for H^+-induced TRPA1 activation, in contrast to the specific roles played by Cys621 in 15d-PGJ_2-induced activation and by Cys641 and Cys665 in NO- or H_2O_2-induced activation of TRPA1. We also monitored the effects of the mutations on 15d-PGJ_2 binding to TRPA1-GFP proteins. Incorporation of biotinylated 15d-PGJ_2 into TRPA1 channel was significantly suppressed by C621S and less extensively by C421S, but not by C414S (Fig. 6g). These results support the above functional data that Cys621 plays a specific role in 15d-PGJ_2-induced activation of TRPA1, while Cys421 is the common site for activation of the TRPA1 channel.

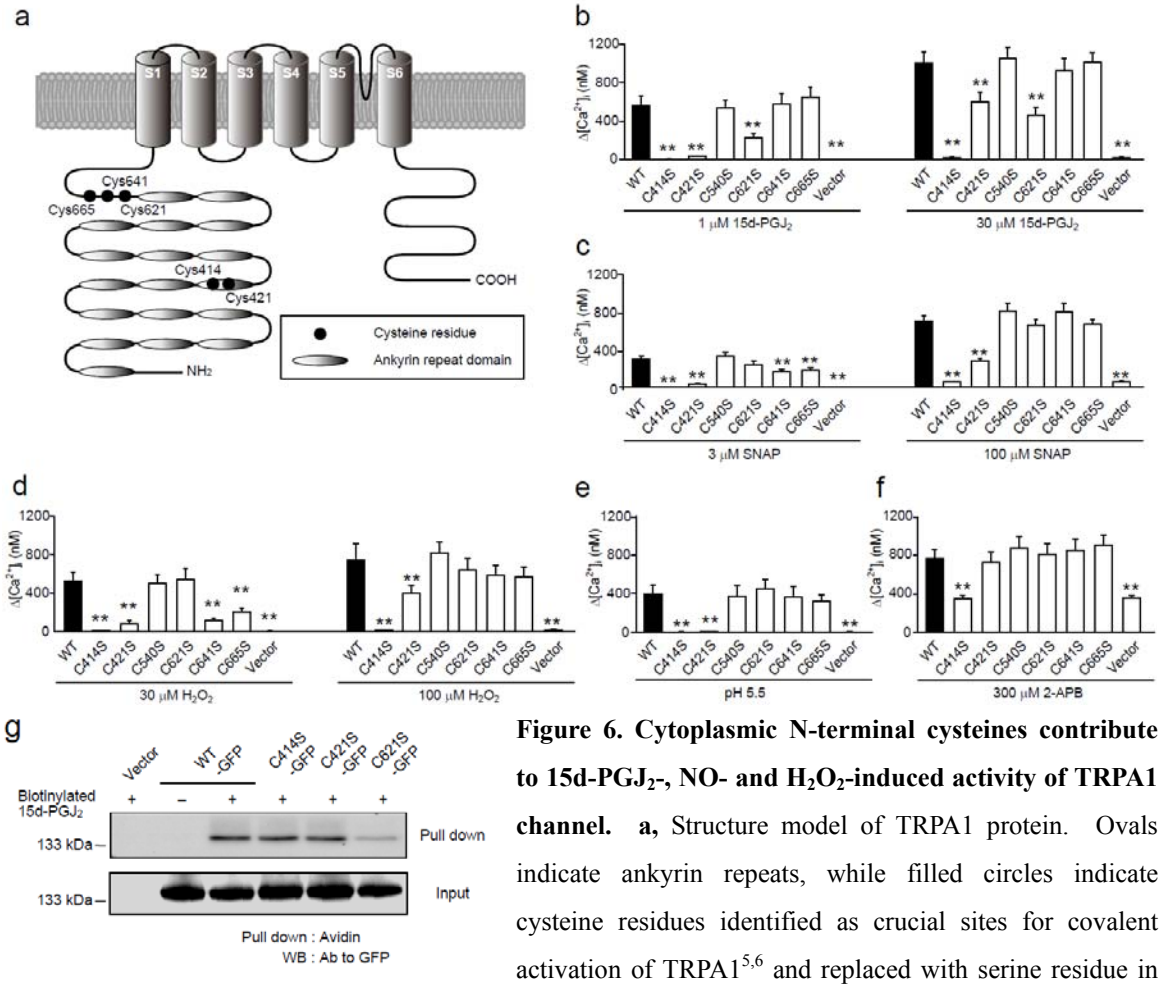

Figure 6. Cytoplasmic N-terminal cysteines contribute to 15d-PGJ$_2$-, NO- and H_2O_2-induced activity of TRPA1 channel. **a,** Structure model of TRPA1 protein. Ovals indicate ankyrin repeats, while filled circles indicate cysteine residues identified as crucial sites for covalent activation of TRPA1[5,6] and replaced with serine residue in the mutagenesis study: C414S, C421S, C621S, C641S and C665S. As a positive control for functional TRPA1, we also subject Cys540 to replacement with serine, that does not affect AITC and acrolein sensitivity.[5,6] **b–f,** Maximum $[Ca^{2+}]_i$ increases induced by 15d-PGJ$_2$ (**b**), SNAP (**c**), H_2O_2 (**d**), H^+ (**e**) and 2-APB (**f**) in HEK cells expressing TRPA1 mutants. Data points are mean ± s.e.m. $^{**}P < 0.001$, compared to WT. **g,** Effects of mutations C414S, C421S and C621S on biotinylated 15d-PGJ$_2$ incorporation of TRPA1. WB of total cell lysates indicates comparable protein expression of TRPA1 constructs (Input).

Discussion

Recent studies have shown that AITC, allicin and other exogenous irritants with electrophilic groups directly activate TRPA1[5,6]. However, regulation of TRPA1 by endogenous substances is poorly understood. Our studies address this issue by demonstrating agonist actions on TRPA1 of 15d-PGJ$_2$, NO, H_2O_2 and H^+, which play important roles in inflammation. By targeting TRPA1 at the cytoplasmic N-terminal tail,

15d-PGJ_2, NO, H_2O_2 and H^+ resemble environmental irritants, such as AITC and allicin[5,6].

The biological activities of PGs are mostly mediated by specific G protein-coupled receptors. However, information concerning specific transmembrane receptors for 15d-PGJ_2 is very limited in contrast to other PGs[42]. Recent studies indicated that 15d-PGJ_2 has agonist activity on prostaglandin D_2 receptors (DP_2), exclusively expressed in Th2 cells, T cytotoxic cells, eosinophils and basophils[43]. In eosinophils, it was shown that 15d-PGJ_2 activated DP_2 and elicited Ca^{2+} influx with a potency nearly equal to that of prostaglandin D_2, the principal ligand for the receptor[44–46]. However, our evidence supports that this mechanism is unlikely to contribute to the activation of TRPA1 by 15d-PGJ_2. Firstly, DP_2 is expressed in Th2 cells, T cytotoxic cells, eosinophils and basophils[43] but not in HEK cells, which we use in the present study, and in sensory neurons, where TRPA1 is expressed predominantly *in vivo*. Secondly, our labeling assay demonstrates incorporation of 15d-PGJ_2 in TRPA1 channel (Fig. 2b). Thirdly, our site-directed mutagenesis studies reveal that Cys421 and Cys621 are involved in 15d-PGJ_2 induced activity of TRPA1 and its incorporation into TRPA1 (Fig. 6b, g). Thus, it is highly likely that TRPA1 is activated by 15d-PGJ_2 via a direct protein modification.

It is not unreasonable to assume that 15d-PGJ_2 is membrane-impermeable, considering its carboxylate group. However, 15d-PGJ_2 seemingly exerts its effects intracellularly through nuclear receptors as well as other proteins, whose function is modified by covalent interaction with 15d-PGJ_2[18–20]. Although the exact mechanism of 15d-PGJ_2 entry into cells is unknown, 15d-PGJ_2 may enter via an active transport system as described previously for the cyclopentenone PGs[47].

Redox-sensitive cysteine residues have been implicated in activation or modulation of ion channels, such as TRPC5[4], cyclic nucleotide-gated channels[48], NMDA-type

glutamate receptor channels[49] or skeletal muscle ryanodine receptors[50]. In these channels, oxidative modification of cysteines by NO or H_2O_2 has been proposed to serve as a common pathway of channel activation or modulation[21]. Our site-directed mutagenesis and pharmacological experiments support the notion that Cys421, Cys 641 and Cys665 are involved in modification by NO and H_2O_2 via nitrosylation and oxidation, respectively (Figs. 4b, c and 6c, d), which may suggest that activation of TRPA1 by NO and H_2O_2 is mediated through direct mechanisms as activation by 15d-PGJ_2. However, it is well known that indirect, modification-independent pathways are responsible for activation of some other channels by NO or H_2O_2. Indeed, the synthesis of NO was classically related to the activation of the enzyme guanylate cyclase, after binding to its heme group, leading to an increase in the rate of conversion of GTP to cGMP and an activation of protein kinase G (PKG)[51]. In the heart, NO activates the ATP-dependent K^+ channel (K_{ATP})[52] and the voltage-dependent L-type Ca^{2+} channel through a cGMP/PKG-dependent mechanism[53]. H_2O_2 activates the TRPM2 channel indirectly via the release of ADP-ribose from mitochondria[54]. Therefore, we cannot exclude the possibility that NO and H_2O_2 activate TRPA1 through indirect mechanisms.

In ryanodine receptor 1 (RyR1), which is a redox-sensitive Ca^{2+} channel, only 12 of the 100 cysteine residues are redox-modified ("hyper-reactive" cysteines). Of the 12 hyper-reactive cysteines of RyR1, two are *S*-nitrosylated but not *S*-glutathionylated, whereas for a further two, the reverse applies[55]. In Kelch-like ECH-associated protein 1 (Keap1), which is thought to be a molecular sensor for intracellular redox changes, different cysteine residues have been reported to display different preferences for alkylating reagents[56–58]. Human TRPA1 protein harbors 29 cysteine residues. Our characterization of site-directed cysteine mutants indicates that the sites of action of 15d-PGJ_2 are partly different from those of NO and H_2O_2 (Fig. 6b–d). This characteristic can be attributed to a difference in mechanisms underlying modification of

free sulfhydryl groups of cysteine residues in TRPA1 proteins between 15d-PGJ_2 and NO or H_2O_2: 15d-PGJ_2 modifies sulfhydryl groups through the Michael addition reaction, while NO or H_2O_2 modifies sulfhydryl groups through the redox reaction. As shown here, mutations C421S, C641S and C665S significantly suppress TRPA1 responses to both 3 μM SNAP and 30 μM H_2O_2 (C414S probably has deleterious effects on channel function at large) (Fig. 6c, d, f). Interestingly, however, TRPA1 mutants C641S and C665S retain sensitivity to SNAP and H_2O_2 at relatively higher concentrations (both 100 μM), while C421S displays a weakened but significant sensitivity (Fig. 6 c, d, f). These results suggest that Cys421, Cys641 and Cys665 are primary targets for NO and H_2O_2, but these compounds may additionally act on other residues. Interestingly, similar partial disruption by the triple TRPA1 mutation has been reported for the TRPA1 response to AITC[5].

Protons are capable of modulating the activity of a number of receptors and ion channels, such as TRPV1 and acid-sensing ion channels (ASICs), expressed by primary afferent nociceptors. Our result suggests that in addition to TRPV1 and ASICs, TRPA1 can also act as a sensor for decreases in extracellular pH with a dynamic range between 5 and 7 (Fig. 3c, f), which corresponds well with the pH range of local acidosis attained during most forms of tissue injury[33]. Recent studies have shown that an extracellular glutamate residue in the region linking the fifth transmembrane domain with the putative pore-forming region of the channel is the key regulatory site for the proton-induced potentiation of TRPC4, TRPC5 and TRPV1 activity[59,60]. Although we did not investigate the mechanism by which H^+ activates TRPA1 in this study, it is possible that the same extracellular glutamate residue plays an important role in H^+-induced activation of TRPA1. Alternatively, cysteine residues such as Cys421 can be deprotonated by nearby basic residues to form thiolate anion in resting states and protonated by acidic pH in activated states. This is a likely possibility, as thiolate anion exerts nucleophilic

attack on 15d-PGJ_2, NO and H_2O_2. Indeed, according to the structural model by Gaudet for TRPA1, Cys421 is spatially located close to the basic residue His418 on the same side of an α helix[61]. Importantly, the resistance to DTT addition but sensitivity to wash out suggests that oxidative cysteine modification is not involved in H^+-induced TRPA1 activation (Fig. 4d, e). It is also important to note a possibility that mechanisms other than direct amino acid protonation of TRPA1 proteins are involved in the H^+-induced activation as suggested in NO- or H_2O_2-induced activation (see above).

Our studies using cultured DRG neurons have revealed that sensory neurons are responsive to 15d-PGJ_2, NO, H_2O_2 and H^+ (Fig. 5). The TRP channel blocker ruthenium red almost completely blocked responses to 1 μM 15d-PGJ_2 and 30 μM SNAP, whereas it partially blocked responses to 30 μM H_2O_2 and H^+ (pH 5.5) only in portions of responsive cells (62.5 and 66.7 % for H_2O_2 and H^+, respectively). Based on these data, we assume that TRPA1 forms an important but not sole site for the action of 15d-PGJ_2, NO, H_2O_2 and H^+ in nociceptive sensory neurons. Indeed, our previous studies have shown that TRPV and TRPM2 channels are susceptible to activation by NO and H_2O_2 (refs. 4, 45). The ability of H^+ to directly activate nociceptors has been classically demonstrated in dissociated sensory neurons[62]. Although the repertoire of ion channels responsible for H^+ responsiveness is not fully known, TRPV1 and ASICs are believed to be important constituents. In heterologous expression systems, it has been reported TRPV1 generates a sustained cationic current in response to a pH below 6 (ref. 41), whereas ASICs generate characteristic transient, rapidly inactivating currents in response to a pH below 7 (ref. 63). Interestingly, we observed two types of $[Ca^{2+}]_i$ responses to H^+ (pH 5.5) in cultured neurons: sustained $[Ca^{2+}]_i$ increases comprised of capsazepine-sensitive and capsazepine-insensitive, ruthenium red-sensitive components (Fig. 5d, upper panel), and transient $[Ca^{2+}]_i$ increases (Fig. 5d, lower panel). These results suggest that native TRPA1 makes an important contribution to H^+-induced responses of DRG neurons.

At inflamed sites, a large amount of ROS, reactive nitrogen species (RNS), and reactive carbonyl species (RCS) are produced mainly by immunocytes. Classically, ROS and RCS were considered nonspecific toxins that cause random damage to cellular components including membrane lipids, DNA and proteins[27]; however, recently, they are believed to be signal-transduction molecules[64]. Sensitization of nociceptors to elicit pain sensation at inflamed sites can be regulated by these reactive species. In this scenario, a variety of reactive electrophiles commonly produced during inflammatory processes may contribute to nociception by directly activating TRPA1 at local sites of inflammation. This novel nociceptive and inflammatory pathway potentially represents an important target for the development of analgesic and anti-inflammatory drugs effective for treatments for a variety of tissue injuries and degenerative conditions that promote inflammation and chronic pain.

During preparation of this manuscript, other studies reported activation of TRPA1 by 15d-PGJ_2 (refs. 65–67), H_2O_2 (refs. 67–69) and NO[69]. These results are generally in agreement with our data. However, as discussed above, our paper represents the first study that reveals the direct action of 15d-PGJ_2 using the biotinylated analogue and the agonistic effect of H^+ on TRPA1. It must be also noted that our comprehensive characterization of mutants suggests that relative importance of each candidate cysteine action site varies among inflammatory mediators including H^+.

Methods

Reagents. Chemicals and drugs were obtained from the following sources: 15-deoxy-$\Delta^{12,14}$-prostaglandin J_2 (Cayman Chemical, Ann Arbor, MI, USA), SNAP (Dojindo Laboratories, Kumamoto, Japan), Hydrogen Peroxide (Wako Pure Chemical, Osaka, Japan) and 2-APB (Calbiochem, San Diego, CA, USA). Preparation of biotinylated 15d-PGJ_2 was described previously[18].

Molecular cloning. Human TRPA1 (GenBank accession No. NM007332.1) was cloned from human brain cDNA library by applying a PCR-based approach, and was subcloned into the expression vector pCI-neo (Promega Corporation, Madison, WI, USA).

Cell culture and cDNA expression. The human TRPA1 was fused at the C terminus with GFP (TRPA1-GFP) using an pEGFP-N1 vector (Clontech Laboratories, Palo Alto, CA, USA). For point mutations to reactive cysteine residues of which environmental irritants, such as isothiocyanates and acrolein, activate TRPA1 through covalent modification, we followed established protocols. Briefly, overlap extension PCR[70] was used to perform site-directed mutagenesis of the reactive cysteine residues. The five residues reported to be involved in activating TRPA1 through covalent modification are in positions Cys414, Cys421, Cys621, Cys641 and Cys665[5,6]. We exchanged the amino acids in these positions to serine (C414S, C421S, C540S, C621S, C641S and C665S). The primer pairs used for C414S and C421S were as follows: C414S, 5'-ACTCACTATAGGCTAGCCTCGAGAATTCGGG-3' (forward) and 5'-CAGGGCCCCCCTGTCTACATGCATAATGTAGAGGAGTACTCCCATCG-3' (reverse); C421S, 5'-ACTCACTATAGGCTAGCCTCGAGAATTCGGG-3' (forward) and 5'-CAGGGCCCCCCTGTCTACTTGCATAATGTAG-3' (reverse). The different PCR products carrying the corresponding mutation were cloned into the *Xho*I / *Apa*I sites of TRPA1. The primer pairs used for C540S, C621S, C641S and C665S were as follows: external primers, 5'-AGCTGGTAATGGATGAAGACAACGATG-3' (forward) and

5’-CTCCATCTTCTGAATGATCAGTTTAATGAGC-3’ (reverse); C540S, 5’-GATACTAATTTGAAGAGCACAGATCGCTTGG-3’ (forward) and 5’-CCAAGCGATCTGTGCTCTTCAAATTAGTATC-3’ (reverse); C621S, 5’-CTCCAGGCAATAAAAGTCCAATTACAG3’ (forward) and 5’-CTGTAATTGGACTTTTATTGCCTGGAG-3’ (reverse); C641S, 5’-GTACTTTTAGATTTCAGCATGTTGCATTCCAC-3’ (forward) and 5’-GTGGAATGCAACATGCTGAAATCTAAAAGTAC-3’ (reverse); C665S, 5’-CAAATATCTTCAAAGTCCATTAGAATTCACC-3’ (forward) and 5’-GGTGAATTCTAATGGACTTTGAAGATATTTG-3’ (reverse). The different PCR products carrying the corresponding mutation were cloned into the *Apa*I / *Bgl*II sites of TRPA1. The nucleotide sequences of the mutants were verified by sequencing the corresponding cDNA. HEK cells (HEK293 cells from American Type Culture Collection) were cultured in Dulbecco’s modified Eagle’s medium (DMEM) containing 10% fetal bovine serum (FBS), 30 units ml^{-1} penicillin and 30 μg ml^{-1} streptomycin at 37^{o}C under 5% CO_2. HEK cells were co-transfected with pEGFP-F (Clontech Laboratories, Palo Alto, CA, USA) and either pCI-neo-TRPA1 or the vector pCI-neo. Transfection was carried out using SuperFect Transfection Reagent (QIAGEN, Valencia, CA, USA). Cells were trypsinized and diluted by DMEM and plated onto glass coverslips 24 h after transfection. Then cells were subjected to measurements 8–24 h after plating on the coverslips.

Fluorescent $[Ca^{2+}]_i$ measurements and electrophysiology. The fura-2 fluorescence was measured in HEPES-buffered saline (HBS) containing the following: NaCl, 107 mM; KCl, 6 mM; $MgSO_4$, 1.2 mM; $CaCl_2$, 2 mM; glucose, 11.5 mM; HEPES, 20 mM; adjusted to pH 7.4 with NaOH. Fluorescence images of the cells were recorded and analyzed with a video image analysis system (ARGUS-50/CA, Hamamatsu Photonics, Shizuoka, Japan) according to the manufacturer’s instructions. The 340:380-nm ratio

images were obtained on a pixel-by-pixel basis. Fura-2 measurements were carried out at 21 ± 1°C in HBS adjusted to pH 7.4. The 340:380-nm ratio images were converted to Ca^{2+} concentrations by *in vivo* calibration using 5 μM ionomycin as described previously[71]. Whole-cell currents were recorded at room temperature (> 24°C) to avoid complications of exposing the channels to cool temperatures using the conventional whole-cell mode of the patch-clamp technique with EPC9 amplifier (HEKA Elektronik, Lambrecht, Germany) as described previously[54]. Voltage-clamp experiments were performed at a holding potential of –60 mV, and recordings were sampled at 2.0 kHz and filtered at 2.9 kHz. The current-voltage relationships were determined using a 180-ms voltage ramp from +80 mV to –100 mV. Current density (pA/pF) was measured. Standard bath solution contained the following: NaCl, 140 mM; KCl, 5 mM; $MgCl_2$, 2 mM; $CaCl_2$, 2 mM; HEPES, 10 mM; glucose 10 mM; adjusted to pH 7.4 with NaOH. The pipette solution contained the following; potassium gluconate, 135 mM; KCl, 5 mM; $MgCl_2$, 7 mM; $CaCl_2$, 0.5 mM; Na_2ATP, 5 mM; EGTA, 5 mM; HEPES, 5 mM; adjusted to pH 7.2 with Tris-base. Compounds were usually added from 1,000–10,000-fold stock solution in DMSO.

Biotinylated 15d-PGJ_2 labeling assay. The biotinylated 15d-PGJ_2 labeling assay was performed as described previously[18] with a few modifications. HEK cells (5×10^6) transfected with TRPA1-GFP or vector were incubated with 5 μM biotinylated 15d-PGJ_2 for 10 min. The cells were washed with phosphate-buffered saline (PBS), harvested, and lysed in RIPA buffer (pH 8.0) containing 150 mM NaCl, 1% Nonidet P-40, 0.5% sodium deoxycholate, 0.1% SDS, 50 mM Tris, 1 mM PMSF and 10 μg ml^{-1} leupeptin. Cell lysates containing 100 μg of protein were incubated batch-wise with 100 μl of NeutrAvidin-Plus beads at 4°C with constant shaking for 4 h. The beads were rinsed seven times with RIPA buffer. The proteins were eluted in SDS sample buffer containing DTT (50 mM) at room temperature for 30 min. The protein samples were

fractionated by 7.5% SDS-PAGE and electrotransferred onto a nitrocellulose membrane. The blots were incubated with an antibody to GFP (Clontech Laboratories, Palo Alto, CA, USA) and stained using the enhanced chemiluminescence (ECL) system (GE Healthcare, Buckinghamshire, UK).

Isolation and culture of mouse DRG neurons. DRG from thoracic and lumbar spinal cord of adult mice were cut in small pieces and incubated for 1 h at 37°C in the solution contained the following: NaCl, 124 mM; KCl, 5 mM; KH_2PO_4, 1.2 mM; $MgSO_4$, 1.3 mM; $CaCl_2$, 2.4 mM; $NaHCO_3$, 24 mM; Glucose, 10 mM; collagenase type II (Sigma-Aldrich, St Louis, MO, USA), 1.6 mg ml^{-1}; trypsin (Difco Laboratories, Detroit, MI, USA), 1.6 mg ml^{-1}; gassed with 95% O_2/5% CO_2. They were gently triturated with a fire-polished glass pipette and the resulting solution was centrifuged at 800 rpm for 8 min. The pellet obtained was resuspended in DRG culture medium contained the following: DMEM, 45%; Ham's F-12 medium (GIBCO Invitrogen Life Technologies, Grand Island, NY, USA), 45%; FBS, 10%; penicillin, 30 units ml^{-1}; streptomycin, 30 μg ml^{-1}. Cells were plated onto coverslips coated with poly-L-lysine (Sigma-Aldrich, St Louis, MO, USA) and laminin (Becton Dickinson, Bedford, MA, USA). The cells were cultured in the DRG culture medium at 37°C under 5% CO_2. $[Ca^{2+}]_i$ imaging experiments were performed 18–36 h after plating. All animal experiments were performed in accordance with protocols approved by the Institutional Animal Care and Use Committees of the Graduate School of Engineering, Kyoto University.

Statistical analysis. All data are expressed as means ± s.e.m.. The data were accumulated under each condition from at least three independent experiments. Statistical significance was evaluated using the Student's *t*-test for comparisons between two mean values. Multiple comparisons between more than three groups were carried out using an ANOVA followed by Tukey–Kramer test.

References

1. Woolf, C. J. & Salter, M. W. Neuronal plasticity: Increasing the gain in pain. *Science* **288,** 1765–1768 (2000).
2. Clapham, D. E. TRP channels as cellular sensors. *Nature* **426,** 517–524 (2003).
3. Guenther, S., Reeh, P. W. & Kress, M. Rises in $[Ca^{2+}]_i$ mediate capsaicin- and proton-induced heat sensitization of rat primary nociceptive neurons. *Eur. J. Neurosci.* **11,** 3143–3150 (1999).
4. Yoshida, T. *et al.* Nitric oxide activates TRP channels by cysteine S-nitrosylation. *Nat. Chem. Biol.* **2,** 596–607 (2006).
5. Hinman, A., Chuang, H. H., Bautista, D. M. & Julius, D. TRP channel activation by reversible covalent modification. *Proc. Natl Acad. Sci. USA* **103,** 19564–19568 (2006).
6. Macpherson, L. J. *et al.* Noxious compounds activate TRPA1 ion channels through covalent modification of cysteines. *Nature* **445,** 541–545 (2007).
7. Bautista, D. M. *et al.* TRPA1 mediates the inflammatory actions of environmental irritants and proalgesic agents. *Cell* **124,** 1269–1282 (2006).
8. Kwan, K. Y. *et al.* TRPA1 contributes to cold, mechanical, and chemical nociception but is not essential for hair-cell transduction. *Neuron* **50,** 277–289 (2006).
9. Story, G. M. *et al.* ANKTM1, a TRP-like channel expressed in nociceptive neurons, is activated by cold temperatures. *Cell* **112,** 819–829 (2003).
10. Nagata, K., Duggan, A., Kumar, G. & García-Añoveros, J. Nociceptor and hair cell transducer properties of TRPA1, a channel for pain and hearing. *J. Neurosci.* **25,** 4052–4061 (2005).
11. Jordt, S. E. *et al.* Mustard oils and cannabinoids excite sensory nerve fibres through the TRP channel ANKTM1. *Nature* **427,** 260–265 (2004).
12. Macpherson, L. J. *et al.* The pungency of garlic: activation of TRPA1 and TRPV1 in response to allicin. *Curr. Biol.* **15,** 929–934 (2005).
13. Bandell, M. *et al.* Noxious cold ion channel TRPA1 is activated by pungent compounds and bradykinin. *Neuron* **41,** 849–857 (2004).
14. Tilley, S. L., Coffman, T. M. & Koller, B. H. Mixed messages: modulation of inflammation and immune responses by prostaglandins and thromboxanes. *J. Clin. Invest.* **108,** 15–23 (2001).
15. Shibata, T. *et al.* 15-deoxy-$\Delta^{12,14}$-prostaglandin J_2. A prostaglandin D_2 metabolite generated during inflammatory processes. *J. Biol. Chem.* **277,** 10459–10466 (2002).
16. Gilroy, D. W. *et al.* Inducible cyclooxygenase may have anti-inflammatory properties. *Nat. Med.* **5,** 698–701 (1999).
17. Kondo, M. *et al.* 15-Deoxy-$\Delta^{12,14}$-prostaglandin J_2: The endogenous electrophile that induces

neuronal apoptosis. *Proc. Natl Acad. Sci. USA* **99,** 7367–7372 (2002).

18. Shibata, T. *et al.* Thioredoxin as a molecular target of cyclopentenone prostaglandins. *J. Biol. Chem.* **278,** 26046–26054 (2003).
19. Rossi, A. *et al.* Anti-inflammatory cyclopentenone prostaglandins are direct inhibitors of IκB kinase. *Nature* **403,** 103–108 (2000).
20. Straus, D. S. *et al.* 15-deoxy-$\Delta^{12,14}$-prostaglandin J_2 inhibits multiple steps in the NF-κB signaling pathway. *Proc. Natl Acad. Sci. USA* **97,** 4844–4849 (2000).
21. Hess, D. T. *et al.* Protein S-nitrosylation: purview and parameters. *Nat. Rev. Mol. Cell Biol.* **6,** 150–166 (2005).
22. Takanishi, C. L., Ma, L. H. & Wood, M. J. A genetically encoded probe for cysteine sulfenic acid protein modification in vivo. *Biochemistry* **46,** 14725–14732 (2007).
23. Wei, X. Q. *et al.* Altered immune responses in mice lacking inducible nitric oxide synthase. *Nature* **375,** 408–411 (1995).
24. Grabowski, P. S. *et al.* Immunolocalization of inducible nitric oxide synthase in synovium and cartilage in rheumatoid arthritis and osteoarthritis. *Br. J. Rheumatol.* **36,** 651–655 (1997).
25. Osborne, M. G. & Coderre, T. J. Effects of intrathecal administration of nitric oxide synthase inhibitors on carrageenan-induced thermal hyperalgesia. *Br. J. Pharmacol.* **126,** 1840–1846 (1999).
26. Holthusen, H. & Arndt, J. O. Nitric oxide evokes pain at nociceptors of the paravascular tissue and veins in humans. *J. Physiol.* **487,** 253–258 (1995).
27. Henricks, P. A. J. & Nijkamp, F. P. Reactive oxygen species as mediators in asthma. *Pulm. Pharmacol. Ther.* **14,** 409–421 (2001).
28. Lambeth, J. D. NOX enzymes and the biology of reactive oxygen. *Nat. Rev. Immunol.* **4,** 181–189 (2004).
29. Huang, H. S., Pan, H. L., Stahl, G. L. & Longhurst, J. C. Ischemia- and reperfusion-sensitive cardiac sympathetic afferents: influence of H_2O_2 and hydroxyl radicals. *Am. J. Physiol.* **269,** H888–H901 (1995).
30. Karashima, Y. *et al.* Modulation of the transient receptor potential channel TRPA1 by phosphatidylinositol 4,5-biphosphate manipulators. *Pflugers Arch.* **457,** 77–89 (2008).
31. Atsmon, J. *et al.* Formation of thiol conjugates of 9-deoxy-delta 9,delta 12(E)-prostaglandin D2 and delta 12(E)-prostaglandin D2. *Biochemistry* **29,** 3760–3765 (1990).
32. Atsmon, J. *et al.* Conjugation of 9-deoxy-Δ^9,Δ^{12}(E)-prostaglandin D_2 with intracellular glutathione and enhancement of its antiproliferative activity by glutathione depletion. *Cancer Res.* **50,**

1879–1885 (1990).

33. Steen, K. H., Reeh, P. W., Anton, F. & Handwerker, H. O. Protons selectively induce lasting excitation and sensitization to mechanical stimulation of nociceptors in rat skin, in vitro. *J. Neurosci.* **12,** 86–95 (1992).
34. Steen, K. H., Steen, A. E., Kreysel, H. W. & Reeh, P. W. Inflammatory mediators potentiate pain induced by experimental tissue acidosis. *Pain* **66,** 163–170 (1996).
35. Issberner, U., Reeh, P. W. & Steen, K. H. Pain due to tissue acidosis: a mechanism for inflammatory and ischemic myalgia? *Neurosci. Lett.* **208,** 191–194 (1996).
36. Kobayashi, K. *et al.* Distinct expression of TRPM8, TRPA1, and TRPV1 mRNAs in rat primary afferent neurons with Aδ/C-fibers and colocalization with Trk receptors. *J. Comp. Neurol.* **493,** 596–606 (2005).
37. Chen, C. C. *et al.* A role for ASIC3 in the modulation of high-intensity pain stimuli. *Proc. Natl Acad. Sci. USA* **99,** 8992–8997 (2002).
38. Caterina, M. J. *et al.* Impaired nociception and pain sensation in mice lacking the capsaicin receptor. *Science* **288,** 306–313 (2000).
39. Davis, J. B. *et al.* Vanilloid receptor-1 is essential for inflammatory thermal hyperalgesia. *Nature* **405,** 183–187 (2000).
40. Kang, S. W., Baines, I. C. & Rhee, S. G. Characterization of a mammalian peroxiredoxin that contains one conserved cysteine. *J. Biol. Chem.* **273,** 6303–6311 (1998).
41. Tominaga, M. *et al.* The cloned capsaicin receptor integrates multiple pain-producing stimuli. *Neuron* **21,** 531–543 (1998).
42. Scher, J. U. & Pillinger, M. H. 15d-PGJ_2: the anti-inflammatory prostaglandin? *Clin. Immunol.* **114,** 100–109 (2005).
43. Hirai, H. *et al.* Prostaglandin D2 selectively induces chemotaxis in T helper type 2 cells, eosinophils, and basophils via seven-transmembrane receptor CRTH2. *J. Exp. Med.* **193,** 255–261 (2001).
44. Monneret, G. *et al.* 15-Deoxy-$\Delta^{12,14}$-prostaglandins D_2 and J_2 are potent activators of human eosinophils. *J. Immunol.* **168,** 3563–3569 (2002).
45. Powell, W. S. 15-deoxy-$\Delta^{12,14}$-PGJ_2: endogenous PPARγ ligand or minor eicosanoid degradation product? *J. Clin. Invest.* **112,** 828–830 (2003).
46. Monneret, G. *et al.* 15*R*-methyl-prostaglandin D_2 is a potent and selective CRTH2/DP_2 receptor agonist in human eosinophils. *J. Pharmacol. Exp. Ther.* **304,** 349–355 (2003).
47. Narumiya, S. & Fukushima, M. Site and mechanism of growth inhibition by prostaglandins. I.

Active transport and intracellular accumulation of cyclopentenone prostaglandins, a reaction leading to growth inhibition. *J. Pharmacol. Exp. Ther.* **239,** 500–505 (1986).

48. Broillet, M. C. & Firestein, S. Direct activation of the olfactory cyclic nucleotide-gated channel through modification of sulfhydryl groups by NO compounds. *Neuron* **16,** 377–385 (1996).
49. Choi, Y. B. *et al.* Molecular basis of NMDA receptor-coupled ion channel modulation by S-nitrosylation. *Nat. Neurosci.* **3,** 15–21 (2000).
50. Xu, L., Eu, J. P., Meissner, G. & Stamler, J. S. Activation of the cardiac calcium release channel (ryanodine receptor) by poly-S-nitrosylation. *Science* **279,** 234–237 (1998).
51. Ignarro, L. J. Nitric oxide. A novel signal transduction mechanism for transcellular communication. *Hypertension* **16,** 477–483 (1990).
52. Baker, J. E. *et al.* Nitric oxide activates the sarcolemmal K_{ATP} channel in normoxic and chronically hypoxic hearts by a cyclic GMP-dependent mechanism. *J. Mol. Cell. Cardiol.* **33,** 331–341 (2001).
53. Jiang, L. H. *et al.* Regulation of cloned cardiac L-type calcium channels by cGMP-dependent protein kinase. *J. Biol. Chem.* **275,** 6135–6143 (2000).
54. Hara, Y. *et al.* LTRPC2 Ca^{2+}-permeable channel activated by changes in redox status confers susceptibility to cell death. *Mol. Cell* **9,** 163–173 (2002).
55. Aracena-Parks, P. *et al.* Identification of cysteines involved in S-nitrosylation, S-glutathionylation, and oxidation to disulfides in ryanodine receptor type 1. *J. Biol. Chem.* **281,** 40354–40368 (2006).
56. Dinkova-Kostova, A. T. *et al.* Direct evidence that sulfhydryl groups of Keap1 are the sensors regulating induction of phase 2 enzymes that protect against carcinogens and oxidants. *Proc. Natl Acad. Sci. USA* **99,** 11908–11913 (2002).
57. Eggler, A. L. *et al.* Modifying specific cysteines of the electrophile-sensing human Keap1 protein is insufficient to disrupt binding to the Nrf2 domain Neh2. *Proc. Natl Acad. Sci. USA* **102,** 10070–10075 (2005).
58. Hong, F., Sekhar, K. R., Freeman, M. L. & Liebler, D. C. Specific patterns of electrophile adduction trigger Keap1 ubiquitination and Nrf2 activation. *J. Biol. Chem.* **280,** 31768–31775 (2005).
59. Semtner, M., Schaefer, M., Pinkenburg, O. & Plant, T. D. Potentiation of TRPC5 by protons. *J. Biol. Chem.* **282,** 33868–33878 (2007).
60. Jordt, S. E., Tominaga, M. & Julius, D. Acid potentiation of the capsaicin receptor determined by a key extracellular site. *Proc. Natl Acad. Sci. USA* **97,** 8134–8139 (2000).
61. Gaudet, R. A primer on ankyrin repeat function in TRP channels and beyond. *Mol. Biosyst.* **4,**

372–379 (2008).

62. Krishtal, O. A. & Pidoplichko, V. I. A receptor for protons in the nerve cell membrane. *Neuroscience* **5,** 2325–2327 (1980).
63. Lingueglia, E. Acid-sensing ion channels in sensory perception. *J. Biol. Chem.* **282,** 17325–17329 (2007).
64. Dröge, W. Free radicals in the physiological control of cell function. *Physiol. Rev.* **82,** 47–95 (2002).
65. Taylor-Clark, T. E. *et al.* Prostaglandin-Induced Activation of Nociceptive Neurons via Direct Interaction with Transient Receptor Potential A1 (TRPA1). *Mol. Pharmacol.* **73,** 274–281 (2008).
66. Maher, M. *et al.* Activation of TRPA1 by farnesyl thiosalicylic acid. *Mol. Pharmacol.* **73,** 1225–1234 (2008).
67. Andersson, D. A., Gentry, C., Moss, S. & Bevan, S. Transient receptor potential A1 is a sensory receptor for multiple products of oxidative stress. *J. Neurosci.* **28,** 2485–2494 (2008).
68. Bessac, B. F. *et al.* TRPA1 is a major oxidant sensor in murine airway sensory neurons. *J. Clin. Invest.* **118,** 1899–1910 (2008).
69. Sawada, Y., Hosokawa, H., Matsumura, K. & Kobayashi, S. Activation of transient receptor potential ankyrin 1 by hydrogen peroxide. *Eur. J. Neurosci.* **27,** 1131–1142 (2008).
70. Ho, S. N. *et al.* Site-directed mutagenesis by overlap extension using the polymerase chain reaction. *Gene* **77,** 51–59 (1989).
71. Nishida, M. *et al.* Amplification of receptor signalling by Ca^{2+} entry-mediated translocation and activation of PLCγ2 in B lymphocytes. *EMBO J.* **22,** 4677–4688 (2003).

Chapter 3

TRPA1 senses O_2 availability in non-carotid body chemoreceptors

Summary

Oxygen (O_2) intake is tightly controlled in order to secure energy production while minimizing the risk of oxidative damage in aerobic organisms. Mammals' respiratory systems have evolved to respond to changes in O_2 availability via the carotid body and other chemoreceptors. However, molecular mechanisms underlying O_2 sensing in chemoreceptors are still elusive. Here, our functional examination of the TRP cation channels expressed in mouse vagal chemoreceptors reveals that the TRPA1 channel is activated by O_2 and mediates ionic currents in hyperoxia via its prominent sensitivity to cysteine-mediated oxidation. TRPA1 is also activated in hypoxia through relief from O_2-dependent inhibition by prolyl hydroxylases. In *Trpa1*-deficient mice, hyperoxia- and hypoxia-induced vagal afferent nerve activities and their consequent ventilatory responses are severely impaired; pulmonary inflammation and hypertension are abnormally induced in normoxia, and are aggravated in hyperoxia and hypoxia, respectively. Thus, TRPA1 is an O_2 sensor that regulates O_2 supply *in vivo*.

Introduction

Molecular oxygen (O_2) is the engine of life essential for cellular respiration in all aerobic organisms[1]. In hypoxia, deprivation of O_2 threats survival, and is critical in the pathogenesis of major causes of mortality such as stroke and myocardial infarction[2]. At the same time, O_2 exerts toxicity through the production of reactive oxygen species (ROS); O_2 is an important cause of aging and of respiratory disorders and eventually death in hyperoxia[1,3]. Thus, due to the ambivalent physiological nature of O_2, the control of adequate O_2 provision to the tissues and the capability of generating adaptive responses to changes in *in vivo* O_2 levels are fundamental challenges for aerobic life forms[3].

Mammals have developed several systems to respond to changes in O_2 levels. At the whole organ level, hyperoxia diminishes but hypoxia increases respiratory drive, leading to suppression and to a rise of O_2 supply to the tissues and organs, respectively. The ventilatory responses are believed to be triggered primarily by the carotid body[4]. The chemosensory inputs are carried within the carotid sinus nerve toward medullary centres and the ventilatory pattern is then changed. The importance of ventilatory responses has also been documented for non-carotid body peripheral chemoreceptors[5–8]. In response to changes in O_2 availability and to chemical substances, breathing tempo is regulated, for example, by pulmonary and airway vagal afferents such as unmyelinated bronchopulmonary C-fibers of vagal nerves, myelinated vagal fibers innervating lung airway neuroepithelial bodies (NEBs) and vagal branch superior laryngeal nerves[5,7,9–15]. With regard to the mechanisms underlying O_2-sensing in the carotid body, it is generally accepted that hypoxia inhibits K^+ channels to depolarize chemoreceptor glomus cells, leading to the activation of voltage-dependent Ca^{2+} channels and exocytosis, while hyperoxia reduces depolarization and inhibits exocytosis[4,16]. Controversy remains about the exact channel subtypes and direct mediators responsible for O_2 sensing[16,17], as well as

the correspondence in O_2-dependence between channel regulation and physiological responses of the carotid body[18]. Even less is known about the molecular mechanisms that directly sense O_2 availability in non-carotid body chemoreceptors[17].

The adaptation to hypoxia involves activation of a transcription factor, hypoxia inducible factor-1 (HIF-1), which subsequently leads to a systemic response, including an increase in red blood cell mass and stimulus of new blood vessel growth[19]. Hydroxylation of the HIF-1α subunit at proline (Pro) residues by prolyl hydroxylases (PHD1–3), which utilize molecular O_2 and 2-oxoglutarate as substrates, targets HIF-1α to the 26*S* proteasome for degradation[20]. Importantly, because Michaelis constant (K_m) values of PHDs, representing the substrate concentration at which half of the enzyme active sites are occupied, are close to the atmospheric O_2 concentration, physiological reductions in O_2 concentration result in increased levels of HIF-1α[21]. A hydroxylation of the asparagine residue in the transactivation domain of HIF-1α by an asparaginyl hydroxylase, known as factor inhibiting HIF (FIH), represents a second mechanism of O_2-dependent repression of HIF-1α[20]. PHDs and FIH are thus central to hypoxia-sensing pathways as a result of their absolute requirement upon O_2 as a cofactor for enzymatic activity[20]. With regard to hyperoxia, different classes of enzymatic and nonenzymatic antioxidants are upregulated by mitogen-activated protein kinases[3] to scavenge ROS in the prevention from hyperoxia-evoked damage for adaptation[22]. However, hyperoxic O_2 sensors that mediate respiratory defense mechanisms to avoid toxicity of O_2 are still unknown.

The *Drosophila* transient receptor potential (TRP) protein and its homologues are polypeptide subunits that assemble into tetramers to form cation channels activated by sensing diverse stimuli from the extracellular environment and from inside the cell[23,24]. Recently, a number of TRP channels have emerged as cell sensors for changes in redox status[25–27]. TRPM2 channels are activated indirectly by H_2O_2 via nicotinamide adenine

dinucleotide and its metabolites[25,28], while certain members of the TRPC and TRPV subfamily, including TRPC5 and TRPV1, are activated by nitric oxide, oxidants and reactive disulfides through modification of cysteine (Cys) free sulfhydryl groups[26]. TRPC5 is also activated by reducing substances such as thioredoxin[27]. Oxidative Cys modification by pungent compounds and inflammatory mediators[14,29–31] are important activation triggers of TRPA1 in addition to noxious cold (< 17°C)[32] and other stimulants[15,33,34]. Notably, as polymodal receptors for noxious stimuli at nerve endings in somatosensory and vagal afferent neurons[15,32,35,36], TRPV1 and TRPA1 sense environmental irritants including oxidants in the airway and lung to evoke defensive reflexes such as coughing and changes in respiration pattern[13–15].

Here we identify TRPA1 as a molecular entity of an O_2 sensor in non-carotid body chemoreceptors. Our studies using *Trpa1* knockout (KO) mice[37] have revealed that TRPA1 detects O_2 availability and triggers the respiratory reflex, which controls O_2 supply *in vivo*.

Results

Characterization of TRPA1 as an O_2 sensor in non-carotid body chemoreceptors.

In order to identify possible target chemoreceptors in the search for molecular O_2 sensors, we examined the effects of bilateral sectioning of cervical vagal trunks, superior laryngeal branches of the vagal nerve and glossopharyngeal nerves including carotid sinus branches on respiratory frequency (Rf) in hyperoxia and hypoxia in mice (Fig. 1a). Notably, bilateral sectioning of cervical vagal trunks and superior laryngeal nerves innervating the mucosa of the larynx significantly impaired Rf changes induced by hyperoxia and mild hypoxia (13 or 15% O_2), while that of glossopharyngeal nerves attenuated the Rf increase by a more severe hypoxia (10% O_2) (Fig. 1b). The same sectioning operations failed to affect the Rf increase in response to hypercapnia (10% CO_2) (Fig. 1c), which originates mainly from the central chemoreceptor[38]. Thus, non-carotid body chemoreceptors have characteristic O_2 sensitivity compared to the carotid body in mice.

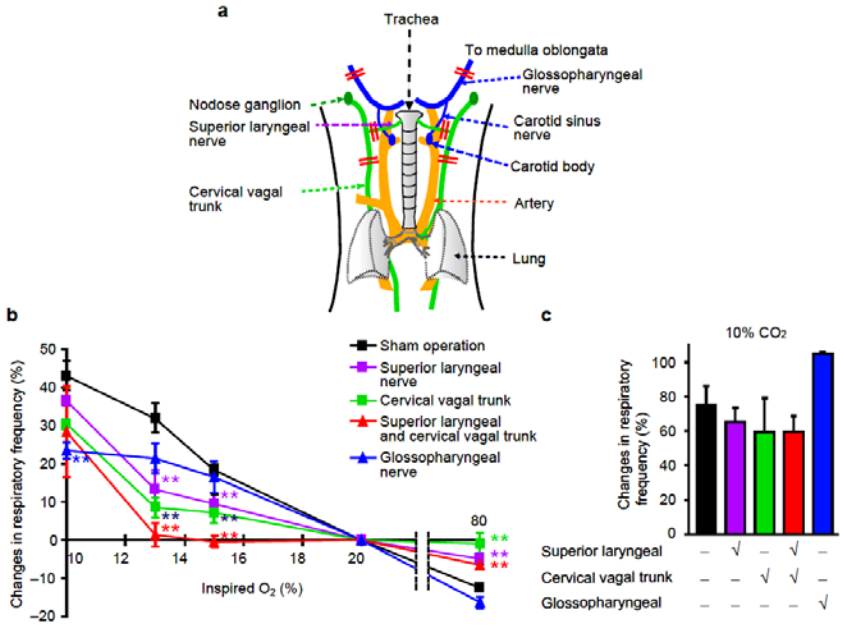

Figure 1. O_2 dependency of Rf changes induced by exposure to hyperoxic or hypoxic gas via peripheral chemoreceptors in anesthetized mice. **a,** Cervical vagal trunks, superior laryngeal nerves and glossopharyngeal nerves are subjected alone or in combination to bilateral sectioning at the transection sites indicated by the red double lines. **b, c,** Percentage changes in Rf induced by hyperoxia (**b**), hypoxia (**b**) or hypercapnia (**c**) from the base lines obtained by initial exposure to 20% O_2 are shown (n = 4–7). $^{**}P < 0.01$ compared to sham operation, ANOVA with Turkey–Kramer post-hoc test.

Responses of the non-carotid body chemoreceptors to changes in O_2 availability were examined in neurons isolated from the mouse nodose ganglion, in which the cell bodies of vagal and superior laryngeal nerves are located. We observed robust increases in intracellular Ca^{2+} concentration ($[Ca^{2+}]_i$) upon application of hyperoxic and hypoxic solutions in a subset of cells responsive to 60 mM KCl, which activates voltage-dependent Ca^{2+} channels in neurons (Fig. 2a and Table 1). The majority of hyperoxia- and hypoxia-responsive cells also responded to the C-fiber-specific sensory irritant capsaicin[9] (Table 1), suggesting that a subset of C-fibers senses O_2 changes in hyperoxia and hypoxia. Whole-cell current amplitudes were augmented by hyperoxic and hypoxic solutions in nodose neurons (Fig. 2b).

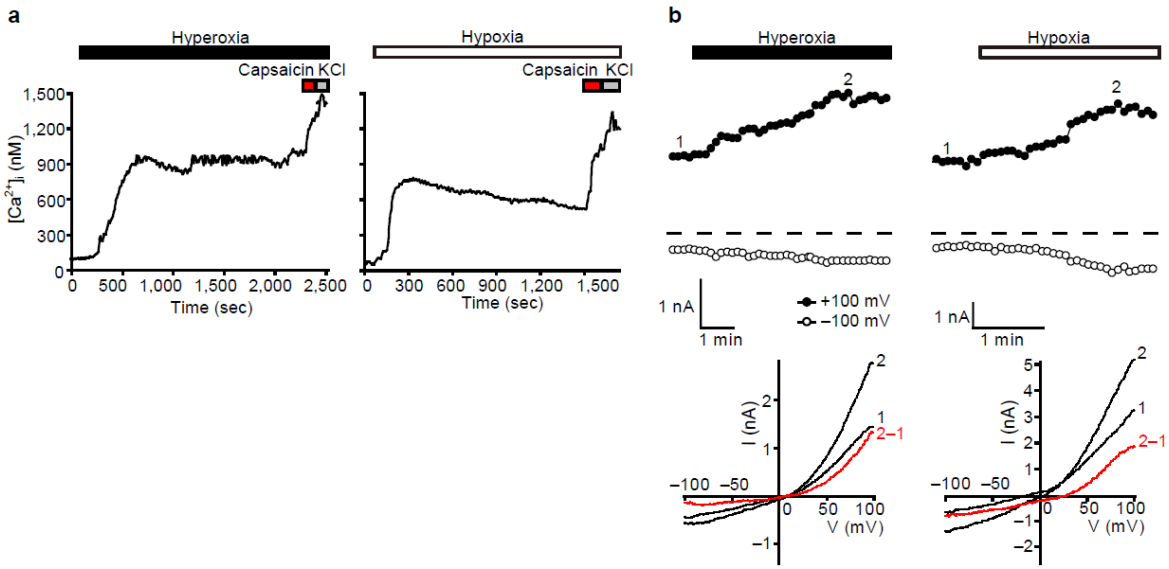

Figure 2. Hyperoxia and hypoxia activate nodose ganglion neurons. **a,** Representative Ca^{2+} responses evoked in hyperoxic (left) or hypoxic solutions (right) and by application of 3 μM capsaicin and 60 mM KCl in mouse nodose ganglion neurons. **b,** Representative time courses of outward and inward currents recorded at +100 and –100 mV, respectively, by whole cell patch clamp method under ramp clamp in hyperoxic (left) or hypoxic (right) solution in mouse nodose ganglion neurons (top). Corresponding *I-V* relationships at the time points 1 and 2, and those of evoked currents (2–1) are shown (bottom). 21 out of 84 cells and 12 out of 50 cells showed evoked currents in hyperoxia and hypoxia, respectively.

Table 1. The percentages of hyperoxia- and hypoxia-responding nodose ganglion or DRG neurons.

	DRG	Nodose ganglion
Capsaicin-responding cells;		
WT	41.3% (102/247)	48.5% (81/167)
Trpa1 KO	39.1% (61/156)	45.5% (102/224)
Hyperoxia-responding cells;		
WT	40.0% (32/80)	28.6% (8/28)
Trpa1 KO	12.1% (4/33)	4.84% (3/62)
Hyperoxia- and capsaicin-responding cells;		
WT	25.0% (20/80)	25.0% (7/28)
Trpa1 KO	0.03% (1/33)	0.02% (1/62)
Hypoxia-responding cells;		
WT	21.6% (36/167)	12.2% (17/139)
Trpa1 KO	7.31% (9/123)	3.09% (5/162)
Hypoxia- and capsaicin-responding cells;		
WT	10.8% (18/167)	12.2% (17/139)
Trpa1 KO	0.81% (1/123)	0.00% (0/162)

Because O_2 is an oxidant itself that induces changes of cellular redox status[3], we hypothesized that redox-sensitive TRP channels mediate the O_2-sensing function of chemoreceptors. RNA expression of TRPM2, TRPM7, TRPC1, TRPC3, TRPC4, TRPC6, TRPV1, TRPV2 and TRPA1 was identified in the mouse nodose ganglion (Fig. 3a). In human embryonic kidney (HEK) 293 cells expressing recombinant TRPA1, hyperoxia and hypoxia induced a robust $[Ca^{2+}]_i$ elevation, which was suppressed by the TRPA1-specific blocker AP-18 (10 μM)[39] in the presence of extracellular Ca^{2+} (Fig. 3), indicating that the TRPA1 channel mediates Ca^{2+} entry in response to hyperoxia and hypoxia. By contrast, other TRPs identified in the nodose ganglion failed to induce such $[Ca^{2+}]_i$ rises, except for TRPM7 causing marginal $[Ca^{2+}]_i$ elevation in response to hypoxia, as reported previously[40] (Fig. 3b, c). Interestingly, TRPA1 activation showed an inverted bell-shaped O_2-dependency curve with a minimum at the partial O_2 pressure (PO_2) of 140 mmHg (18%), which is slightly below the atmospheric PO_2 (152 mmHg) (Fig. 1d). Notably, TRPA1 protein was identified by immunohistochemistry in a subset of nodose ganglion neurons projecting to the lung and airway in mice[13] (Fig. 4a), while TRPA1 RNA was undetectable in the mouse carotid body (Fig. 4b).

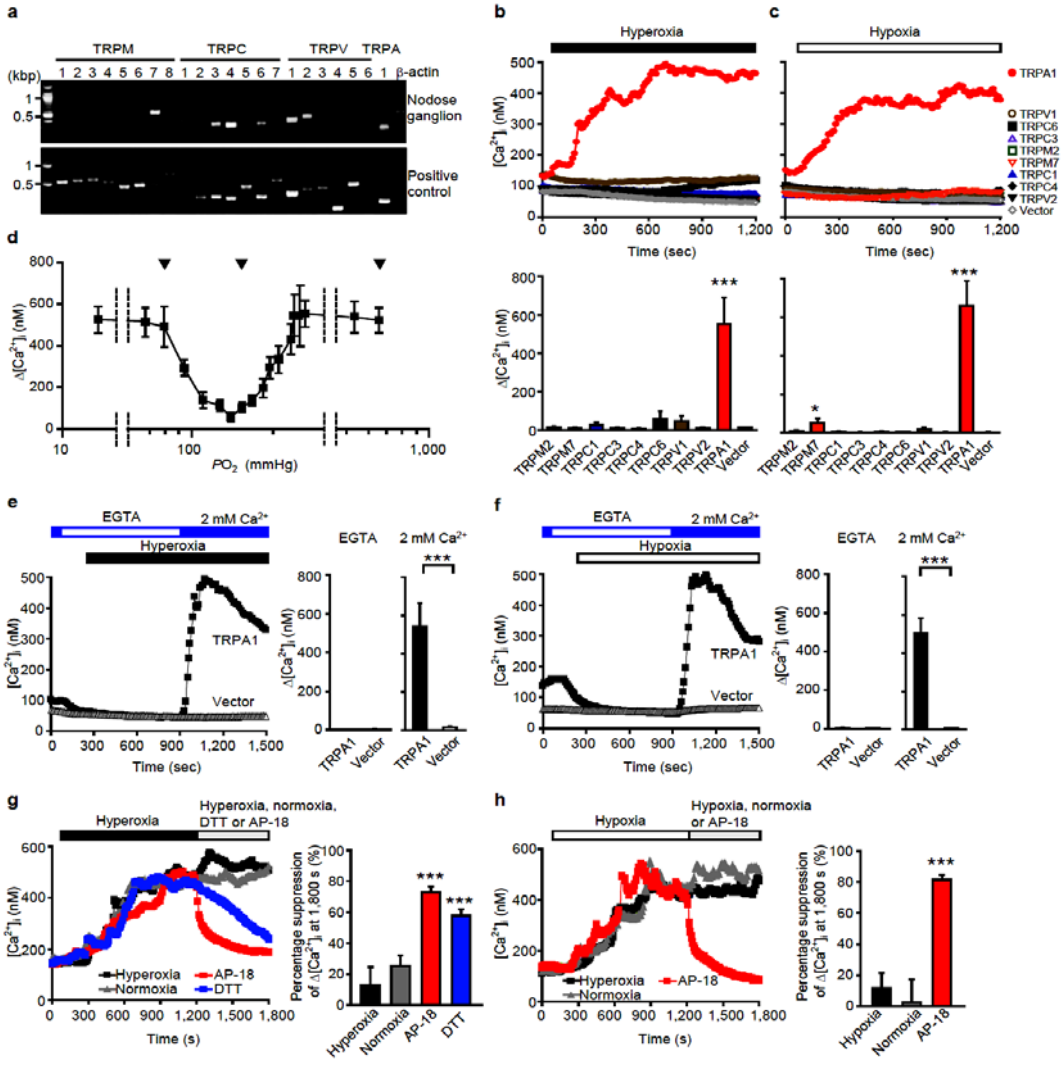

Figure 3. TRPA1 mediates Ca^{2+} influx upon hyperoxia and hypoxia. **a,** RNA expression of TRP channels detected by RT-PCR in mouse nodose ganglion neurons. See Methods for sources of positive control RNAs. **b, c,** $[Ca^{2+}]_i$ rises evoked by hyperoxic (**b**) and hypoxic (**c**) solutions in HEK293 cells transfected with TRP homologues detected in nodose ganglion neurons. Averaged time courses (top) and maximum $[Ca^{2+}]_i$ rises ($\Delta[Ca^{2+}]_i$) (bottom) (n = 16–40). $^{*}P < 0.05$ and $^{***}P < 0.001$ compared to vector. **d,** The relationship between PO_2 and maximum Ca^{2+} responses mediated by TRPA1 (n = 21–41). Arrowheads indicate, from left to right, PO_2 values for hypoxia (10% O_2), normoxia (20% O_2) and hyperoxia (86% O_2) in examining *in vitro* cellular response to O_2. PO_2 measured in the hypoxic, normoxic and hyperoxic solutions are 79 ± 3, 152 ± 1 and 655 ± 32 mmHg, respectively. **e, f,** Averaged time courses (left) and maximum $[Ca^{2+}]_i$ rises induced by hyperoxia (**e**) (n = 11–28) or hypoxia (**f**) (n = 16–27) in Ca^{2+}-free, 0.5 mM EGTA- (middle) or 2 mM Ca^{2+}-containing solution (right) are shown for HEK293 cells transfected with TRPA1 or vector. $^{***}P < 0.001$. **g, h,** Suppression of hyperoxia- (**g**) and hypoxia-induced Ca^{2+} responses (**h**) via TRPA1 by 10 μM AP-18 (**g, h**) or 10 mM DTT (**g**). Averaged time courses (left) and percentage suppression of $[Ca^{2+}]_i$ rises (right) at 1,800 sec relative to maximal rises in TRPA1-expressing HEK293 cells (n = 18–26). Data points are mean ± s.e.m.. In **f, g,** $^{***}P < 0.001$ compared to cells treated with normoxic solution.

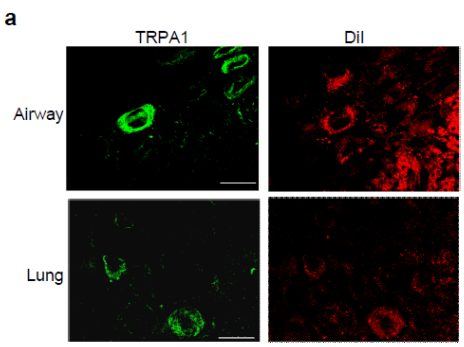

Figure 4. Expression of TRPA1 in nodose ganglion neurons and the carotid body. **a,** Expression of TRPA1 proteins in a subset of nodose ganglion neurons innervating the airway (top) and the lung (bottom). Confocal images of immunostaining with TRPA1-specific antibody (green). Retrograde labeling of nodose ganglion neurons projecting to airway or lung with DiI (red) are attained by its instillation into the airway lumen or by transdermal injection into the lung, respectively. The bar indicates 20 μm. Data points are mean ± s.e.m.. **b,** RNA expression of TRPA1 is undetectable in the mouse carotid body. RNAs are subjected to RT-PCR from the mouse carotid body and that from DRG as a positive control of TRPA1 expression. Identification of carotid body is confirmed by the detection of tyrosine hydroxylase (TH) RNA, a specific marker for carotid body in the carotid artery region[41].

In TRPA1-expressing HEK293T cells, hyperoxia or hypoxia dramatically increased whole cell currents inhibited by AP-18 (Fig. 5). Hyperoxia- and hypoxia-induced currents showed similar current-voltage (*I-V*) relationships (Fig. 5a, b). Single-channel currents were significantly enhanced by hyperoxic solution but not by hypoxic solution, when applied from the intracellular side of cell-free excised inside-out patches at a holding potential (V_h) of –60 mV (Fig. 6a–c). With regard to hyperoxia-induced unitary activities, the open probability was reduced by AP-18 (10 μM) (Fig. 6d, e) and conductance was 97.3 ± 2.0 pS at –80 - +20 mV and 180.6 ± 10.7 pS at +40 - +80 mV, as previously reported[36] (Fig. 6f). These results imply that TRPA1 is activated by direct action of O_2 in hyperoxia and by intracellular O_2-sensing mediators in hypoxia.

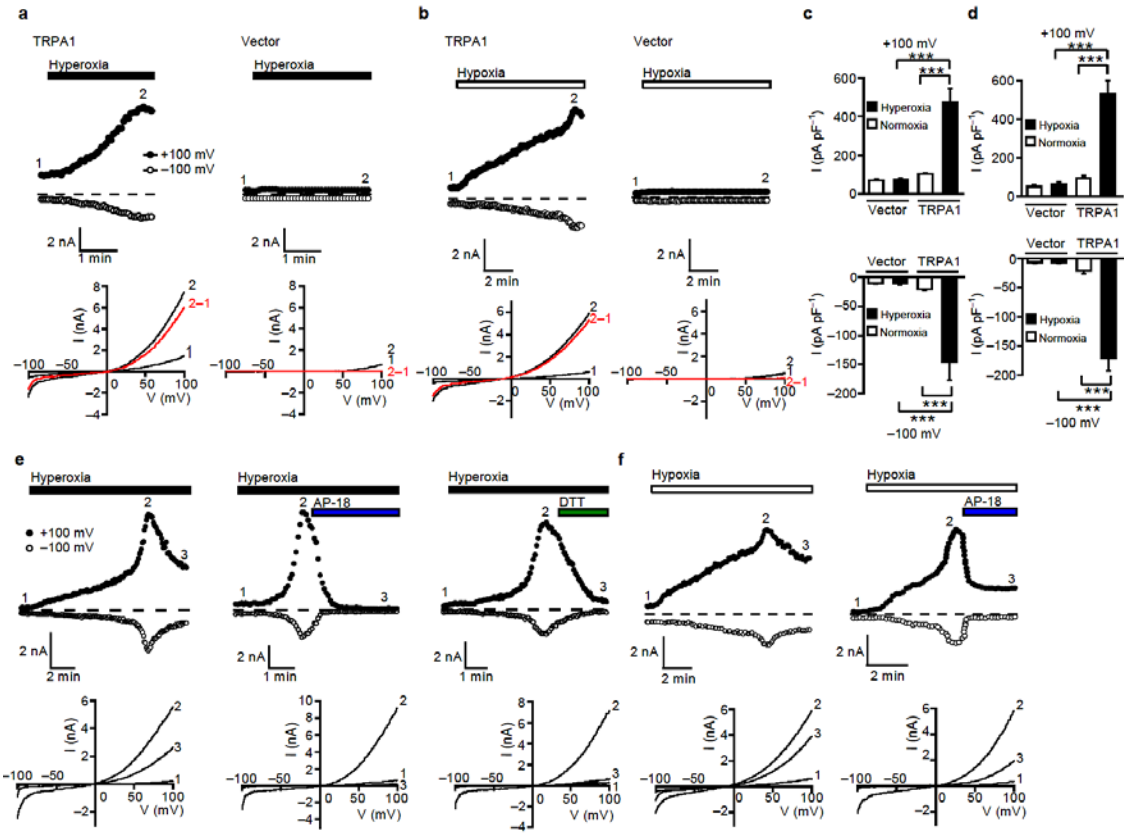

Figure 5. Hyperoxia- and hypoxia-evoked current through TRPA1. Measurement of ionic currents evoked by hyperoxia or hypoxia using whole cell patch clamp method with a Cs^+-based pipette solution and a Na^+-based bath solution in TRPA1-expressing HEK293T cells. **a, b,** Representative time courses of outward and inward currents recorded at +100 and –100 mV, respectively, under ramp clamp in hyperoxic (**a**) or hypoxic (**b**) solution in HEK293T cells transfected with TRPA1 (left) or vector (right) (top). Corresponding *I-V* relationships at the time points 1 and 2, and those of evoked currents (2–1) are shown (bottom). **c, d,** Peak current densities at +100 (top) and –100 mV (bottom) in normoxic (**c, d**), hyperoxic (**c**) and hypoxic (**d**) conditions (n = 6–18). $^{***}P < 0.001$. **e,** Suppression of hyperoxia-evoked whole cell currents by 10 μM AP-18 and 10 mM DTT in TRPA1-expressing HEK293T cells. Representative time courses of outward and inward currents recorded at +100 and –100 mV, respectively, under ramp clamp (top). Corresponding *I-V* relationships at the time points 1–3 (bottom) **f,** Suppression of hypoxia-evoked whole cell currents by AP-18 in TRPA1-expressing HEK293T cells. Representative time courses (top) and corresponding *I-V* relationships (bottom). **g,** Suppression of hyperoxia-activated TRPA1 currents by 10 μM AP-18 (n = 7) and 10 mM DTT (n= 5) at +100 (top) and –100 mV (bottom). Percentage suppression of the current at 3-min after the peak relative to that at the peak. **h,** Suppression of hypoxia-activated TRPA1 currents by AP-18 at +100 (top) and –100 mV (bottom) (n = 10). Data points are mean ± s.e.m.. In **g** and **h**, $^{*}P < 0.05$, $^{**}P < 0.01$ and $^{***}P < 0.001$ compared to cells maintained in hyperoxia (**g**) or hypoxia (**h**) without the agents.

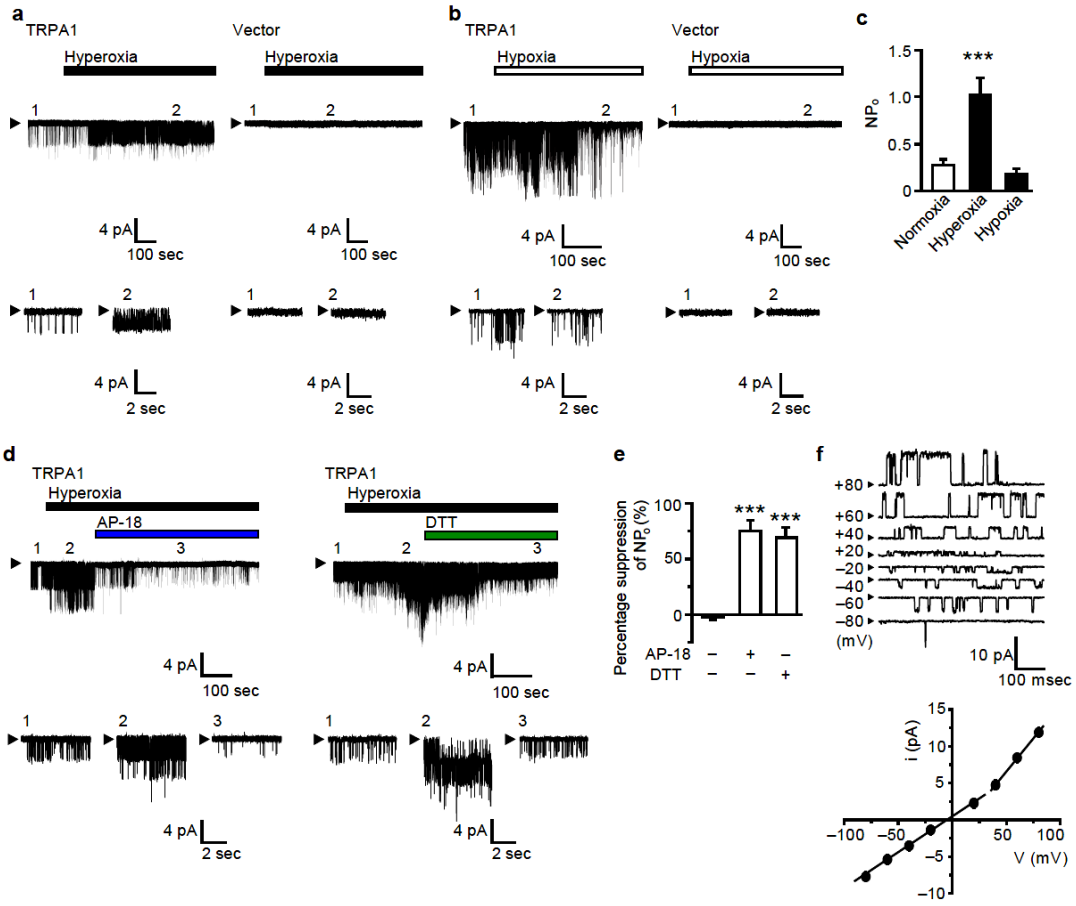

Figure 6. Single TRPA1 channel currents activated by hyperoxia. **a, b,** Single channel activities evoked by application of hyperoxic (**a**) and hypoxic (**b**) solutions at –60 mV in inside-out patches excised from HEK293T cells transfected with TRPA1 (left) or vector (right). Time-expanded current traces before (trace 1) and during (trace 2) application are also shown in the bottom panels. Arrowheads represent the closed state. **c,** Averages of NP_O (N, number of channels; P_O, open probability) representing single TRPA1 channel activity in normoxia (n = 35), hyperoxia (n = 20) and hypoxia (n = 14). $^{***}P < 0.001$ compared to normoxia. **d,** Suppression of hyperoxia-evoked single channel currents by AP-18 and DTT at –60 mV in inside-out patches excised from HEK293T cells expressing TRPA1. Time-expanded current traces in normoxia (trace 1) and in hyperoxia without (trace 2) and with the agents (trace 3) are shown in the bottom panels. Arrowheads represent the closed state. **e,** Percentage suppression of hyperoxia-induced NP_O in control (n = 29) and after application of AP-18 (n = 8) or DTT (n = 11). Data points are mean ± s.e.m.. $^{***}P < 0.001$ compared to cells maintained in hyperoxia without the agents. **f,** Representative current traces of single TRPA1 channel evoked by hyperoxia at different voltages in inside-out patches excised from TRPA1-expressing HEK293T cells (top). Arrowheads represent the closed state. Current-voltage (i-V) relationship for unitary currents (n = 5–8) (bottom).

O_2-sensing mechanisms in TRPA1 channels.

To quantitatively understand the physicochemical basis of the O_2 sensitivity of TRPA1, redox-sensitive TRP channels[26] were assessed using a congeneric series of reactive disulfides[42]. A strong dependence of the redox potentials on substituents (Table 2) suggests that the resulting changes in the electron density distribution of the aromatic ring affect the reduction propensity of the disulfide bond, indicating that redox potential is an excellent index for electrophilicity of reactive disulfides as electron acceptors (Fig. 7a). Indeed, plotting of $[Ca^{2+}]_i$ rises against redox potentials of reactive disulfide stimuli revealed positive correlations between these parameters, and threshold redox potentials (x-intercepts) for respective TRPs (Fig. 7b, left panel). This strongly suggests that Cys free sulfhydryl(s) acting as an electron donor(s) attacks disulfide bonds of compounds and induces disulfide exchange reactions in activation of redox-sensitive TRP channels (Fig. 7a). Strikingly, among the TRPs tested, only TRPA1 responded to inert electrophiles with a redox potential of –3,050 mV. The redox potential of O_2 (–2,765 mV) was less negative than the threshold redox potential for TRPA1 but was more negative than that for TRPV1, TRPV2, TRPV3, TRPV4 and TRPC5. Indeed, these TRPs failed to respond to hyperoxia (Fig. 7b). Thus, TRPA1 is unique in having a prominent susceptibility to Cys oxidation, such that it is activated by the weak oxidant O_2.

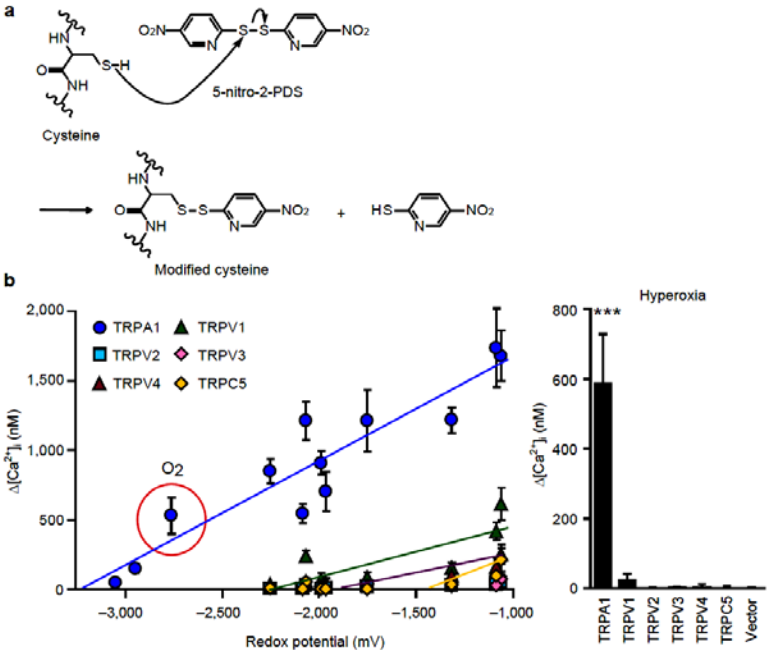

Figure 7. Oxidation sensitivity of TRP channels. **a,** A likely chemical mechanism underlying the action of a reactive disulfide compound, 5-nitro-2-PDS, via Cys sulfhydryls on TRPA1. **b,** Plots of $[Ca^{2+}]_i$ rises induced by 10 μM reactive disulfides (see Table 2) and O_2 in HEK293 cells expressing redox-sensitive TRP channels against redox potentials of respective substances (left) (n = 13–33). O_2 is applied at a hyperoxic level with PO_2 of 655 ± 32 mmHg (corresponding to 1.13 mM). The plotted data are fit to straight lines by the least squares method. Maximum $[Ca^{2+}]_i$ rises evoked by O_2 in HEK293 cells expressing redox-sensitive TRP channels (right) (n = 15–28). $^{***}P < 0.001$ compared to vector.

Table 2. Redox potentials ($E_{1/2}$ values) of reactive disulfides determined by rotating disk-electrode voltammetry.

Reactive disulfide compound	Structure	Redox potential ($E_{1/2}$ value)
5-nitro 2-pyridyl disulfide (5-nitro 2-PDS)	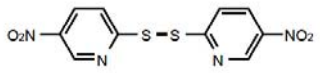	−1,064 mV
4-nitro phenyl disulfide	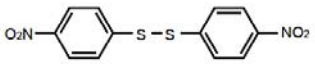	−1,088 mV
4-pyridyl disulfide	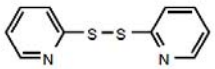	−1,316 mV
3-nitro phenyl disulfide	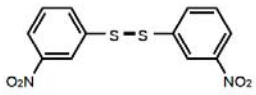	−1,754 mV
4-chloro phenyl disulfide	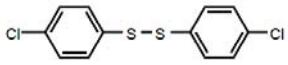	−1,966 mV
4-tolyl disulfide	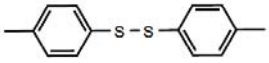	−1,990 mV
phenyl disulfide	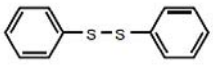	−2,071 mV
4-methoxy phenyl disulfide	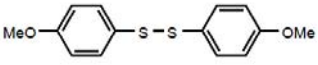	−2,085 mV
4-amino phenyl disulfide	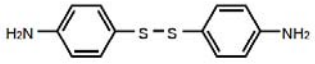	−2,252 mV
diallyl disulfide	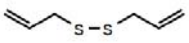	−2,950 mV
dipropyl disulfide	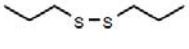	−3,050 mV

Cys-to-serine TRPA1 mutants C173S, C192S, C414S, C421S, C633S, C641S, C665S, C786S, C834S and C856S showed significantly suppressed responses to hyperoxia (Fig. 8a), as well as to diallyl disulfide (10 μM) having a redox potential similar to O_2 (Fig. 8b). In C414S, C421S, C786S and C834S, mutations likely have deleterious effects on channel function at large, because they significantly suppressed responses to 100 μM 2-aminoethyl diphenylborinate (2-APB) (Fig. 8c), which activates TRPA1 independently of Cys modification[29]. The mutants with impaired responses to hyperoxia were further assessed by the patch clamp method at fixed membrane potentials and under a defined and optimized intracellular composition, using pipette solution containing polytriphosphate (10 mM) and Ca^{2+} (30 nM), which sensitizes activity and prevents inactivation, respectively, of TRPA1[36,43]. Other than those non-functional mutants, C633S, C856S and the double mutant C633S·C856S showed severely suppressed hyperoxia-induced currents, suggesting that Cys633 and Cys856 are main target sites of O_2 in hyperoxia (Fig. 8d). C633S, C856S and C633S·C856S showed significantly suppressed O_2 responses, and required stronger reactive disulfides such as 5-nitro-2-PDS at higher concentrations for full activation compared to wild-type (WT) (Fig. 8e–g). Incorporation of DTNB-2Bio, which is the reactive disulfide DTNB derivative with two biotin groups attached for detection[26], into green fluorescent protein-tagged TRPA1 (GFP-TRPA1) was abolished by C633S but not by C856S (Fig. 8h). These findings, together with the complete suppression of hyperoxia-induced TRPA1 response by DTT (Figs. 3g, 5e, g and 6d, e), suggest that the free sulfhydryls of Cys633 and Cys856 act as nucleophiles to directly attack electrophiles such as O_2 and reactive disulfides, and this oxidative modification is stably maintained for Cys633 in TRPA1 activation (Fig. 7a).

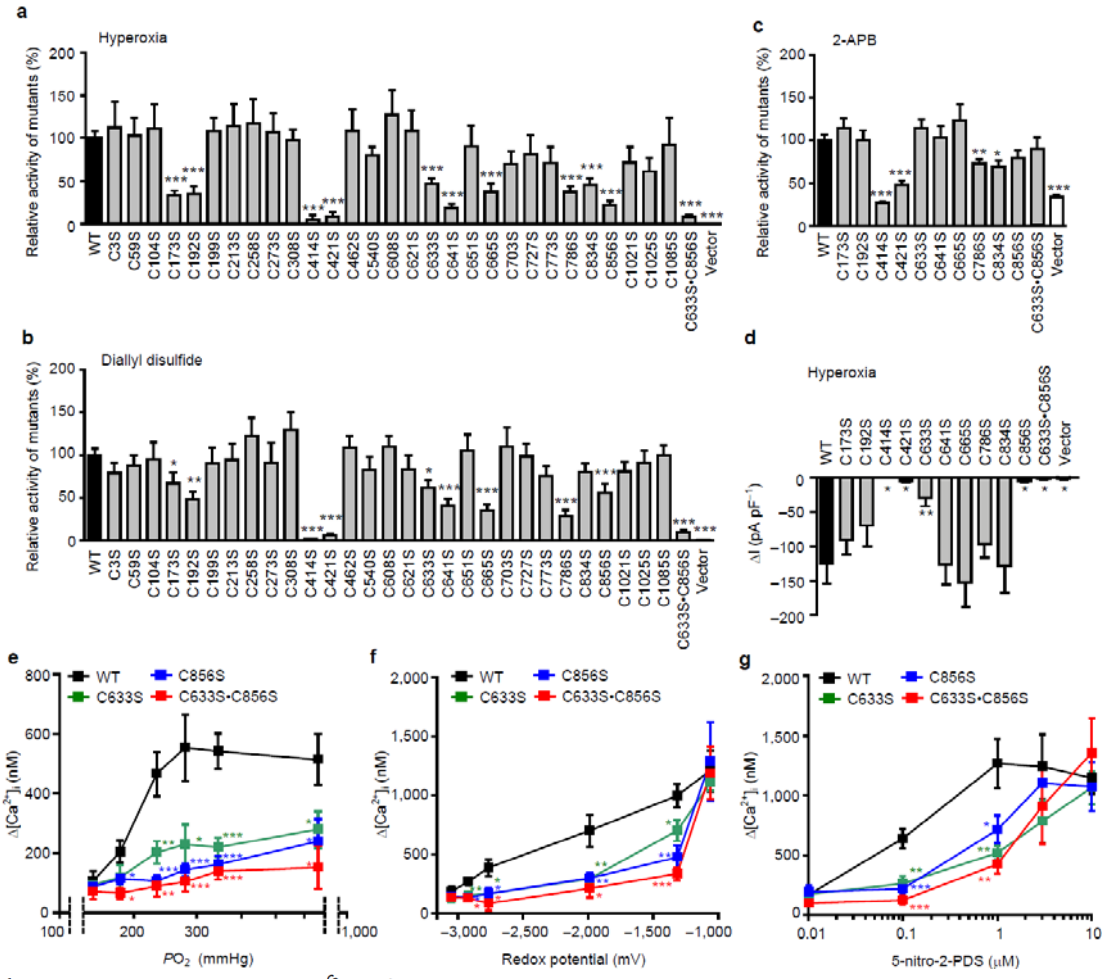

Figure 8. O_2 activates TRPA1 through Cys modification. **a,** Relative Ca^{2+} responses to O_2 of TRPA1 Cys mutants in HEK293 cells (n = 17–109). **b,** Relative Ca^{2+} responses of TRPA1 Cys mutants to 10 μM diallyl disulfide, which has a redox potential comparable to O_2, in HEK293 cells (n = 16–44). **c,** Relative Ca^{2+} responses to 100 μM 2-APB of TRPA1 Cys mutants, which showed impaired response to hyperoxia, in HEK293 cells (n = 20–67). $^{*}P < 0.05$, $^{**}P < 0.01$ and $^{***}P < 0.001$ compared to WT. **d,** O_2-evoked current responses (ΔI) of TRPA1 Cys mutants. The basal density of whole cell inward currents in normoxia is subtracted from that recorded after the O_2 treatment at –100 mV (n = 5–18). **e,** The relationships between PO_2 and maximum $[Ca^{2+}]_i$ rises mediated by WT TRPA1, C633S, C856S or C633S·C856S in HEK293 cells (n = 17–43). **f,** Plots of $[Ca^{2+}]_i$ rises induced by 10 μM dipropyl disulfide, diallyl disulfide, 4-tolyl disulfide, 4-pyridyl disulfide, 5-nitro-2-PDS and O_2 in HEK293 transfected with TRPA1 constructs against redox potentials of respective substances (n = 19–40). **g,** Dose-response relationships of 5-nitro-2-PDS-induced maximum $[Ca^{2+}]_i$ rises in HEK293 cells transfected with TRPA1 constructs (n = 23–45). $^{*}P < 0.05$, $^{**}P < 0.01$ and $^{***}P < 0.001$ compared to WT. **h,** Effects of mutations C633S and C856S on DTNB-2Bio incorporation into TRPA1 proteins. Western blotting (WB) of total lysates indicates comparable TRPA1 expression (lysates). Data points are mean ± s.e.m..

Alignment of the consensus sequences for the prolyl hydroxylation motif[20,21] and the asparaginyl hydroxylation motif[20,44] with the amino-acid sequence of TRPA1 revealed conservation of these motifs in the N-terminal cytoplasmic ankyrin repeat of TRPA1 (Fig. 9a, b). This prompted us to hypothesize that decreased activity of PHDs and FIH expressed in the nodose ganglion (Fig. 9c) underlies TRPA1 activation in hypoxia. Indeed, the pan-hydroxylase inhibitor dimethyloxalylglycine (DMOG) induced Ca^{2+} responses (Fig. 9d) and currents via TRPA1 that were suppressed by AP-18 (Fig. 9e–h). Furthermore, cotransfection of catalytically dead dominant negative mutants for PHD1 (PHD1-Mut), PHD2 (PHD2-Mut) and PHD3 (PHD3-Mut), but not that for FIH (FIH-Mut), elevated basal $[Ca^{2+}]_i$ indicative of constitutive TRPA1 activation, and abolished TRPA1 responses to hypoxia and DMOG (Fig. 10a, b). By contrast, all hydroxylase mutants failed to affect TRPA1 responses to both 2-APB and hyperoxia (Fig. 10c, d). The TRPA1 mutant P394A carrying alanine substitution for Pro394 of the prolyl hydroxylation motif[20,21] significantly elevated basal TRPA1 activity, and abrogated TRPA1 responses to hypoxia and DMOG (Fig. 11a–e) but not to 2-APB and hyperoxia (Fig. 11f, g). Furthermore, GFP-TRPA1 showed coimmunoprecipitation with PHD1–3-Flag, which was reduced in GFP-P394A (Fig. 12a). These results suggest that hydroxylation of Pro394 by PHDs inhibits TRPA1 channels in normoxia, while a decrease in O_2 concentration diminishes PHD activity, to relieve TRPA1 from inhibition, leading to channel activation in hypoxia. Interestingly, among the Cys mutants, C641S and C665S showed significantly suppressed responses to hypoxia (Fig. 12b). Modification of Cys641 and Cys665 may be also involved in sensing low O_2 availability.

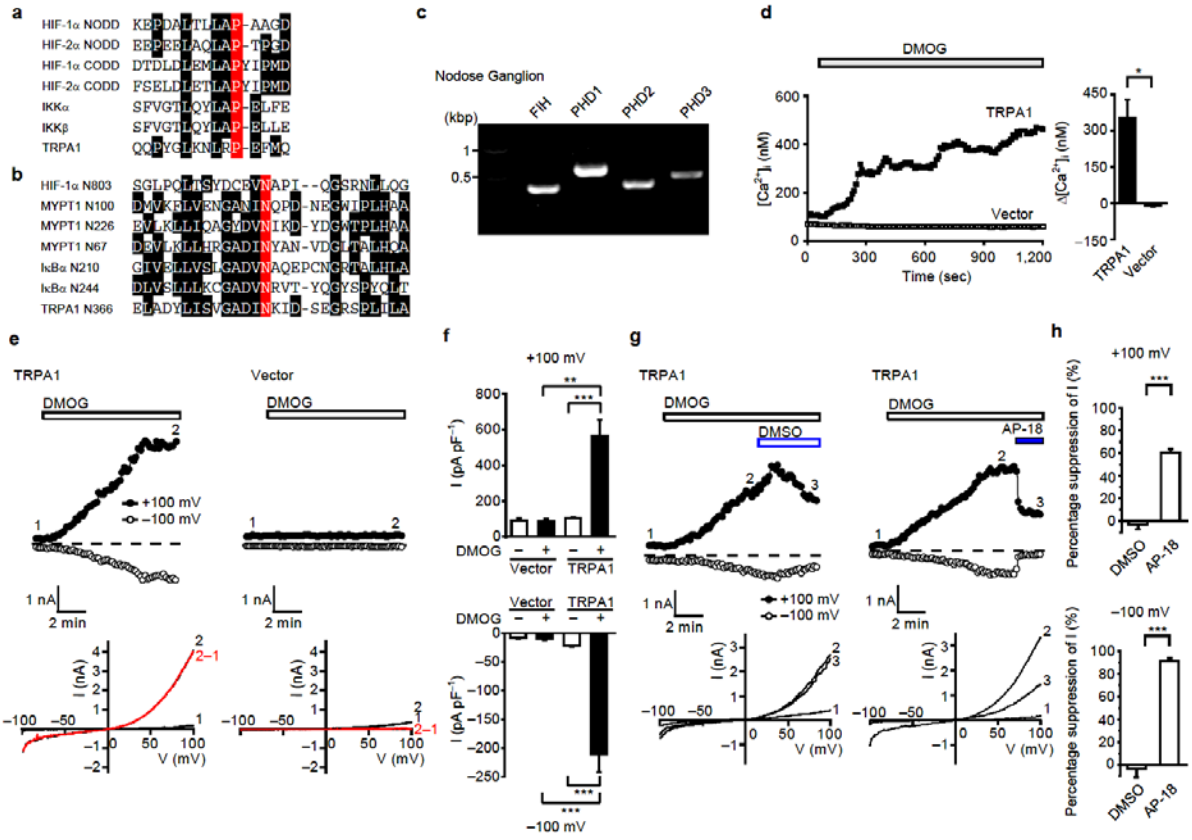

Figure 9. Inhibition of prolyl and asparaginyl hydroxylase elevates TRPA1 activity. **a,** Alignment of amino acid residues 384–398 of human TRPA1 with conserved prolyl hydroxylation motif within N-terminal and C-terminal O_2-dependent degradation domain (NODD and CODD, respectively) of HIF-1α and HIF-2α, IKKα and IKKβ. **b,** Alignment of amino acid residues 353–379 of human TRPA1 with asparaginyl hydroxylation motif within HIF-1α, myosin phosphatase targeting subunit 1 (MYPT1) and inhibitor of NF-κB (IκBα). **c,** RNA expression of FIH and PHD1–3 detected by RT-PCR in mouse nodose ganglion neurons. **d,** Ca^{2+} responses of TRPA1 to 3 mM DMOG in HEK293 cells. Averaged time courses (left) and $[Ca^{2+}]_i$ rises at 1,080–1,200 sec (right) (n = 23–40). **e,** Representative time courses of 3 mM DMOG-evoked outward and inward currents recorded at +100 and –100 mV, respectively, under ramp clamp in HEK293T cells transfected with TRPA1 (left) or vector (right) (top). Corresponding *I-V* relationships at the time points 1 and 2, and those of evoked currents (2–1) are shown (bottom). **f,** Peak current densities at +100 (top) and –100 mV (bottom) in the presence or absence of DMOG (n = 7–21). $^{**}P < 0.01$ and $^{***}P < 0.001$. **g,** Suppression of 3 mM DMOG-evoked whole cell currents by 10 μM AP-18 in TRPA1-expressing HEK293T cells. Cells exposed to DMOG are treated with 0.1% DMSO (left) or AP-18 (right). Representative time courses of outward and inward currents recorded at +100 and –100 mV, respectively, under ramp clamp (top). Corresponding *I-V* relationships at the time points 1–3 (bottom). **h,** Percentage suppression of DMOG-activated TRPA1 current at 3-min after the peak relative to that at the peak in the presence of DMOG (n = 7).

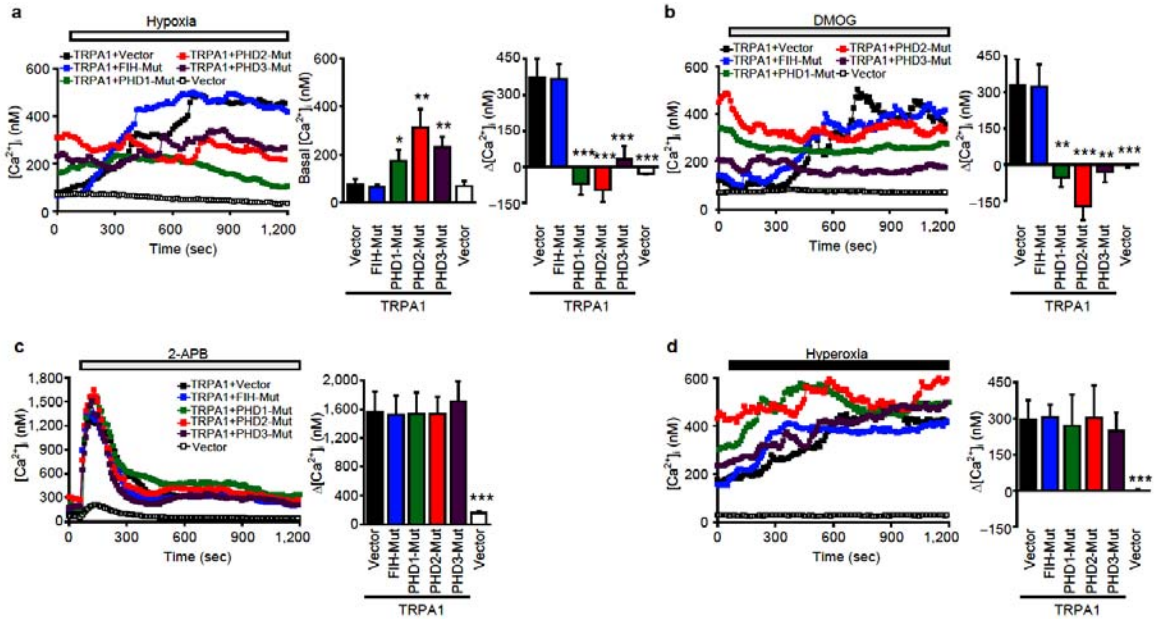

Figure 10. Inhibition of PHDs elevates basal TRPA1 activity and abrogates TRPA1 responses to hypoxia and DMOG. **a, b,** Inhibition of PHD1–3 activates TRPA1 without hypoxic stimulus (**a**) or 3 mM DMOG (**b**). Averaged time courses (left), basal $[Ca^{2+}]_i$ levels (middle in **a**) and $[Ca^{2+}]_i$ rises at 1,080–1,200 sec (right) in TRPA1-expressing HEK293 cells cotransfected with catalytically dead mutants (FIH-Mut, PHD1-Mut, PHD2-Mut or PHD3-Mut) (n = 13–50). **c, d,** Ca^{2+} responses of TRPA1 to 100 μM 2-APB (**c**) (n = 18–26) and hyperoxia (**d**) (n = 16–29) are unaffected by inhibition of PHD1–3 and FIH. Averaged time courses (left) and $[Ca^{2+}]_i$ rises (right) at the maximum (**c**) and at 1,080–1,200 sec (**d**). $^{*}P < 0.05$, $^{**}P < 0.01$ and $^{***}P < 0.001$ compared to cotransfection of TRPA1 with vector.

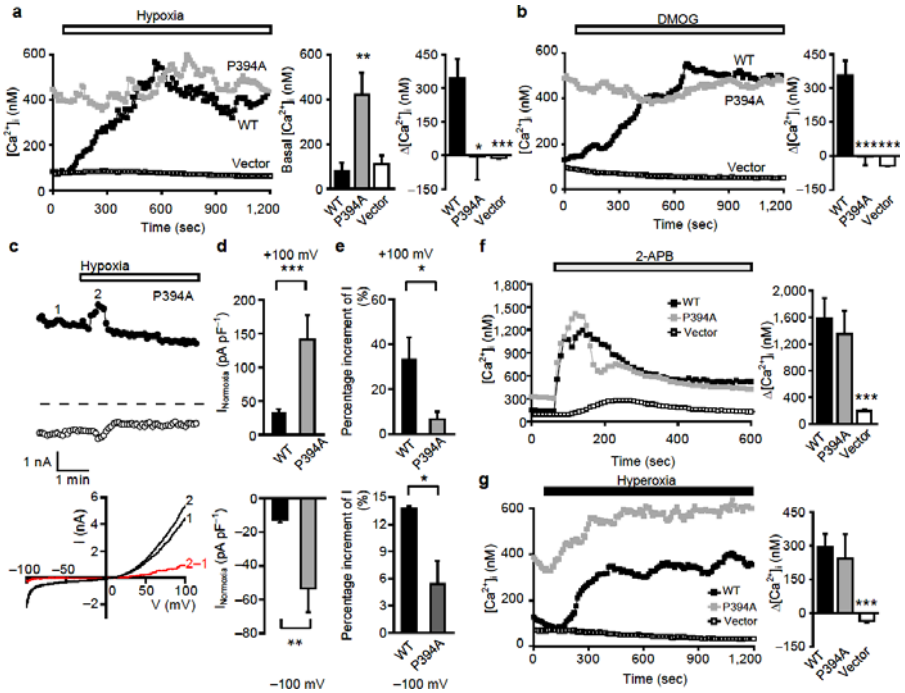

Figure 11. P394A mutation induces spontaneous activation of TRPA1 without hypoxic stimulus or DMOG. **a, b,** Averaged time courses (left), basal $[Ca^{2+}]_i$ levels (middle in **a**) and hypoxia- (**a**) or 3 mM DMOG-evoked $[Ca^{2+}]_i$ rises (**b**) at 1,080–1,200 sec (right) in HEK293 cells transfected with TRPA1 costructs (n = 15–27). $^{*}P < 0.05$, $^{**}P < 0.01$ and $^{***}P < 0.001$ compared to WT. **c,** Representative time courses of outward and inward currents recorded at +100 and –100 mV, respectively, by whole cell patch clamp method under ramp clamp in hypoxic solution in P394A-expressing HEK293T cells (top).

Corresponding *I-V* relationships at the time points 1 and 2, and those of hypoxia-evoked current (2–1) are shown (bottom). **d,** Peak current densities at +100 (top) and –100 mV (bottom) in normoxic condition in HEK293T cells transfected with TRPA1 constructs (n = 23–38). **e,** Percentage increment of the current at the peak in hypoxia relative to that in normoxia (n = 6–24). $^{*}P < 0.05$, $^{**}P < 0.01$ and $^{***}P < 0.001$. **f, g,** Ca^{2+} responses of TRPA1 to 2-APB (**f**) (n = 18–24) and hyperoxic solution (**g**) are unaffected by P394A mutation (n = 16–20). Averaged time courses (left) and $[Ca^{2+}]_i$ rises (right) at the maximum (**f**) and at 1,080–1,200 sec (**g**) in HEK293 cells transfected with TRPA1 constructs. Data points are mean ± s.e.m.. $^{***}P < 0.001$ compared to WT.

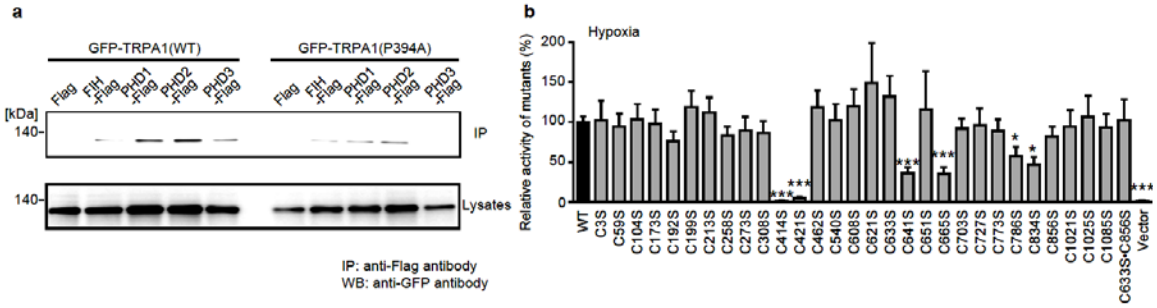

Figure 12. Co-immunoprecipitation of TRPA1(WT) or TRPA1(P394A) with FIH and PHD1–3. a, Immunoprecipitates (IP) with antibody to Flag are subjected to WB with antibody to GFP. **b,** Relative Ca^{2+} responses to hypoxia of TRPA1 Cys mutants in HEK293 cells (n = 14–48). Data points are mean ± s.e.m.. $^{*}P < 0.05$ and $^{***}P < 0.001$ compared to WT.

TRPA1 controls respiratory reflexes *in vivo* in hyperoxia and hypoxia.

Ionic currents and Ca^{2+} responses induced by hyperoxia and hypoxia were substantially blocked by AP-18 in nodose ganglion neurons (Fig. 13). The majority of hyperoxia- and hypoxia-responsive cells also responded to the TRPV1 agonist capsaicin (Table 1), as reported previously[13]. Notably, hyperoxia- and hypoxia-induced ionic currents and Ca^{2+} responses were largely absent in nodose neurons isolated from *Trpa1* KO mice (Fig. 13). Nodose neurons prepared from *Trpa1* KO mice responded well to capsaicin and to membrane depolarization induced by 60 mM KCl, indicating intact TRPV1 and voltage-dependent Ca^{2+} channels (Fig. 13c, d). KCl-responsive sensory neurons from dorsal root ganglia (DRG) of WT mice exhibited robust responses to hyperoxia and hypoxia, while those of *Trpa1* KO mice exhibited impaired responses to hyperoxia and

hypoxia (Fig. 14). These results suggest that hyperoxia and hypoxia activate native TRPA1 channels in mouse nodose ganglion neurons and sensory neurons.

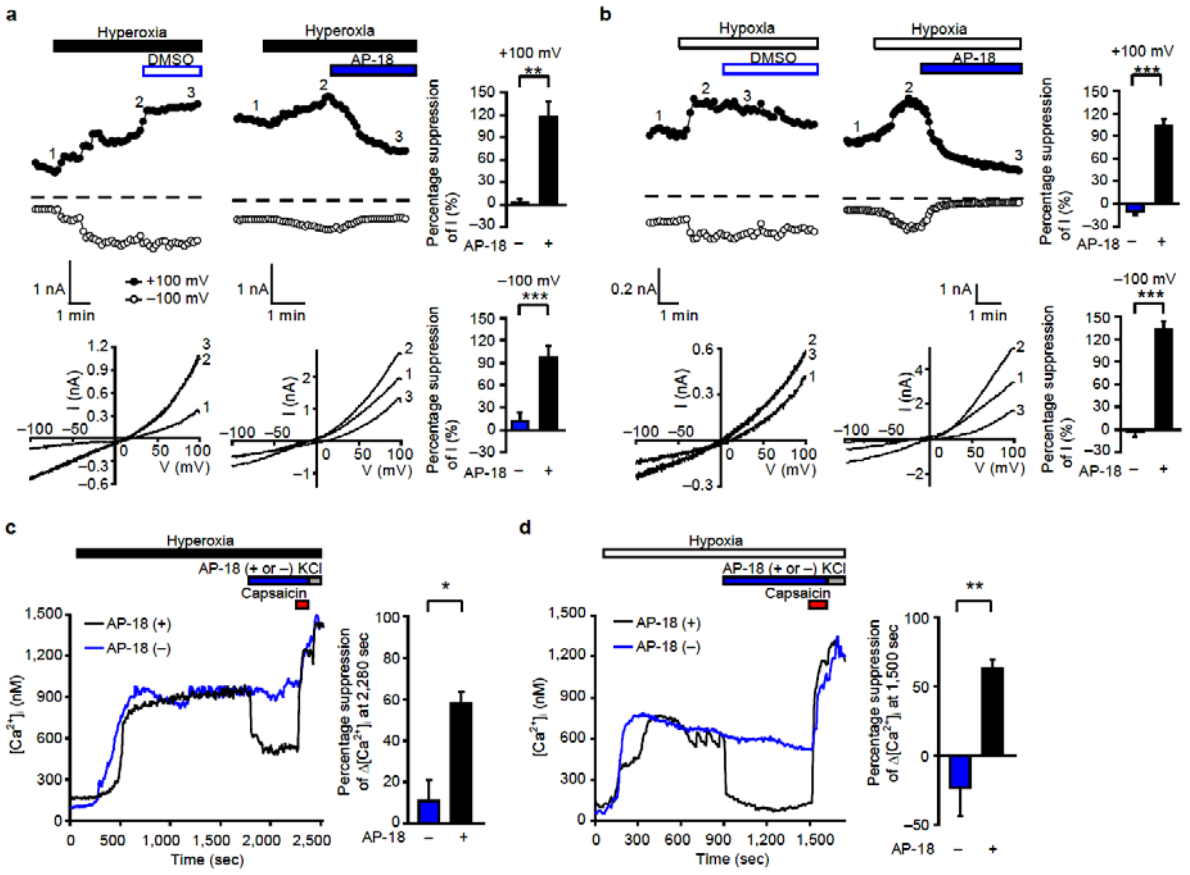

Figure 13. TRPA1 mediates hyperoxia- and hypoxia-induced Ca^{2+} responses and ionic currents in mouse nodose ganglion neurons. **a, b,** Suppression of hyperoxia- (**a**) (n = 6–7) and hypoxia-evoked whole cell currents (**b**) (n = 5–7) by 10 μM AP-18 in WT nodose ganglion neurons. Representative time courses of outward and inward currents recorded at +100 and –100 mV, respectively, under ramp clamp in hyperoxic (**a**) or hypoxic (**b**) solution (top). Corresponding *I-V* relationships at the time points 1–3 (bottom). Right panels show percentage suppression of the currents at 3-min after the peak relative to that at the peak. **c, d,** Suppression of hyperoxia- (**c**) and hypoxia-induced Ca^{2+} responses (**d**) by AP-18 in WT nodose ganglion neurons. Representative time courses (left) and percentage suppression of $[Ca^{2+}]_i$ rises (right) at 2,280 sec (**c**) and 1,500 sec (**d**) relative to maximal rises in hyperoxia- (**c**) and hypoxia-responding neurons (**d**), respectively (n = 6–11). Data points are mean ± s.e.m.. $^{*}P < 0.05$, $^{**}P < 0.01$ and $^{***}P < 0.001$.

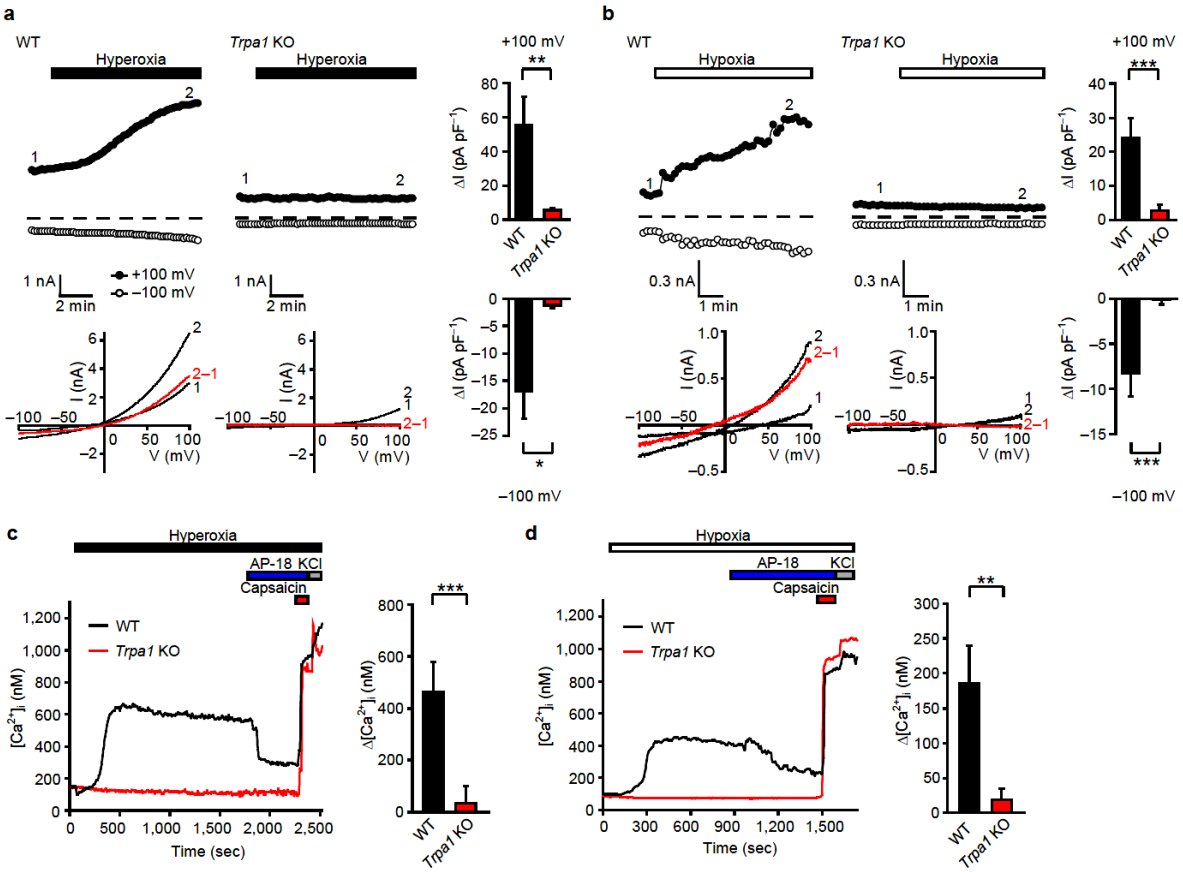

Figure 14. Ablated responses to hyperoxia and hypoxia in *Trpa1* KO nodose ganglion neurons. **a, b,** Hyperoxia- (**a**) and hypoxia-induced currents (**b**) are abolished in *Trpa1* KO nodose ganglion neurons (n = 16 and 19). Representative time courses of outward and inward currents recorded at +100 and –100 mV, respectively, under ramp clamp in hyperoxic (**a**) or hypoxic (**b**) solution in nodose ganglion neurons isolated from WT or *Trpa1* KO mice (top). Corresponding *I-V* relationships at the time points 1 and 2, and those of evoked currents (2–1) (bottom). Right panels show hyperoxia- (**a**) and hypoxia-induced current densities (**b**) evoked at +100 and –100 mV. $^{*}P < 0.05$, $^{**}P < 0.01$ and $^{***}P < 0.001$. **c, d,** Ablated hyperoxia- (**c**) and hypoxia-induced Ca^{2+} responses (**d**) in *Trpa1* KO nodose ganglion neurons. Representative time courses (left) and maximum $[Ca^{2+}]_i$ rises at 60–1,800 sec (**c**) or 60–900 sec (**d**) (right) in capsaicin-sensitive neurons (n = 13–46). Data points are mean ± s.e.m.. $^{*}P < 0.05$, $^{**}P < 0.01$ and $^{***}P < 0.001$.

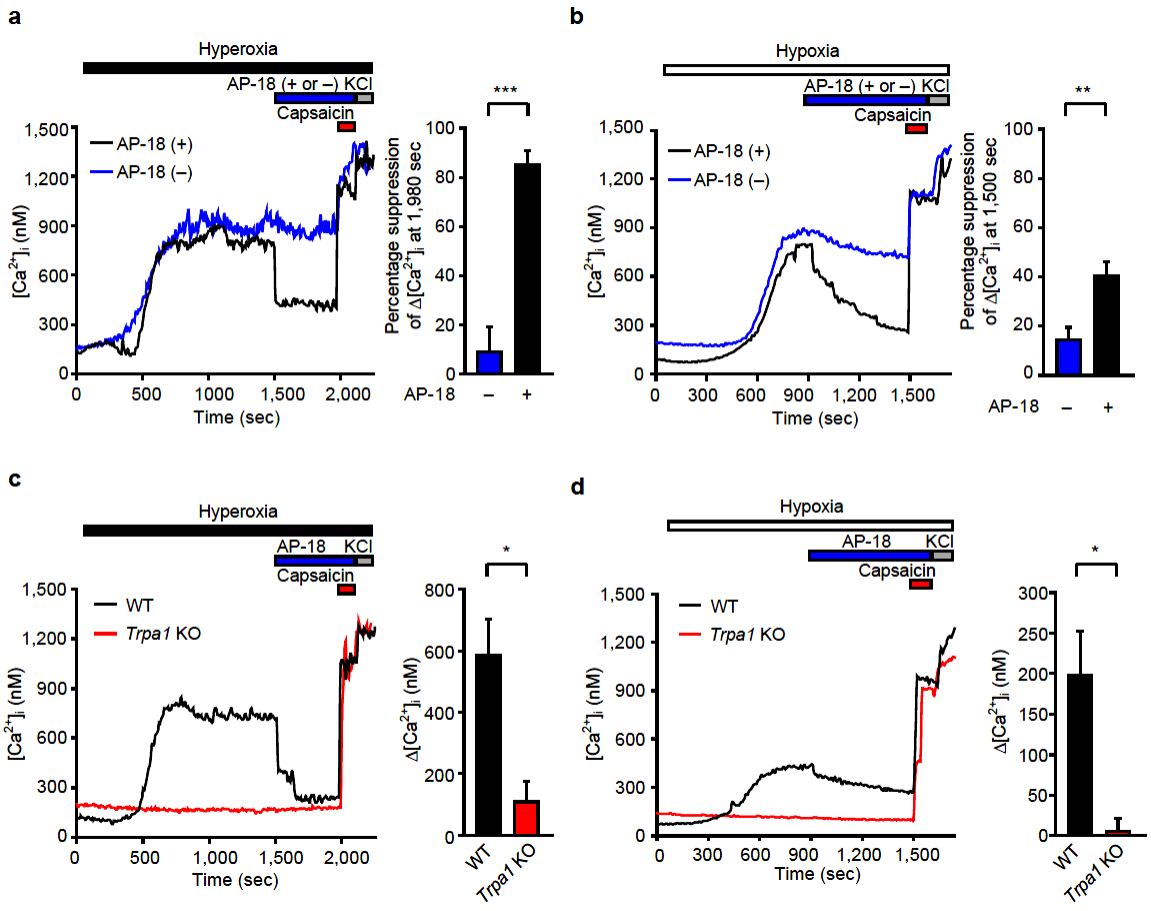

Figure 14. Hyperoxia and hypoxia evoke TRPA1 responses in mouse DRG neurons. **a, b,** Suppression of hyperoxia- (**a**) and hypoxia-induced Ca^{2+} responses (**b**) by AP-18 in WT DRG neurons. Representative time courses (left) and percentage suppression of $[Ca^{2+}]_i$ rises (right) at 1,980 sec (**a**) and 1,500 sec (**b**) relative to maximal rises in neurons responding to hyperoxia (**a**) and hypoxia (**b**), respectively (n = 11–35). **c, d,** Ablated Ca^{2+} responses to hyperoxia (**c**) and hypoxia (**d**) in *Trpa1* KO DRG neurons. Representative time courses (left) and maximum $[Ca^{2+}]_i$ rises at 60–1,500 sec (**c**) or 60–900 sec (**d**) in capsaicin-sensitive neurons (n = 12–49). Data points are mean ± s.e.m.. $^{*}P < 0.05$, $^{**}P < 0.01$ and $^{***}P < 0.001$.

We then evaluated the roles of TRPA1 *in vivo* in regulating vagal activities under systemic hyperoxia and hypoxia. Exposure of WT mice to hyperoxic (100% O_2) or hypoxic gas (10, 13 and 15% O_2) via a tracheal cannula significantly enhanced discharges of afferents in the cervical vagal trunk (Fig. 15) and superior laryngeal afferents (Fig. 16) as shown by multifiber neurogram. In *Trpa1* KO mice, the enhancement of nerve discharges by hyperoxia and mild hypoxia (15% O_2) was abolished, while that by severe

hypoxia (10 and 13% O_2) was intact. Basal activity in normoxia (20% O_2) of vagal and superior laryngeal afferents in *Trpa1* KO mice was indistinguishable from that in WT mice. Interestingly, only severe hypoxia (10% O_2) increased the discharge of glossopharyngeal afferents, which was unaffected by *Trpa1* deficiency (Fig. 17). Thus, TRPA1 regulates discharges in vagal and superior laryngeal afferents stimulated by hyperoxia and mild hypoxia (15% O_2), but not those in vagal, superior laryngeal and glossopharyngeal afferents stimulated by severe hypoxia (10 or 13% O_2). It should be noted that the O_2 levels that enhance discharges via TRPA1 in vagal and superior laryngeal afferents correspond well with the O_2 levels that trigger ventilatory responses via these nerves as demonstrated in the sectioning experiment (Fig. 1b).

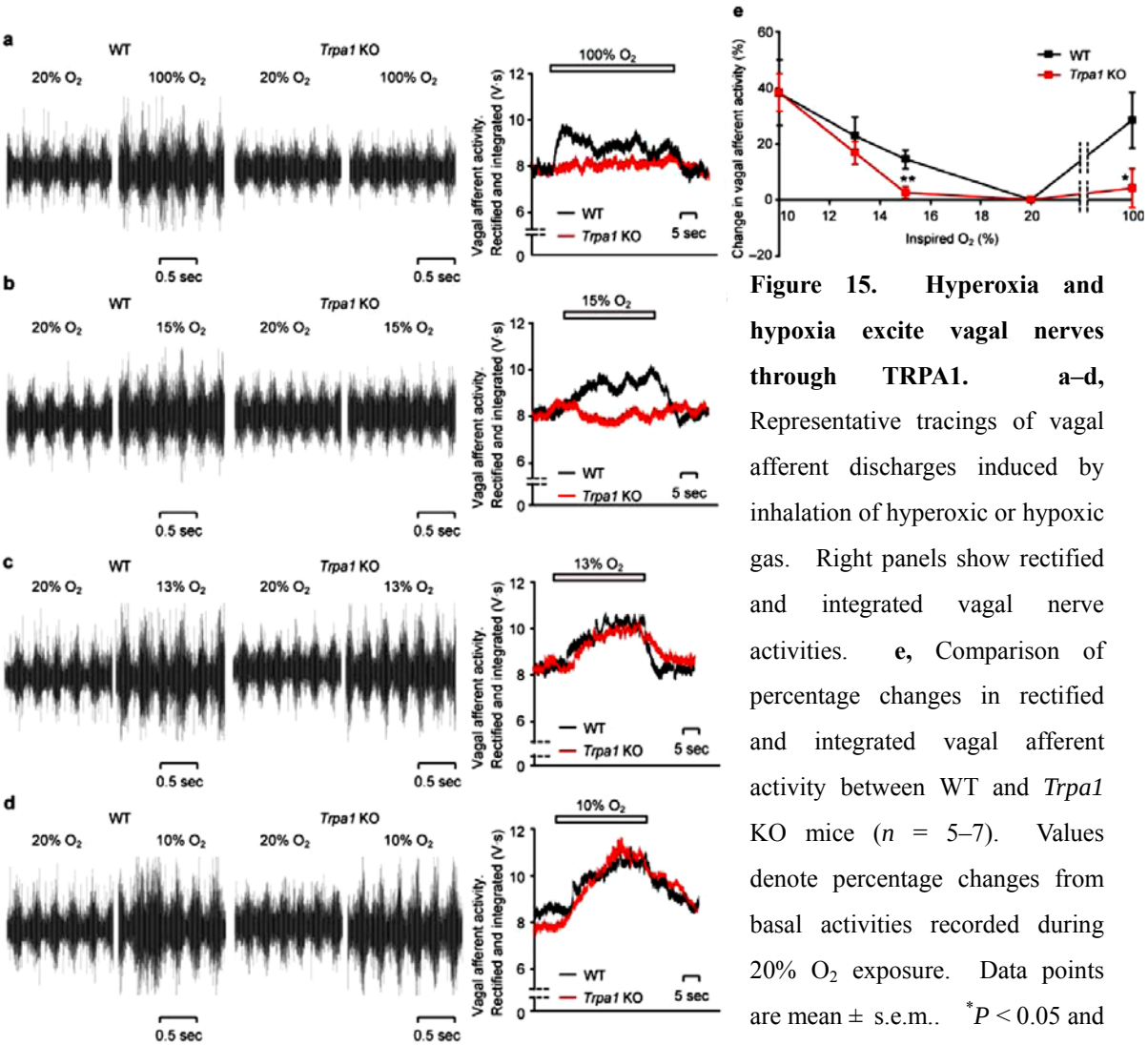

Figure 15. Hyperoxia and hypoxia excite vagal nerves through TRPA1. a–d, Representative tracings of vagal afferent discharges induced by inhalation of hyperoxic or hypoxic gas. Right panels show rectified and integrated vagal nerve activities. **e,** Comparison of percentage changes in rectified and integrated vagal afferent activity between WT and *Trpa1* KO mice (n = 5–7). Values denote percentage changes from basal activities recorded during 20% O_2 exposure. Data points are mean ± s.e.m.. $^{*}P < 0.05$ and $^{**}P < 0.01$ compared to WT mice.

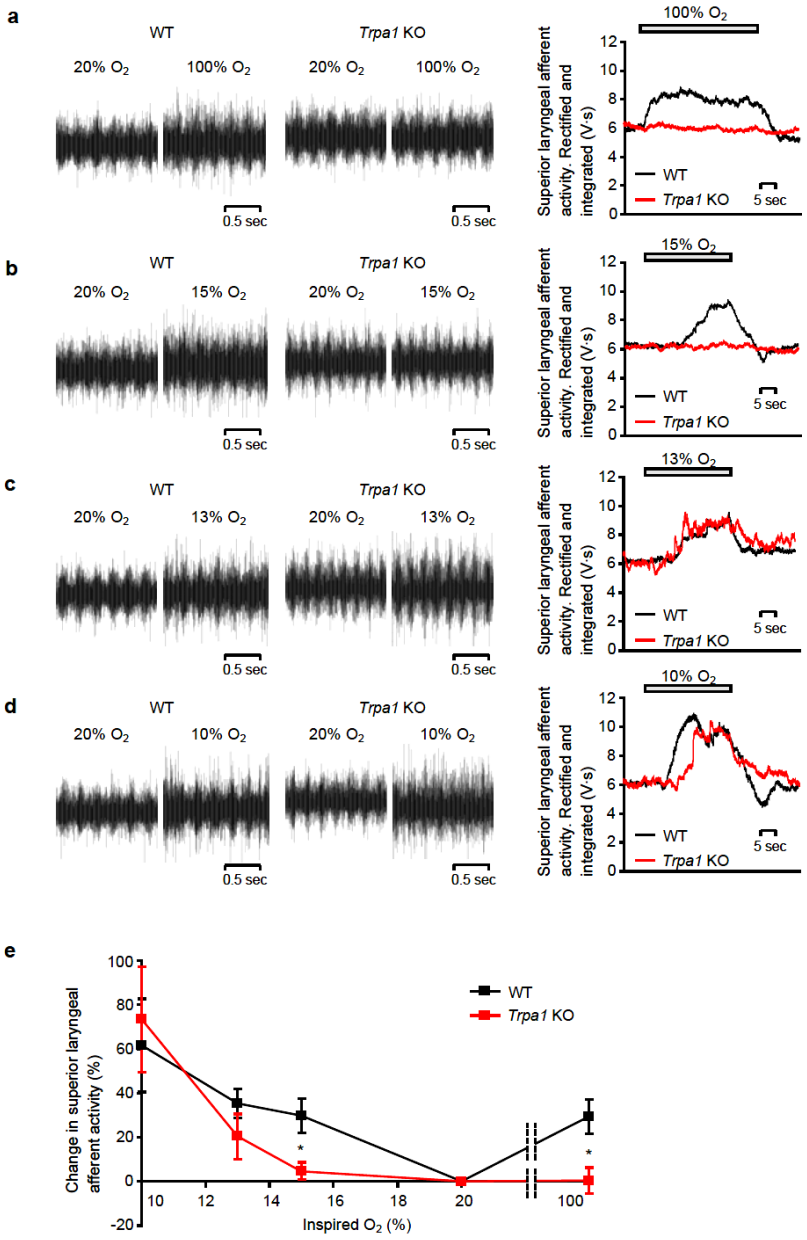

Figure 16. Defects of superior laryngeal afferent discharges under systemic hyperoxia and mild hypoxia (15% O_2) in *Trpa1* KO mice. **a–d,** Representative tracings of superior laryngeal afferent discharges induced by inhalation of hyperoxic or hypoxic gas. Right panels show rectified and integrated superior laryngeal afferent activities. **e,** Comparison of percentage change in rectified and integrated superior laryngeal nerve activity between WT and *Trpa1* KO mice (n = 4–7). Values denote percentage changes from basal activities recorded during 20% O_2 exposure. Data points are mean ± s.e.m.. $^{*}P < 0.05$ compared to WT.

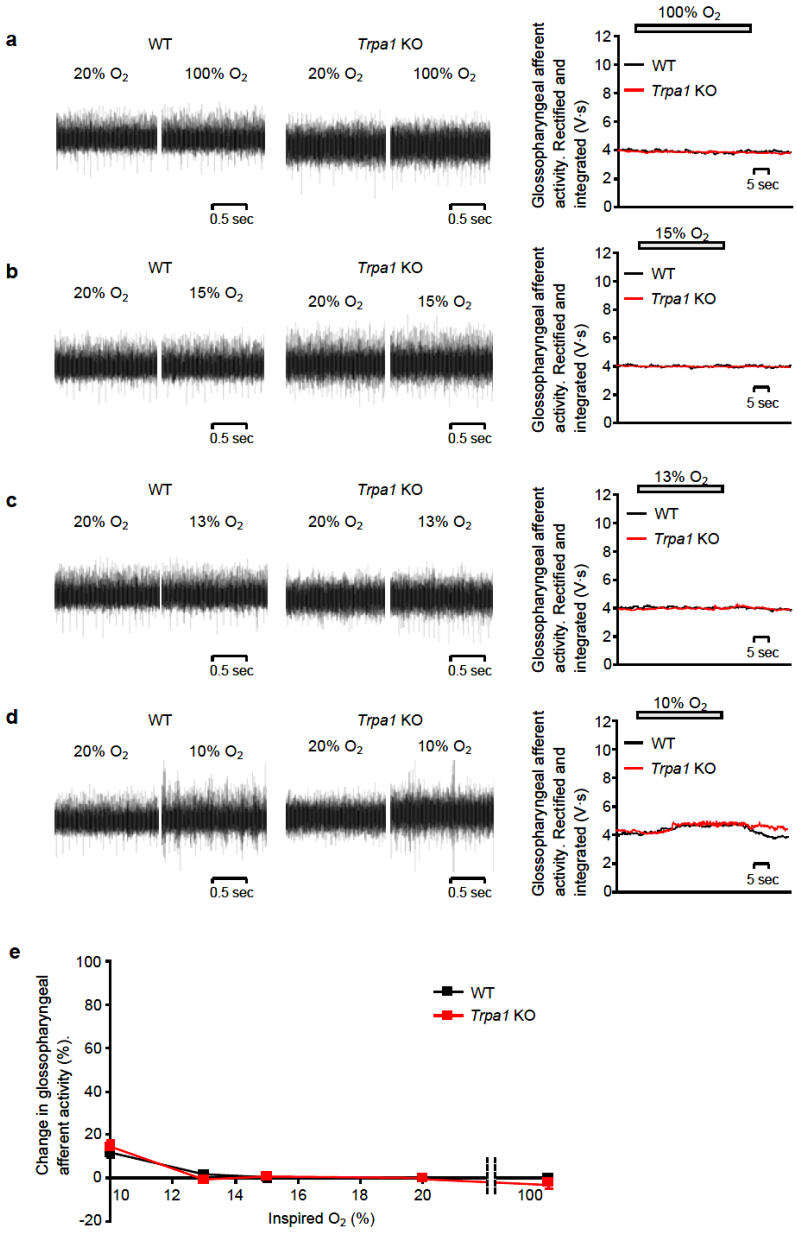

Figure 17. Intact responses of glossopharyngeal afferent discharges to systemic hyperoxia and hypoxia in *Trpa1* KO mice. a–d, Representative tracings of glossopharyngeal afferent discharges induced by inhalation of hyperoxic or hypoxic gas. Right panels show rectified and integrated glossopharyngeal afferent activities. **e,** Comparison of percentage change in rectified and integrated glossopharyngeal nerve activity between WT and *Trpa1* KO mice (n = 4–5). Values denote percentage changes from basal activities recorded during 20% O2 exposure. Data points are mean ± s.e.m.. No significant differences are observed between WT and *Trpa1* KO mice.

We studied the roles of TRPA1 in ventilatory responses in conscious mice, as measured by unrestrained plethysmography. Rf and minute volume (MV) were controlled by O_2 levels in WT mice: the magnitudes of Rf and MV were decreased by hyperoxia (50 and 80% O_2) but increased by hypoxia (10 and 15% O_2) (Fig. 18). Hyperoxia and hypoxia failed to affect tidal volume in WT mice (data not shown). Ventilatory responses to hyperoxia and mild hypoxia (15% O_2), but not to severe hypoxia (10% O_2), were inhibited by aerosolized AP-18. In *Trpa1* KO mice, ventilatory

responses to hyperoxia and mild hypoxia (15% O_2), but not to severe hypoxia (10% O_2), were significantly impaired (Fig. 19a, b). Ventilatory responses were unaffected by AP-18 in mutant mice (Fig. 19c, d). These results suggest that TRPA1 selectively mediates respiratory reflexes induced by hyperoxia and mild hypoxia.

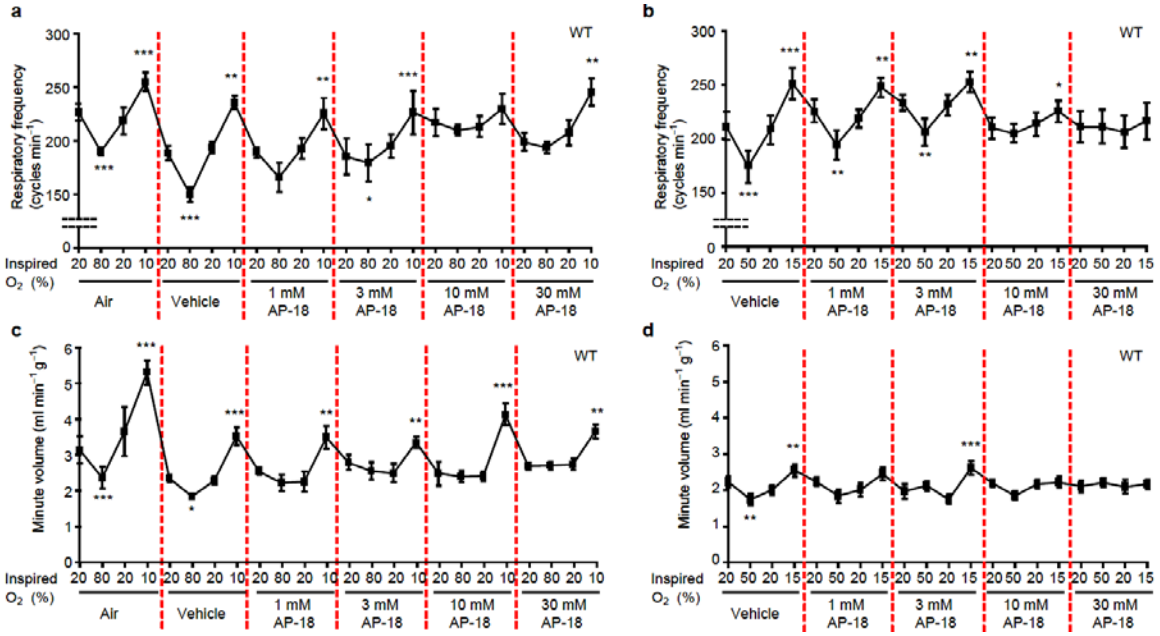

Figure 18. Ventilatory responses to hyperoxia and mild hypoxia (15% O_2) are likely mediated by TRPA1. Time-related changes in Rf (**a, b**) and MV (**c, d**) during exposure to aerosol of increasing dose of AP-18 in conscious WT, as measured by unrestrained plethysmography (n = 6–17). In **a** and **c**, mice are subjected to sequential exposure to 20% O_2 (20 min), 80% O_2 (5 min), 20% O_2 (20 min) and finally to 10% O_2 (5 min) without any aerosols. This is followed sequentially by the same protocol conducted in the presence of vehicle (20% EtOH in saline) aerosol, 1 mM AP-18 aerosol, 3 mM AP-18 aerosol, 10 mM AP-18 aerosol and finally 30 mM AP-18 aerosol. In **b** and **d**, mice are subjected to sequential exposure to 20% O_2 (20 min), 50% O_2 (5 min), 20% O_2 (20 min) and finally to 15% O_2 (5 min) without any aerosols. This is followed sequentially by the same protocol conducted in the presence of vehicle, 1 mM AP-18 aerosol, 3 mM AP-18 aerosol, 10 mM AP-18 aerosol and finally 30 mM AP-18 aerosol. To avoid hyperventilation-induced hypocapnia, inspired gas also contains 2% CO_2 throughout the experiment. Data points are mean ± s.e.m.. $^{*}P < 0.05$, $^{**}P < 0.01$ and $^{***}P < 0.001$ compared to preceding 20% O_2 periods. Repeated-measures ANOVA.

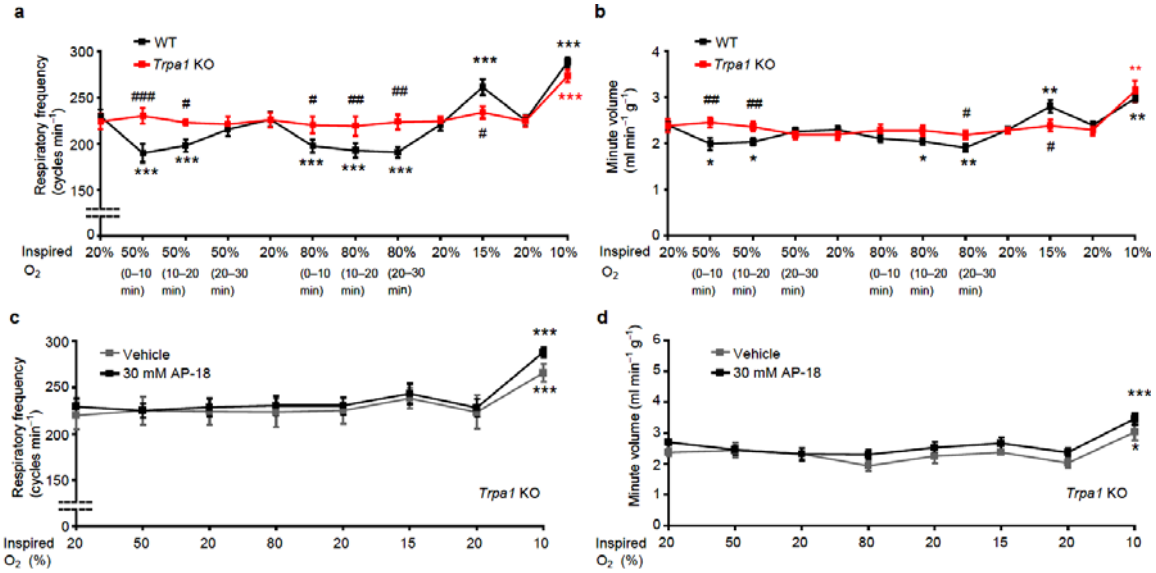

Figure 19. Defects of ventilatory responses to hyperoxia and mild hypoxia in *Trpa1* KO mice.TRPA1 controls ventilatory responses to hyperoxia and mild hypoxia in mice. **a, b,** Time-related changes in Rf (**a**) and MV (**b**) in conscious WT mice, as measured by unrestrained plethysmography (n = 8–9). Mice are subjected to sequential exposure to 20% O_2 (20 min), 50% O_2 (30 min), 20% O_2 (20 min), 80% O_2 (30 min), 20% O_2 (20 min), 15% O_2 (5 min), 20% O_2 (20 min) and to 10% O_2 (5 min). $^{\#}P$<0.05, $^{\#\#}P$<0.01, $^{\#\#\#}P$ <0.001 compared to WT mice. **c, d,** Ventilatory responses are unaffected by aerosolized AP-18 in *Trpa1* KO mice. Time-related changes in Rf (**c**) and MV (**d**) during exposure to aerosolized vehicle or 30 mM AP-18 in conscious *Trpa1* KO mice, as measured by unrestrained plethysmography (n =5). *Trpa1* KO mice are subjected to sequential exposure to 20% O_2 (20 min), 50% O_2 (5 min), 20% O_2 (20 min), 80% O_2 (5 min), 20% O_2 (20 min), 15% O_2 (5 min), 20% O_2 (20 min) and finally to 10% O_2 (5 min) in the presence of vehicle or 30 mM AP-18 aerosol. To avoid hyperventilation-induced hypocapnia, inspired gas also contains 2% CO_2 throughout the experiment. Data points are mean ± s.e.m.. $^{*}P < 0.05$, $^{**}P < 0.01$ and $^{***}P < 0.001$ compared to preceding 20% O_2 periods. Repeated-measures ANOVA.

The question remains why hyperoxia and hypoxia elicit a respiratory reflex in the opposite direction through the TRPA1 channel in vagal afferents? Hyperoxia decreases but hypoxia increases Rf and MV. It is possible that the directionality of changes in respiratory parameters upon vagal afferent stimulus depends on the pattern of evoked neuronal discharges; the frequency of discharges may be a determinant for resultant Rf and MV. Indeed, external electric stimulus of vagal and superior laryngeal afferents at lower frequencies (0.2 and 0.5 Hz) increased Rf, while that at higher frequencies (2, 5 and 10 Hz) decreased Rf (Fig. 20). Thus, nerve discharges at different oscillation

frequencies may underlie opposite ventilatory responses to hypoxia and hyperoxia in terms of Rf changes.

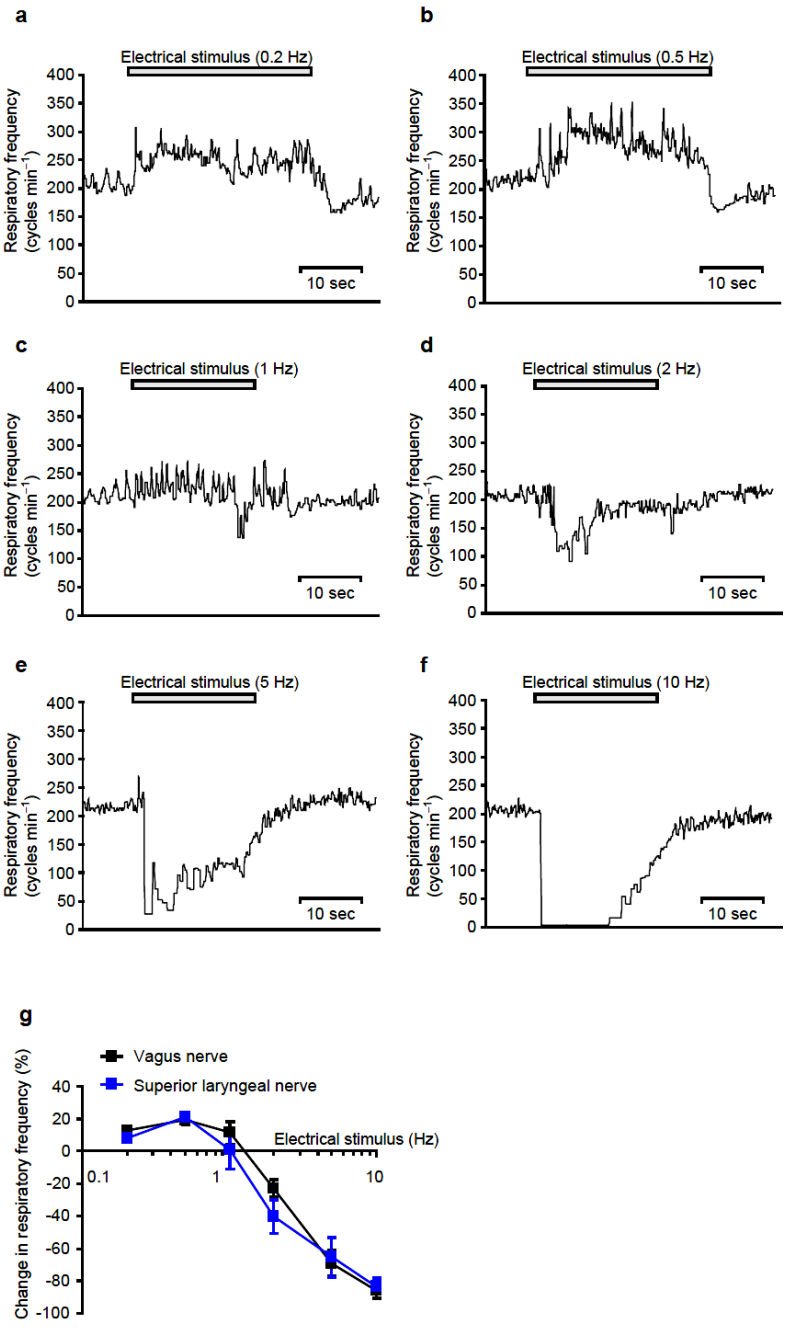

Figure 20. The frequency of electrical stimulus of vagal and superior laryngeal afferents determines the directionality of changes in Rf. a–f, Representative tracing of Rf when vagal afferents are exposed to electrical stimulus at a frequency of 0.2 Hz (**a**), 0.5 Hz (**b**), 1 Hz (**c**), 2 Hz (**d**), 5 Hz (**e**) or 10 Hz (**f**). The stimulus voltage and the pulse duration are maintained at 10 V and for 1 msec, respectively. **g,** Percentage changes in Rf when vagal or superior laryngeals are exposed to electrical stimulus at different frequencies (n = 6–7). Values denote percentage changes in Rf from the base lines observed without stimulus. Data points are mean ± s.e.m..

Arterial PO_2 was more dramatically decreased by hypoxic gas (15% O_2) and increased by hyperoxic gas (50 and 80% O_2) in mutant mice compared to WT mice (Fig. 21). Importantly, the mean arterial PO_2s corresponding to 15, 50 and 80% of inspired

O_2 were 82.4 ± 5.1, 294.5 ± 5.4 and 453.2 ± 7.9 mmHg, respectively, which fully activated TRPA1 in WT mice (Fig. 3d). These results support that TRPA1 acts as an O_2 sensor to control respiratory reflexes in regulation of O_2 supply *in vivo*.

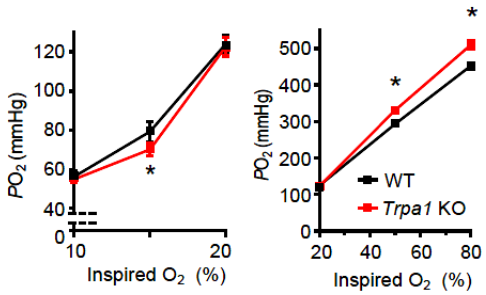

Figure 21. Arterial PO_2 in WT and *Trpa1* KO mice under hyperoxia or hypoxia. Mice are challenged with five levels of O_2 (10, 15, 20, 50 and 80% O_2) for 5 min each. $^*P < 0.05$ compared to WT mice (n = 6–9). To avoid hyperventilation-induced hypocapnia, inspired gas also contains 2% CO_2 throughout the experiment.

Trpa1 deficiency exacerbates pulmonary injury and hypertension.

To obtain further evidence that TRPA1 is an O_2 sensor *in vivo*, we examined acute pulmonary injury induced by hyperoxia and pulmonary hypertension by hypoxia[22,45]. Interestingly, under normoxic conditions, bronchoalveolar lavage fluid (BALF) analysis and immunohistochemical staining revealed a greater accumulation of macrophages and neutrophils in the lungs of *Trpa1* KO mice compared to WT mice (Figs. 22 and 23a). Hyperoxia (> 95% O_2) induced a more pronounced infiltration of cells including macrophages and neutrophils in *Trpa1* KO mice compared to WT mice (Figs. 22 and 23b, c). These results suggest that TRPA1 protects the lung from O_2 injury.

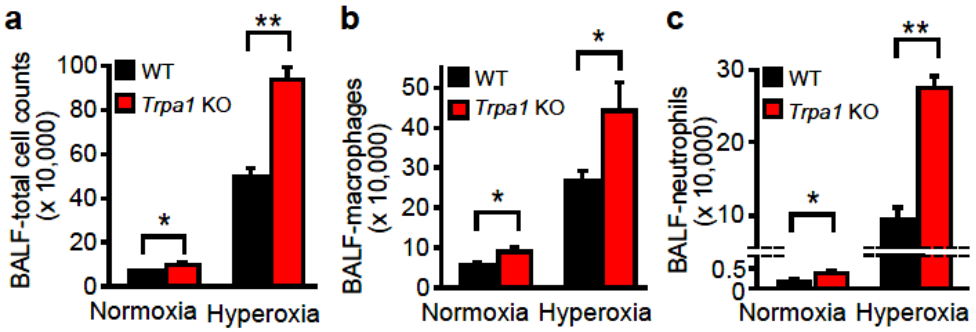

Figure 22. *Trpa1* deficiency exacerbates acute pulmonary injury induced by hyperoxia (> 95% O_2, 72 h) in mice. Numbers of total cells (**a**), macrophages (**b**) or neutrophils (**c**) in the BALF from WT or *Trpa1* KO mice exposed to normoxia and hyperoxia (n = 6).

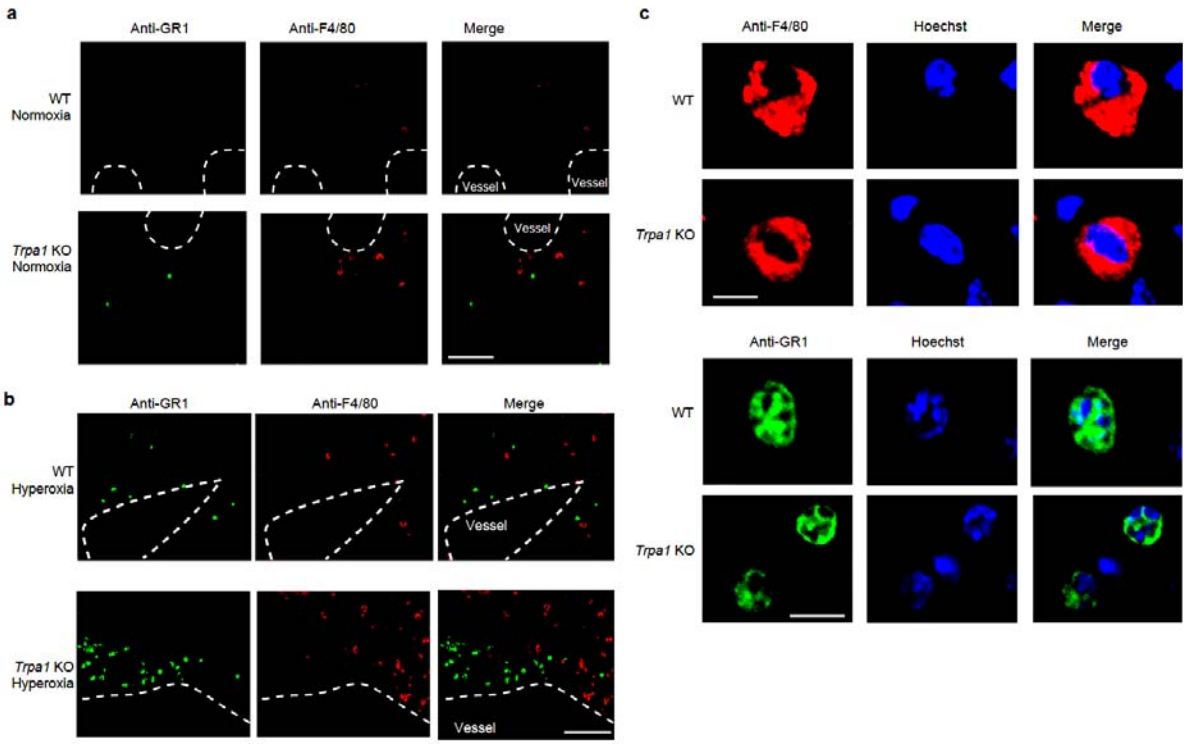

Figure 23. Immunostaining for neutrophils and macrophages infilterating into the lung. a, b, Frozen lung sections from mice exposed to normoxia (**a**) or hyperoxia (> 95% O_2, 72 h) (**b**) are stained with FITC-conjugated anti-GR1 antibody for neutrophils (green) and R-PE-conjugated anti-F4/80 antibody for macrophages (red). **c,** Fluorescent images of neutrophils or macrophages with nuclear stains in frozen lung sections from mice exposed to hyperoxia. Nuclear staining with Hoechst 33342 (blue) reveals that GR1-positive cells show multilobulated nucleus observed for neutrophils but F4/80-positive cells a round nucleus observed for macrophages. Scale bars, 5 μm.

Right ventricular hypertrophy (RVH) is a hallmark of hypoxia-induced pulmonary hypertension resulting from right ventricular systolic pressure (RVSP) overload. Interestingly, RVSP and the ratio of right ventricular (RV) weight to left ventricle (LV) plus septum (S) weight [RV/(LV + S)] in *Trpa1* KO mice were slightly larger than those in WT mice under a normoxic condition (Fig. 23a–c). Hypoxia (O_2 maintained at 15 ± 1.0%) induced greater increases of RVSP and [RV/(LV + S)] in *Trpa1* KO mice compared to WT mice (Fig. 23a–c). In addition, histological analyses of lung sections revealed a slight thickening of arteriol walls in *Trpa1* KO mice under a normoxic condition (Fig. 23d, e). After hypoxic exposure, wall thickness was increased more extensively in *Trpa1* KO mice than WT (Fig. 23d, e). These findings indicate that *Trpa1* deficiency increases

active vasoconstriction and aggravates pulmonary vascular remodeling with hypoxic RVH in mice. Therefore, TRPA1 channels modulate ventilation to protect the body against O_2 deprivation in hypoxia and O_2 excess in hyperoxia. This function of TRPA1 is likely to be important for the adjustment of ventilatory responses in normoxia.

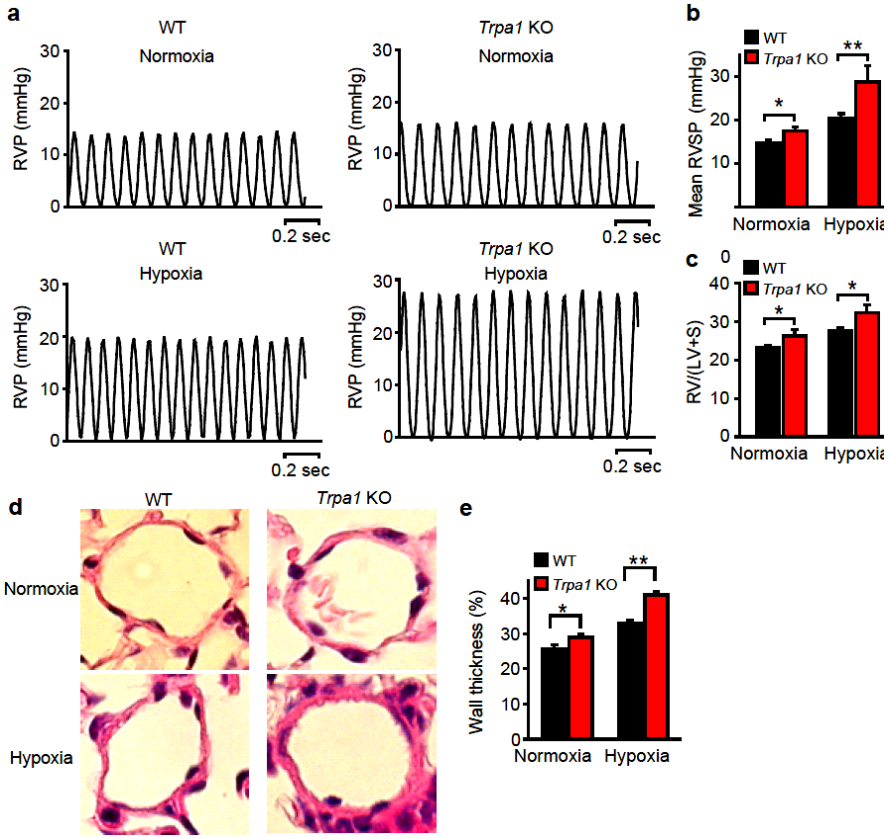

Figure 24. *Trpa1* deficiency exacerbates pulmonary hypertension induced by hypoxia (15 ± 1.0%, 8–9 days) in mice. **a,** Representative polygraph tracing of right ventricular pressure (RVP) obtained from WT (left) and *Trpa1* KO (right) mice exposed to normoxia (top) or hypoxia (bottom) for 8–9 days. **b,** Mean RVSP (n = 7–9). **c,** Development of right ventricular hypertrophy determined by the [RV/(LV + S)] ratio (n = 7–8) as describe in Methods. **d,** Hematoxylin and eosin staining of lung sections. Each field shows a representative pulmonary arteriole. Scale bar, 10 μm. **e,** Percent wall thickness in arterioles of comparable size based on analysis of area as described in Methods. Data points are mean ± s.e.m.. $^{*}P <$ 0.05 and $^{**}P < 0.01$.

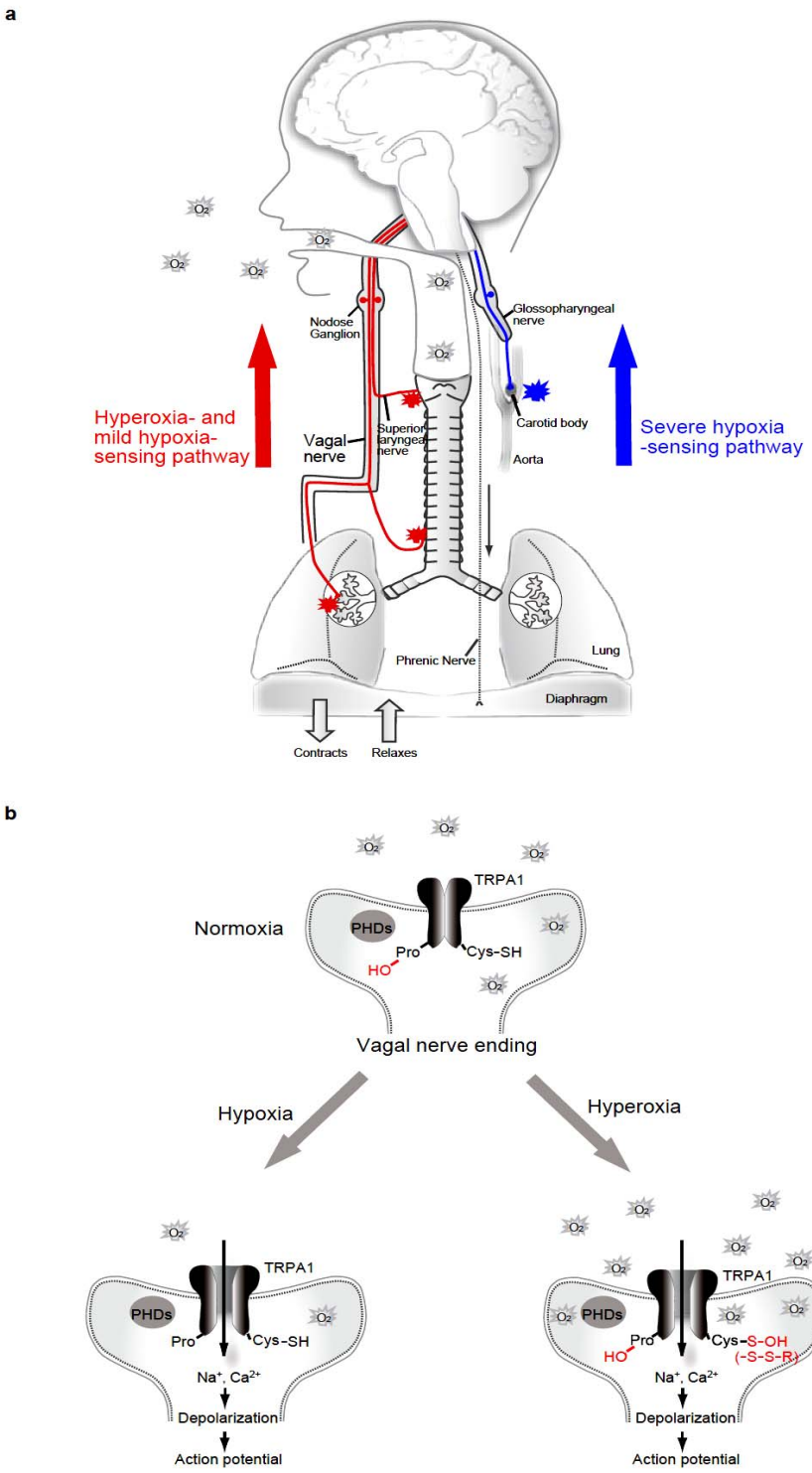

Figure 25. Model for O_2 sensing mechanisms. **a,** Hyperoxia and relatively mild hypoxia are detected by vagal afferents innervating the mucosa of larynx, airway or lungs, while relatively severe hypoxia is detected by carotid body. **b,** Molecular mechanism underlying O_2-sensing at the vagal nerve ending. PHDs hydroxylate conserved Pro394 within the N-terminus ankyrin repeat of TRPA1 in normoxia, while a decrease in O_2 concentrations diminishes PHD activity and relieves TRPA1 from inhibition, leading to its activation in hypoxia. O_2 in hyperoxia oxidizes Cys633 (and possibly Cys856), thereby activating TRPA1. This Cys oxidation may dominate the inhibition by Pro hydroxylation to activate TRPA1.

Discussion

The present study identifies TRPA1 as a novel O_2 sensor. TRPA1 detects changes in O_2 availability and control ventilation in hypoxia, hyperoxia and normoxia to maintain cellular O_2 concentrations sufficient for tissue demands, and low enough to minimize O_2 toxicity (Fig. 25).

In mice, nerve section experiments and discharge recordings suggest that non-carotid body chemoreceptors sense relatively mild hypoxia and hyperoxia, being different from the carotid body which detects severe hypoxia. This difference can be attributable to differences in O_2-sensing molecules. TRPA1 most likely plays a major role in O_2 sensing at the non-carotid body chemoreceptor terminals, because the O_2 sensitivity of non-carotid body chemosensors corresponds well with that of TRPA1 channels and is abolished in *Trpa1* KO mice. NEBs innervated by myelinated vagal fibers may also express TRPA1 to detect O_2. Notably, TRPA1 represents the first example of a channel where the activation is controlled by prolyl hydroxylation. PHDs hydroxylate conserved Pro394 within the N-terminus ankyrin repeat of TRPA1[20,21] and inhibit TRPA1 channels in normoxia, while a decrease in O_2 concentrations diminishes PHD activity and relieves TRPA1 from inhibition, leading to its activation in hypoxia. The relief can be achieved by surface expression of newly sythesized TRPA1 proteins through membrane recycling[20,21], or by dehydroxylation through an unidentified molecular mechanism. Importantly, O_2 dependence of enzymatic activities of PHDs and FIH is consistent with the major role played by PHDs but not by FIH in inhibiting TRPA1 activity: normoxic O_2 concentration of 200 μM (152 mmHg) is comparable to K_m values of 230–250 μM (175–190 mmHg) by O_2 concentrations for PHDs but it is higher than the K_m value of 90 μM (68 mmHg) for FIH[21]. On the other hand, in the carotid body, it has been documented that hypoxic inhibition of a variety of K^+ channels is crucial to initiate reflexes directed to improve tissues' O_2 supply. For triggering hypoxic inhibition of K^+

channels, the importance of mitochondrial function has been suggested, because mitochondria are the largest consumers of O_2, and as such are the key determinants of cytosolic O_2 concentration[18]. Energy metabolism and ROS generation linked to cellular redox status are mitochondrial functions that have been considered to be involved in hypoxia, but the exact roles of these processes remain controversial[16]. Interestingly, in TRPA1, mutations of Cys641 and Cys665 suppressed both constitutive and hypoxia-induced activation (Fig. 12b). Cys641 and Cys665 may be susceptible to attack of ROS produced upon hypoxia[16]. Alternatively, these Cys residues may form a disulfide bond and, after its cleavage in hypoxic reducing conditions[16], may coordinate with metal ions such as Zn^{2+} (refs 46, 47). Therefore, it is possible that Cys modification cooperates with prolyl hydroxylation in controlling activation of TRPA1 in hypoxia.

Our results suggest that sensing of hyperoxia is uniquely attributed to the TRPA1 O_2 sensor in non-carotid body chemoreceptors in mice. The possibility cannot be excluded that the carotid body and central chemoreceptors located in medulla oblongata are also involved in detecting hyperoxia, as reported for hypoxia[48]. However, TRPA1 is absent in the carotid body (Fig. 4b) and in the brain of rodents[32,36], suggesting that these tissues only play a minor role. Free Cys sulfhydryls are the key to understanding O_2-sensing ability of TRPA1 in hyperoxia. A high reactivity of Cys633 and Cys856 as electron donors enables TRPA1 to respond to O_2, which is a relatively poor electron acceptor. These Cys oxidations may dominate the inhibition by Pro hydroxylation to activate TRPA1. Contribution of multiple Cys residues to oxidation sensitivity of protein function has also been reported for the transcription factor regulator Kelch-like ECH-associated protein 1 (ref. 49) and other proteins[46,50]. Because sensitivities to O_2 and reactive disulfides are nearly abolished in the double mutant for Cys633 and Cys856 but are only partially reduced in single mutants, these Cys residues are more likely to

contribute to the same molecular determinant for O_2 sensitivity than to separate sites with characteristic oxidation sensitivities. Importantly, to activate TRPA1, our mutation studies suggest that diallyl disulfide and 4-tolyl disulfide, which have redox potentials comparable to O_2 (Table 2), target the same Cys residues, while reactive disulfides with higher oxidizing potency at high concentrations also act on additional Cys residues (Fig. 8f, g). For sensing other covalently modifying substances such as cinnamaldehyde and synthetic Cys-modification reagent *N*-methyl maleimide (NMM), multiple but different Cys residues have been identified[29–31]. The difference may be due to different reaction mechanisms: modification of free sulfhydryls by O_2 is mediated by a redox reaction, while that by cinnamaldehyde and NMM is mediated by the Michael addition reaction. Multiple activation triggers such as temperature are known for TRPA1[24,34]. Our preliminary experiments have suggested that cold-sensitive activation of TRPA1 is in part due to the well known effect of cold temperature to enhance dissolution of O_2. Zn^{2+} is well known to bind Cys residues in proteins and it also activates TRPA1[47]. Some other modes of activation sensitivity may be coupled with redox-sensitivity to finely regulate TRPA1 in response to changes in the environment. Hence, TRPA1, which is abundantly expressed in the vagus innervating the airways and lungs, may play a critical role in the frontline of defense against O_2 toxicity and various noxious chemical challenges.

Hypoxia and hyperoxia affect respiratory parameters in the opposite direction through TRPA1 in vagal afferents in mice. Interestingly, the activation of bronchopulmonary C-fibers by pungent compounds produces changes in Rf, with some animals displaying a fall in Rf[12–15], others a slight increase in Rf[10,12]. As a basis of such a conflicting finding, it has been proposed that Rf changes by capsaicin depend on the route or the dose of administration[12]. Our study provides evidence that the directionality of Rf changes by vagal afferent stimulus depends on the pattern of evoked neuronal discharges; lower frequencies of discharges increase Rf but higher frequencies decrease Rf (Fig. 20), as

previously reported for effects of vagal afferent stimulus on blood pressure reflexes in dogs[51]. Therefore, a likely scenario is that hypoxia induces low frequency discharges to increase Rf, but hyperoxia elicits high frequency discharges to decrease Rf. Molecular determinants of discharge patterns are still unclear in non-carotid body chemoreceptors. K^+ channels, which respond to hypoxia, may play roles in regulating discharges[16].

Even in normoxia, *Trpa1* KO mice developed pulmonary injury, which was derived from O_2 toxicity and observed only in hyperoxia for WT mice; however, *Trpa1* KO mice showed normal basal levels of ventilatory parameters, Rf and MV. In addition, during normoxia, *Trpa1* KO mice showed pulmonary hypertension, which was induced only by hypoxia in WT mice. TRPA1 activity may be necessary for adjusting reflex control of ventilation during changes in body condition or exercise in normoxia.

Methods

Materials. Fura-2 AM ester, 5-nitro-2-pyridyl disulfide (5-nitro-2-PDS), 4-pyridyl disulfide and 1,2-bis(2-aminophenoxy)ethane-*N*,*N*,*N'*,*N'*-tetraacetic acid (BAPTA) were obtained from Dojindo, 2-aminoethyl diphenylborinate (2-APB) and capsaicin from SIGMA, 4-nitro phenyl disulfide, 4-tolyl disulfide and 4-methoxy phenyl disulfide from Aldrich, 3-nitro phenyl disulfide, phenyl disulfide, diallyl disulfide, dipropyl disulfide and sodium tripolyphosphate from Wako, 4-chloro phenyl disulfide and 4-amino phenyl disulfide from Tokyo Chemical Industry, dimethyloxalylglycine (DMOG) from Frontier Scientific, DiI from Invitrogen, dithiothreitol (DTT) from Nacalai Tesque. DTNB-2Bio was synthesized as previously reported[26].

Mice. Mice were housed in a standard environmental condition (12-h light/12-h dark cycle; about 23°C). All experimental procedures were performed in accordance with the National Institute of Health Guide for the Care and Use of Laboratory Animals and approved by the Institutional Animal Use Committees of Kyoto University and Kagoshima University. Experiments were performed using C57BL/6J and *Trpa1* KO mice. *Trpa1* KO mice were purchased from the Jackson Laboratory and genotyped as previously described[37].

Measurement of Rf after nerve section in anesthetized mice. WT mouse was anesthetized with intraperitoneal injection of urethane (1.3 g kg^{-1}). L-shaped cannula (polyethylene tube, OD = 1.20 mm) perforated at the corner was inserted to the trachea through a midline incision to spread gas not only toward lung but also toward throat cavity. One end of the tracheal cannula was connected to the side of vinyl tube to which a consistant volume of air was supplied at a rate of 400 ml min^{-1}. To avoid hyperventilation-induced hypocapnia, inspired gas also contains 2% CO_2 throughout this experiment[52]. Inspired PO_2 and PCO_2 were continuously monitored (model JKO-25, Jikco, Co. Ltd.; Respina IH26, NEC-San-Ei-Instrument, respectively). To evaluate the

effect of acute bilateral sectioning of nerves on Rf, mice were divided into five groups: group I, bilateral cervical vagal trunks were exposed and cut immediately below the point of branching off to the superior laryngeal nerves (cervical vagal trunk); group II, bilateral superior laryngeal nerves were exposed and cut (superior laryngeal nerve); group III, bilateral cervical vagal trunks were exposed and cut immediately below the nodose ganglions (superior laryngeal and cervical vagal trunk); group IV, bilateral glossopharyngeal nerves were exposed and cut distal to the glossopharyngeal ganglions (glossopharyngeal nerve); group V, bilateral vagal, superior laryngeal and glossopharyngeal nerves were exposed only as control (sham operation). Ventilation was measured by pneumotachography as described previously[53]. Baseline Rfs in normoxia (20% O_2-2% CO_2) were measured for at least 5 min before the start of ventilation tests for nerve section or sham operation. The animal was challenged with five levels of inspired O_2 (10, 13, 15, 20 and 80% O_2; 2% CO_2, balance N_2 for each) and hypercapnia (10% CO_2; 20% O_2, balance N_2) before and after nerve section. Normoxic and hyperoxic gas challenges lasted 1 min, and hypoxic and hypercapnic challenges lasted 30 sec, respectively. The order of applied gas conditions was chosen randomly for each experiment, and gas challenge was followed by a 5-min interval in normoxia (20% O_2-2% CO_2). Throughout the experiment, rectal temperature was kept constant at 36.5 ± 1.0°C by a heating pad connected to a thermo controller (ATB-1100, Nihon Koden).

Isolation of mouse nodose ganglion and DRG neurons. Nodose ganglion and DRG neurons were prepared from adult WT and *Trpa1* KO mice using methods described previously[31]. Nodose ganglion and DRG were isolated under a dissecting microscope, cut in small pieces and treated with 0.1% trypsin (Difco Laboratories) and 0.1% collagenase type II (SIGMA) for 1 h at 37°C in the solution contained the following (in mM): 124 NaCl, 5 KCl, 1.2 KH_2PO_4, 1.3 $MgSO_4$, 2.4 $CaCl_2$, 24 $NaHCO_3$ and 10 glucose,

gassed with 95% O_2 and 5% CO_2. They were gently triturated with a fire-polished glass pipette and the resulting solution was centrifuged at 800 rpm for 8 min. The pellet obtained was resuspended in neuron culture medium contained the following: DMEM, 45%; Ham's F-12 medium (Invitrogen), 45%; FBS, 10%; penicillin, 30 units ml^{-1}; streptomycin, 30 μg ml^{-1}. Cells were plated onto coverslips coated with poly-L-lysine and laminin (Becton Dickinson). The cells were cultured in the neuron culture medium at 37°C under 5% CO_2 and subjected to $[Ca^{2+}]_i$ and electrophysiological measurements 8–24 h after plating.

Measurement of changes in $[Ca^{2+}]_i$. The fura-2 fluorescence was measured in HEPES-buffered saline (HBS) containing the following (in mM): 107 NaCl, 6 KCl, 1.2 $MgSO_4$, 2 $CaCl_2$, 11.5 glucose and 20 HEPES (pH adjusted to 7.4 with NaOH). Fluorescence images of the cells were recorded and analyzed with a video image analysis system (AQUACOSMOS; Hamamatsu Photonics) according to the manufacturer's instructions. The 340:380-nm ratio images were obtained on a pixel-by-pixel basis. Fura-2 measurements were carried out at 21 ± 1°C in HBS adjusted to pH 7.4. The 340:380-nm ratio images were converted to Ca^{2+} concentrations by *in vivo* calibration using 5 μM ionomycin as described previously[54]. Hyperoxic solution was achieved by bubbling with 22, 24, 26, 28, 30, 32, 34, 36, 80 or 100% O_2 (balanced with N_2) gas for at least 20 min before cell perfusion. Hypoxic solution was achieved by bubbling with 0, 8, 10, 12, 14, 16 or 18% O_2 (balanced with N_2) gas at least 20 min before cell perfusion and by blowing the respective gas over the surface of the experimental chamber using a modified dish. The concentration of dissolved O_2 in the chamber solution was determined with an O_2 microelectrode (InLab 605; METTLER TOLEDO).

Electrophysiology. For electrophysiological measurements, coverslips with cells were placed in dishes containing the solutions. Currents from cells were recorded at room temperature (22–25°C) using patch-clamp techniques of whole-cell mode and excised

inside-out mode with EPC-9 (*Heka Electronic*) or Axopatch 200B (Molecular devices) patch-clamp amplifier as previously described[55]. The patch electrodes prepared from borosilicate glass capillaries had a resistance of 2–4 MΩ for whole cell recordings and 5–7 MΩ for single-channel recordings. Current signals were filtered at 5 kHz with a four-pole Bessel filter and digitized at 10 or 20 kHz. PULSE (version 8.8; Heka Electronic) or pCLAMP (version 10.0.2; Molecular devices) software was used for command pulse control, data acquisition and analysis. For whole cell recordings, series resistance was compensated (to 70–80%) to minimize voltage errors. Ramp pulses were applied every 5 sec from –100 mV to +100 mV or from +100 mV to –100 mV at a speed of 1.1 mV $msec^{-1}$ from a holding potential of 0 mV. The extracellular (bath) solution was contained the following (in mM): 100 NaCl, 2 Ca gluconate and 10 HEPES (pH adjusted to 7.4 with NaOH, and osmolality adjusted to 320 mmol kg^{-1} with D-mannitol). Intracellular (pipette) solutions contained the following: 100 Cs aspartate, 5 1,2-bis(2-aminophenoxy)ethane-*N*,*N*,*N'*,*N'*-tetraacetic acid (BAPTA), 1.4 Ca gluconate, 2 Na_2ATP, 2 $MgSO_4$, 1 $MgCl_2$, 10 HEPES and 10 $Na_5P_3O_{10}$ (pH 7.4 adjusted with CsOH, and osmolality adjusted to 320 mmol kg^{-1} with D-mannitol). The free Ca^{2+} concentration was 30 nM calculated with CaBuf software (provided by Dr. Droogmans, G., Katholieke Universiteit Leuven, Leuven, Belgium). To measure in nodose ganglion neurons, 1.4 mM Ca gluconate was omitted. Percentage suppression of the current (%) in Figure 2d, h and Figure 4f were calculated according to the following equation; percentage suppression of the current (%) = $100\times(1- I_A/I_{Ctl})$, where I_{Ctl} and I_A are whole cell currents observed before and after 10 μM AP-18 or 10 mM DTT application, respectively. Single-channel recordings were performed in the excised inside-out configuration. The NP_O of single-channels was calculated by dividing the total time spent in the open state by the total time of continuous recording (30 sec) in the patches containing active channels. The amplitude of single-channel currents was measured as

the peak-to-peak distance in Gaussian fits of the amplitude histogram. For inside-out patch recordings, the intracellular side was exposed to bath solution containing the following: 50 Cs aspartate, 50 CsCl, 1 $MgCl_2$, 1 $CaCl_2$, 10 EGTA, 10 $Na_5P_3O_{10}$ and 10 HEPES (pH adjusted to 7.4 with CsOH, and osmolality adjusted to 300 mmol kg^{-1} with D-mannitol). The pipette solution contained the following: 100 CsCl, 1 $MgCl_2$, 1 EGTA and 10 HEPES (pH adjusted to 7.4 with CsOH, and osmolality adjusted to 300 mmol kg^{-1} with D-mannitol). Percentage supression of the NP_O (%) in Figure 2l was calculated according to the following equation; percentage supression of the NP_O (%) = $100\times(1-NP_{O\,A}/NP_{O\,Ctl})$, where $NP_{O\,Ctl}$ and $NP_{O\,A}$ indicate mean NP_O of 60 sec obtained before and after 10 μM AP-18 or 10 mM DTT application, respectively.

RNA isolation and RT-PCR. Total RNA was extracted using ISOGENE (Wako), following the manufacturer's instructions. The concentration and purity of RNA were determined spectrophotometrically. Two hundred nanograms of total RNA were reverse-transcribed into first-strand cDNA by use of the RNA LA PCR kit (TaKaRa) at the final volume of 20 μl. Expression levels of TRPM1–M8, TRPC1–C7, TRPV1–V6, TRPA1, TH, FIH, PHD1–3 and β-actin RNA in mouse nodose ganglion neurons and those of TRPA1 and TH in mouse carotid bodies were determined by RT-PCR. The primers used for PCR amplification are summarized in Table 3. PCR was conducted with a GeneAmp PCR system 9700 (Applied Biosystems) using LA Taq polymerase with GC buffer (TaKaRa) for 32 cycles under the following conditions: initial denaturation was 3 min at 95°C, then 30 sec at 95°C, following by a 30-sec annealing step at 55–61°C (See Table 3) and 30-sec elongation at 72°C, and a final elongation of 7 min at 72°C. Predicted lengths of PCR products are 531, 534, 592, 520, 455, 473, 495, 682, 354, 298, 309, 289, 442, 309, 499, 347, 401, 421, 186, 464, 358, 243, 429, 363, 543, 388, 467 and 440 base pairs (bp) for TRPM1, TRPM2, TRPM3, TRPM4, TRPM5, TRPM6, TRPM7, TRPM8, TRPC1, TRPC2, TRPC3, TRPC4, TRPC5, TRPC6, TRPC7, TRPV1, **Table 3.**

Table 3. Primer sequences used in RT-PCR experiments.

Genes	Primer sequences (5′→ 3′)	Annealing temperatures (°C)
TRPM1	for: AGACCATGTCCAACCCTCTG rev: TTCCTTTGAGCAAGGCAGTT	58
TRPM2	for: ACAACCCTGAAGGACAGTGG rev: CATCACTAGCACCTCCAGCA	58
TRPM3	for: GCCATTCTCTTTCCCAATGA rev: ACGAATTGAAGCGATCATCC	58
TRPM4	for: TGGATGCTCTGCTGAATGAC rev: GACTCTAGGCGAGCCATCAC	58
TRPM5	for: CTGATCGCCATGTTCAGCTA rev: GGAGCCAGTGTATCCGTCAT	58
TRPM6	for: GAGAGGAGGCCACAGTCAAG rev: CAGGCCCTGGTCACTGTAAT	58
TRPM7	for: CTGAAGCTGGGAAAATCAGC rev: ACCAAGTTCCAGGACCACAG	55
TRPM8	for: CAAAACACCCAACCTGGTCATTTC rev: CACAGTGCGTGGTAAAAAGCG	55
TRPC1	for: GATTTTGGGAAATTTCTGGG rev: TGCTATCAGCTGGAAGCT	55
TRPC2	for: GACATGATCCGGTTCATG rev: CTCGATCTTCTGGAAGGA	55
TRPC3	for: GACATATTCAAGTTCATGG rev: CTCGATCTCTTGGTATGA	55
TRPC4	for: TGGGACATGTGGCACCCCAC rev: ACGTGGAAAACGCGTTGTTCTG	55
TRPC5	for: ATTATTCCCAGCCCCAAATC rev: GACAGGCCTTTTTCTTGCAG	58
TRPC6	for: GATATCTTCAAATTCATGGTC rev: CTCAATTTCCTGGAATGAAC	58
TRPC7	for: GCAGCAAGCTAGGACAAACC rev: GAGATGATCTGGGGGTCTGA	58
TRPV1	for: TCGTCTACCTCGTGTTCTTGTTTG rev: CCAGATGTTCTTGCTCTCTTGTGC	55
TRPV2	for: GATGGAGATGAAGAAGGCAGTGC rev: TTGACAAGGGGCTGAGGATTGC	61
TRPV3	for: CCCCATCCTCTTTCTCTTCC rev: CGACGTTTCTGGGAATTCAT	55
TRPV4	for: CGTCCAAACCTGCGAATGAAGTTC rev: CCTCCATCTCTTGTTGTCACTGG	55
TRPV5	for: GAGTTGGTGCCTCTCGCTAC rev: GGCAAAGGTGGCATAGGTAA	58
TRPV6	for: ATCGATGGCCCTGCCAACT rev: CAGAGTAGAGGCCATCTTGTTGCTG	55
TRPA1	for: ACAAGAAGTACCAAACATTGACACA rev: TTAACTGCGTTTAAGACAAAATTC	55
β-actin	for: GATGACGATATCGCTGCGCTG rev: GTACGACCAGAGGCATACAGG	55
TH	for: GGACATTGGACTTGCATCTCTGGG rev: GCTTGGGTCAGGGTGTGCAG	55
FIH	for: CTGCAGCAGACACTCAATGACACC rev: GCCAACCACTGTCTCATAACCAACC	55
PHD1	for: ACCGCGCAGCATTCGTG rev: GGGGCTGGCCATTAGGTAGGTGTA	55
PHD2	for: GCGGGAAGCTGGGCAACTAC rev: TCAACCCTCACACCTTTCTCACC	55
PHD3	for: CTGCGTGCTGGAGCGAGTCAA rev: TCATGTGGATTCCTGCGGTCTG	55

TRPV2, TRPV3, TRPV4, TRPV5, TRPV6, TRPA1, TH, FIH, PHD1, PHD2, PHD3 and β-actin, respectively. Sources of positive control RNAs in Figure 1d are: the eye for TRPM1 and TRPM5; the brain for TRPM2, TRPM3, TRPM4, TRPM6, TRPM7, TRPC1, TRPC2, TRPC3, TRPC4, TRPC5, TRPC6, TRPC7, TRPV2, TRPV4 and β-actin; the DRG for TRPM8, TRPV1 and TRPA1; the colon for TRPV3; the kidney for TRPV5 and TRPV6.

Cell cultures and cDNA expression. HEK293 or HEK293T cells were cultured in Dulbecco's modified Eagle's medium (DMEM) containing 10% fetal bovine serum, 30 units ml^{-1} penicillin and 30 μg ml^{-1} streptomycin under a 95% air-5% CO_2 atmosphere at 37°C. HEK293 and HEK293T cells were co-transfected with recombinant plasmids and pEGFP-F (Clontech) as a transfection marker, using SuperFect Transfection

Reagent (Qiagen) and Lipofectamine 2000 (Invitrogen), respectively. HEK293 cells were plated onto poly-L-lysine-coated glass coverslips 24 h after transfection and subjected to $[Ca^{2+}]_i$ measurement 8–24 h after plating on the coverslips. DTNB-2Bio labeling assay and immunoprecipitation were performed 32–48 h after transfection of HEK293 cells. HEK293T cells were subjected to electrophysiological measurements 32–72 h after transfection.

cDNA c loning and plasmid construction. Human TRPA1, FIH, PHD1, PHD2 and PHD3 (GenBank accession No. NM007332.1, NM017902, BC036051, NM022051 and NM022073, respectively) were cloned from Human Brain, whole Marathon-Ready cDNA (BD Biosciences) by applying a PCR-based approach, and were subcloned into the expression vector pCI-neo (Promega), pEGFP-C (Clontech) and pCMV-tag2 (Stratagene). TRPA1 Cys mutants and Pro mutant were constructed from TRPA1-pCIneo using overlap extension PCR[56]. C414S, C421S, C540S, C621S, C641S and C665S were constructed as previously reported[31]. The primer pairs used for C3S, C59S, C104S, C173S, C192S, C199S, C213S, C258S, C273S, C308S, C462S, C608S, C633S, C651S, C703S, C727S, C773S, C786S, C834S, C856S, C1021S, C1025S, C1085S and P394A are summarized in Table 4. The double mutant C633S·C856S was generated by digesting C633S-pCIneo with *Xho*I and *Spe*I and inserting this fragment containing the mutation into the *Xho*I and *Spe*I sites of C856S-pCIneo. Catalytically dead FIH, PHD1, PHD2 and PHD3 mutants were constructed from FIH-pCIneo, PHD1-pCIneo, PHD2-pCIneo and PHD3-pCIneo, respectively, using overlap extension PCR, as previously reported[57–60]. The primer pairs used for FIH mutant (D201A), PHD1 mutant (H357A), PHD2 mutant (H374A) and PHD3 mutant (H196A) are summarized in Table 4. The nucleotide sequences of the mutants were verified by sequencing the corresponding cDNA.

Table 4. Primer sequences used for overlap extension PCR in producing mutants.

Genes	Mutants	Mutation primer sequences (5' → 3')	External primer sequences (5' → 3')	Restriction sites used for cloning into TRPA1-pCIneo, FIH-pCIneo, PHD1-pCIneo, PHD2-pCIneo or PHD3-pCIneo
TRPA1	C3S	for: CTTCCACCATGAAGAGCAGCCTGAGGAAG rev: CATCTTCCTCAGGCTGCTCTTCATGGTG	for: CTGCAGTGACTCTCTTAAGGTAGCCTTG rev: CTGTCTACATGCATAATGTAGAGGAGTACAC	*Xho*I / *Nhe*I
	C59S	for: GAAATTAAAAACAAGTGACGATATGGAC rev: GTCCATATCGTCACTTGTTTTTAATTTC		
	C104S	for: GGAAATACCCCTCTGCATAGTGCTGTAG rev: CTACAGCACTATGCAGAGGGGTATTTCC		
	C173S	for: GATCATTGCGAGCACCACAAATAATAG rev: TATTTGTGGTGCTCGCAATGATCACAG		
	C192S	for: GGAGCTAAGCCAAGTAAATCAAATAAATG rev: CATTTATTTGATTTACTTGGCTTAGCTCC		
	C199S	for: GGAAGTTTCCCTATTCACCAAGCTGC rev: GCAGCTTGGTGAATAGGGAAACTTCC		
	C213S	for: GGTTCCAAAGAAAGCATGGAAATAATAC rev: GTATTATTTCCATGCTTTCTTTGGAACC		
	C258S	for: GATCAAAATGAGCCTGGACAATGGTG rev: GTGCACCATTGTCCAGGCTCATTTTG		
	C273S	for: GAAGGGAAGGAGCACAGCCATTCATTTTG rev: AATGAATGGCTGTGCTCCTTCCCTTCTC		
	C308S	for: CAACCGATGGAAGTCATGAGACCATGC rev: GCATGGTCTCATGACTTCCATCGGTTG		
TRPA1	C462S	for: GTATCAATACCAGTCAGAGGCTCCTACAAG rev: CTTGTAGGAGCCTCTGACTGGTATTGATACG	for: ACCGATGGATGTCATGAGACCATGCTTC rev: GCAATGTCGCCAACTGCCAAACCAATAAG	*Apa*I / *Bam*HI
	C608S	for: GATGGGATGAAAGTCTTAAGATTTTCAGTC rev: GACTGAAAATCTTAAGACTTTCATCCCATC		
	C633S	for: CTCCCTGAAAGCATGAAGGTACTTTTAG rev: GTACCTTCATGCTTTCAGGGAGGTATTC		
	C651S	for: GACAAGTCCAGCCGAGACTATTATATC rev: GATATAATAGTCTCGGCTGGACTTGTCTTC		
	C703S	for: CTGTGAGTAAAGAATATTTACTCATGAAATGG rev: CCATTTCATGAGTAAATATTCTTTACTCACAG		
	C727S	for: GATGAATTTAGGATCTTACAGTCTTGGTCTC rev: AAGACTGTAAGATCCTAAATTCATCATATGAG		
	C773S	for: CCACGAATTCATATCTAATAAAAACTAGTATG rev: CATACTAGTTTTTATTAGATATGAATTCGTGG		
	C786S	for: GTATATTTGGGTATAGCAAAGAAGCGGG rev: CCCGCTTCTTTGCTATACCCAAATATAC		
	C834S	for: GTGGCAAAGTGGAGCAATTGCTGTTTAC rev: GTAAACAGCAATTGCTCCACTTTGCCAC		
	C856S	for: CAAAGATTTGAAAATAGTGGAATTTTTATTG rev: ATTCCACTATTTTCAAATCTTTGAAGATAC		
TRPA1	C1021S	for: CCATATATTCAGTTTTTTATTTTGCACTGG rev: CCAGTGCAAAATAAAAAACTGAATATATGG	for: CTCAGCTTTTACATCCTCCTGAATTTAC rev: CCTTATCGGATTTTACCACATTTGTAGAG	*Bam*HI / *Xma*I
	C1025S	for: CTGTTTTTTATTTAGCACTGGGGAAATAAG rev: CTTATTTCCCCAGTGCTAAATAAAAAACAG		
	C1085S	for: GATGATGATAGCCATAGTTCTTTTCAAGAC rev: GTCTTGAAAAGAACTATGGCTATCATCATC		
TRPA1	P394A	for: TGCGAGCTGAATTTATGCAGATGCAACA rev: TGTTGCATCTGCATAAATTCAGCTCGCA	for: ACTCACTATAGGCTAGCCTCGAGAATTCGGG rev: CTTGTAGGAGCCTCTGACAGGTATTGATACG	*Xho*I / *Apa*I
FIH	D201A	for: CTCACTATGCTGAGCAGCAGAACTTTTT rev: AAAAAGTTCTGCTGCTCAGCATAGTGAG	for: CACGAATTCTCCACCATGGCGGCGACAGCGGCGGA rev: CACGTCGACCTAGTTGTATCGGCCCTTGATC	*EcoR*I / *Sal*I
PHD1	H357A	for: GAACCCCGCCGAGGTGAAGCCAGCCTATGC rev: GCATAGGCTGGCTTCACCTCGGCGGGGTTC	for: CACGAATTCTCCACCATGGACAGCCCGTGCCAGCC rev: CACGTCGACCTAGGTGGGCGTAGGCGGCTGTG	*EcoR*I / *Sal*I
PHD2	H374A	for: TCGCAACCCTGCTGAAGTACAACCA rev: TGGTTGTACTTCAGCAGGGTTGCGA	for: CACGAATTCTCCACCATGGCCAATGACAGCGGCG rev: CACGTCGACCTAGAAGACGTCTTTACCGAC	*EcoR*I / *Sal*I
PHD3	H196A	for: CGTAGGAACCCAGCCGAAGTGCAG rev: CTGCACTTCGGCTGGGTTCCTACG	for: CACGAATTCTCCACCATGCCCCTGGGACACATCAT rev: CACGTCGACTCAGTCTTCAGTGAGGGCAG	*EcoR*I / *Sal*I

Immunohistochemistry of airway-and lung-identified nodose ganglion neurons. WT mice were anaesthetized with pentobarbital (50 mg kg^{-1}). To label neurons that project fibres into the trachea, mice were orotracheally intubated, and 50 µl of the tracer DiI (dissolved in 100% ethanol and diluted in sterile saline to a final concentration of 0.5 mg ml^{-1} in 1% ethanol) was instilled into the tracheal lumen. On the other hand, in order to label neurons that project fibres deep into the lung, mice were transdermally injected with 50 µl of DiI (0.5 mg ml^{-1}) into the right lung. Eight days after injection, the mice were killed by an overdose of pentobarbital (150 mg kg^{-1}). The nodose ganglions were removed from the mice without perfusion of fixation solution. The samples were then rinsed with PBS, embedded in OCT compound (Sakura Finetek) and 'snap-frozen' in dry ice and acetone and stored at –80°C. Cryostat sections (3 µm in thickness) were affixed to micro slides (MATSUNAMI), dried at room temperature, fixed in cold acetone for 10 min and then dried at room temperature. The samples were rehydrated in Tris-buffered saline (TBS), pH 7.6, and blocked with 1% BSA and 5% NGS in TBS for 1 h at room temperature. The samples were incubated with anti-mouse TRPA1 antibody[33], which was a gift from Y. Kubo, as a first antibody overnight at 4°C, washed with 1% BSA and 5% NGS in TBS at room temperature and then incubated with Alexa-conjugated goat anti-rabbit IgG (Alexa Fluor 488) (Invitrogen) as a second antibody for 2 h at 4°C. Followed by washing with 1% BSA and 5% NGS in TBS, the coverslips were sealed with PermaFluor Aqueous (IMMUNONTM, SHANDON) to prevent evaporation and stored at 4°C before imaging. The fluorescence images were acquired with a confocal laser-scanning microscope using the 488-nm line of an argon laser for excitation and a 505–525 nm band-pass filter for emission and 543-nm line of a He-Ne laser for excitation and a 560-nm long-pass filter for emission. The specimens were viewed at high magnification using plan oil objectives (60×, 1.40 NA, Olympus).

Synthesis of AP-18 ((*Z*)-4-(4-chlorophenyl)-3-methylbut-3-en-2-oxime)[39,61–63]. A

mixture of *p*-chloro benzaldehyde (29.5 g, 210 mmol), methyl vinyl ketone (51.3 ml, 630 mmol), triphenyl phosphine (PPh_3) (11.0 g, 42.0 mmol) and *p*-nitrophenol (8.86 g, 63.0 mmol) in tetrahydrofuran (THF) (500 ml) was stirred for 72 h at room temperature. After removal of the solvent, the resulting mixture was purified by column chromatography (silica, hexane : ethyl acetate = 4 : 1 → 2 : 1) to afford 3-(hydroxy-(4-chlorophenyl)methyl)-but-3-en-2-one (**1**) (25.9 g, 59%) as a colorless oil. ^{1}H-NMR (400 MHz, $CDCl_3$) δ/ppm 7.31 (m, 4H), 6.21 (s, 1H), 5.98 (s, 1H), 5.58 (s, 1H), 2.35 (s, 3H).

In a round bottom flask, **1** (25.3 g, 120 mmol) was dissolved in dichloromethane (100 ml), and then acetic anhydride (Ac_2O) (16.9 ml, 180 mmol) and 4-dimethylaminopyridine (DMAP) (2.93 g, 24.0 mmol) were added. After stirring for 1 h at room temperature, the reaction mixture was diluted with 10% $NaHCO_3$ solution, and extracted with dichloromethane (150 ml × 3). The combined organic layers were dried over $MgSO_4$ and the solvent was evaporated in vacuo. The resulting mixture was purified by column chromatography (silica, hexane : EtOAc = 4 : 1 → 2 : 1) to afford 3-(acetoxy-(4-chlorophenyl)methyl)-but-3-en-2-one (**2**) (14.8 g, 47%) as a white solid. ^{1}H-NMR (400 MHz, $CDCl_3$) δ/ppm 7.30 (m, 4H), 6.69 (s, 1H), 6.23 (s, 1H), 6.10 (s, 1H), 2.31 (s, 3H), 2.10 (s, 3H).

In argon atmosphere, a mixture of **2** (14.0 g, 55.4 mmol), $Pd(OAc)_2$ (0.62 g, 2.77 mmol), 1,2-bis(diphenylphosphino)ethane (DPPE) (3.53 g, 8.86 mmol), formic acid (HCOOH) (6.26 ml, 166 mmol) and triethylamine (NEt_3) (23.0 ml, 166 mmol) in dry THF (300 ml) was refluxed for 3 h. After removal of the solvent, ethyl acetate (200 ml) and hexane (200 ml) were added to the residue. The organic solution was washed with 5% citric acid solution, 10% $NaHCO_3$ solution and brine. The organic layer was dried over $MgSO_4$, and the solvent was evaporated in vacuo. The residue was purified by column chromatography (silica, hexane : ethyl acetate = 8 : 1 → 4 : 1) to afford

(*Z*)-4-(4-chlorophenyl)-3-methyl-3-butene-2-one (**3**) (6.5 g, 60%). ^{1}H-NMR (400 MHz, $CDCl_3$) δ/ppm 7.46–7.26 (m, 5H), 2.46 (s, 3H), 2.04 (s, 3H).

A mixture of **3** (6.50 g, 33.4 mmol) and hydroxylamine hydrochloride ($NH_2OH{\cdot}HCl$) (3.48, 50.1 mmol) in dry ethanol (18 ml) and dry pyridine (36 ml) was stirred overnight at 60°C. After removal of the solvent, ethyl acetate (150 ml) and hexane (150 ml) were added to the residue. The organic solution was washed with 0.1N HCl solution, 10% $NaHCO_3$ solution, and brine. The organic layer was dried over $MgSO_4$, and the solvent was evaporated in vacuo. The residue was purified by recrystallization from ethyl acetate and hexane to afford **AP-18** (6.8 g, 96%) as a white solid. ^{1}H-NMR (400 MHz, $CDCl_3$) δ/ppm 8.51 (s, 1H), 7.35 (d, 2H, J = 8.4 Hz), 7.25 (d, 2H, J = 8.4 Hz), 6.85 (s, 1H), 2.16 (s, 3H), 2.05 (s, 3H). FAB-Mass *m*/*z* 210 [$(M+H)^+$].

Electrochemical characterization of reactive disulfides. Half-wave potential ($E_{1/2}$) values of reactive disulfides and O_2 were determined by rotating disk-electrode voltammetry. The measurements were carried out with a BAS 100B (Bioanalytical Systems) and a RDE-3 rotating disk electrode (Nikko Keisoku) with a SC-5 controller (Nikko Keisoku). The voltammetry was measured in 0.1 M Bu_4NBF_4/DMSO using a glassy carbon working electrode, a platinum wire counter electrode and an Ag/AgCl reference electrode at 2,500 rpm. $E_{1/2}$ is an empirical value that is defined as the midpoint of the rise of current in voltammogram and, as such, it differs from the standard reduction potential (E^o) of the compound. As previously reported[42], the relative nature of $E_{1/2}$ values presented in this study was deemed to be a relevant descriptor of the redox potential of these agents.

DTNB-2Bio labeling assay. The DTNB-2Bio labeling assay was performed as previously described with modifications[26]. HEK293 cells transfected with GFP-TRPA1 (GFP-WT), GFP-C633S, GFP-C856S or vector (~5×10^6) were washed with PBS. The surface membrane was permeabilized by exposure to PBS containing 0.001% digitonin

(SIGMA) for 5 min. The cells were collected and incubated in HBS solution containing 50 μM DTNB-2Bio for 20 min at room temperature. The cells were washed with HBS and lysed in RIPA buffer (pH 8.0) containing 150 mM NaCl, 1% Nonidet P-40, 0.5% sodium deoxycholate, 0.1% SDS, 50 mM Tris. Cell lysates were incubated batch-wise with NeutrAvidin-Plus beads (Thermo Scientific) for 4 h at 4°C with constant shaking. The beads were rinsed three times with RIPA buffer by centrifugation at 15,000 rpm for 1 min. The proteins were eluted in RIPA buffer containing 50 mM DTT for 1 h and denatured in SDS sample buffer containing 50 mM DTT for 30 min at room temperature. The proteins were analyzed by 7.5% SDS-PAGE and WB using an antibody to GFP.

Immunoprecipitation. HEK293 cells (~5×10^6) cotransfected with GFP-TRPA1(WT) or GFP-TRPA1(P394A) and Flag-FIH, Flag-PHD1, Flag-PHD2, Flag-PHD3 or pCMV-Tag2 (vector) are pretreated with 1 mM DMOG for 48 h to stabilize the enzyme-substrate interaction[64]. The cells were lysed in RIPA buffer. Flag-FIH, Flag-PHD1, Flag-PHD2 and Flag-PHD3 were immunoprecipitated with M2 monoclonal antibody to Flag (SIGMA) in the presence of sepharose A-agarose beads (GE Healthcare) rocked for 4 h at 4°C. The immune complexes were washed three times with RIPA buffer and resuspended in SDS sample buffer containing 50 mM DTT for 30 min at room temperature. The proteins were analyzed by 7.5% SDS-PAGE and WB using an antibody to GFP.

Recording of multifiber vagal, superior laryngeal and glossopharyngeal afferent discharges. The recording of multifiber nerve discharges was performed as previously described with modifications[65,66]. WT or *Trpa1* KO mouse was anesthetized with intraperitoneal injection of urethane. L-shaped cannula perforated at the corner was inserted to the trachea. The animal was then artificially ventilated with room air and paralyzed with 0.15 mg kg^{-1} panchronium bromide. Acute unilateral nerve sectioning was performed as follows: right cervical vagal trunk was exposed and cut immediately

below the point of branching off to the superior laryngeal nerve; right superior laryngeal nerve was exposed and cut; right glossopharyngeal nerve was cut immediately below the glossopharyngeal ganglion. To record its afferent activities, the distal cut end was placed on a pair of silver hook electrodes. Multifiber vagal, superior laryngeal and glossopharyngeal nerve discharges were amplified (10,000×, AVB-8, Nihon Kohden) and displayed on an oscilloscope (5113, Tektronix, Beaverton). The lower and higher cut-off frequencies of the recording system were 100 and 3,000 Hz, respectively. Nerve discharges were full-wave rectified, leaky integrated (time constant = 1 sec, EI-601G, Nihon Kohden) and stored in a hard disk through an analog-to-digital converter (PowerLab, ADInstrument) together with original nerve discharges, electrocardiogram, inspired PO_2 and PCO_2 and the event signal. At the end of each experiment, the vagal, superior laryngeal and glossopharyngeal nerves were cut proximally to the recording electrode and the mean level of instrumentation noise was determined over the period of several minutes. At the time of reproduction, rectified and integrated vagal, superior laryngeal and glossopharyngeal nerve activities were subtracted by this noise level to obtain each nerve activity. During the control period, the animal was breathed room air. The animal was then challenged with five levels of inspired O_2 (10, 13, 15, 20 and 100% O_2). Normoxic and hyperoxic gas challenges lasted 1 min, and hypoxic challenge lasted 30 sec, respectively. The order of applied gas conditions was chosen randomly for each experiment, and gas challenge was followed by a 5-min interval in room air. Throughout the experiment, rectal temperature was kept constant at 36.5 ± 1.0°C by a heating pad connected to a thermo controller.

Measurement of ventilation by whole-body plethysmography. Ventilatory response in conscious mice was measured by whole-body plethysmography as described previously[67,68]. WT or *Trpa1* KO mouse was placed into a whole-body plethysmography chamber continuously flushed with normoxic, hyperoxic or hypoxic gas

(see below) at a rate of 500 ml min^{-1}. Tidal volume (TV) was calculated according to the formula used by Epstein et al.[69]. MV was defined as the product of inspiratory TV and Rf, normalized to the animal's body weight. Respiratory parameters were calculated only for quiet wakefullness, because the animal's movement might distort the plethysmographic signals. To avoid hyperventilation-induced hypocapnia, inspired gas also contains 2% CO_2 throughout this experiment[52]. In this series of experiments, the animal initially breathed 20% O_2 (2% CO_2, balance N_2) for 20 min, and baseline values of Rf, TV and MV were calculated. Next, hyperoxic gas of 50% O_2 followed by 80% O_2 were introduced into the chamber for 30 min each. There was a 20-min interval with 20% O_2 breathing between the hyperoxic stimuli. Thereafter, the animal breathed 20% O_2 for 20 min. After the experiments with hyperoxic gases, hypoxic gas of 15% O_2 followed by 10% O_2 were introduced into the chamber for 5 min each. There was a 20-min interval with 20% O_2 breathing between the hypoxic stimuli. In total, eight sequential data values were obtained in each experiment. To confirm the role of TRPA1 on respiratory regulation thoroughly, the respiratory parameters were measured in response to AP-18 aerosol. AP-18 was aerosolized with an ultrasonic nebulizer (NE-U17, Omuron), mixed with air and subsequently distributed into whole-body plethysmography chamber. To reduce animal's burden, the experiments using WT mice were separately divided into Experiment 1 and Experiment 2. In Experiment 1, WT mouse was exposed sequentially to 20% O_2 (20 min), 80% O_2 (5 min), 20% O_2 (20 min) and finally to 10% O_2 (5 min) without any aerosols. This was followed sequentially by the same protocol conducted in the presence of vehicle (20% EtOH in saline) aerosol, 1 mM AP-18 aerosol, 3 mM AP-18 aerosol, 10 mM AP-18 aerosol and finally 30 mM AP-18 aerosol. In Experiment 2, WT mouse was exposed sequentially to 20% O_2 (20 min), 50% O_2 (5 min), 20% O_2 (20 min) and finally to 15% O_2 (5 min) without any aerosols. This was followed sequentially by the same protocol conducted in the

presence of vehicle, 1 mM AP-18 aerosol, 3 mM AP-18 aerosol, 10 mM AP-18 aerosol and finally 30 mM AP-18 aerosol. *Trpa1* KO mice were exposed sequentially to 20% O_2 (20 min), 50% O_2 (5 min), 20% O_2 (20 min), 80% O_2 (5 min), 20% O_2 (20 min), 15% O_2 (5 min), 20% O_2 (20 min) and finally to 10% O_2 (5 min) in the presence of vehicle or 30 mM AP-18 aerosol. At the time of measurement, the supply of air and monitoring of PCO_2 and PO_2, were discontinued by closing inlet and outlet stopcocks.

Measurement of arterial blood gas. In WT or *Trpa1* KO mouse, a catheter was implanted into the right carotid artery under 2–3% isoflurane anesthesia. After recovery from anesthesia for more than 3 h, the animal was placed in the body plethysmography chamber and breathed 20% O_2 (2% CO_2, balance N_2) for 20 min. To avoid hyperventilation-induced hypocapnia, inspired gas also contains 2% CO_2 throughout this experiment. The first few drops were discarded, and 50–100 μl of arterial blood was directly poured into a heparinized sampling glass tube (capillary kit 471819, Ciba-Corning). The animal was then challenged with five levels of inspired O_2 (10, 15, 20, 50 and 80% O_2). These gas challenges lasted 5 min each and the blood sampling was performed while the animal was breathing each level of O_2. The order of applied gas conditions was chosen randomly for each experiment, and gas challenge was followed by a 5-min interval in normoxia (20% O_2-2% CO_2). Arterial PO_2 was determined by the blood gas analyzer (ABL555, Radiometer America Inc.).

External electric stimulus of vagal and superior laryngeal afferents in anesthetized mice. WT mouse was anesthetized with intraperitoneal injection of urethane. Acute unilateral nerve sectioning was performed as follows: right cervical vagal trunk was exposed and cut immediately below the point of branching off to the superior laryngeal nerve; right superior laryngeal nerve was exposed and cut. Its proximal cut end was placed on a pair of silver hook electrodes. The nerve and electrode were immersed in a mixture of liquid paraffin and Vaseline to prevent drying of the tissue. The parameters

of electrical stimulus were varied in a systematic manner using monophasic square wave impulses produced by SEN-7203 (Nihon Kohden). To evaluate the effect of frequency of discharges on Rf, the stimulus voltage and the pulse duration were maintained at 10 V and for 1 msec, respectively. The stimulus frequency was set to 0.2, 0.5, 1, 2, 5 or 10 Hz. Low frequencies of stimuli (0.2 and 0.5 Hz) were applied for 30 sec, while high frequencies (1, 2, 5 or 10 Hz) were applied for 20 sec. Ventilation was measured by pneumotachography as described in METHODS.

Hyperoxic exposure. WT and *Trpa1* KO mice were exposed continuously to hyperoxic conditions using 100% O_2 gas flow at a rate of 1 L min^{-1} in an airtight vinyl glove box. The concentration of O_2 in the glove box was monitored continuously with model OXY-1/1S (Jikco, Co. Ltd.) and maintained to > 95%, except for 30 min day^{-1} when the cages were opened to room air during periods of cleaning and general maintenance. The mice were provided *ad libitum* access to food and water and were observed continuously for signs of discomfort and O_2 toxicity. Mice used in this experiment were sacrificed at 72 h after hyperoxic exposure.

Bronchoalveolar lavage. The mice exposed to hyperoxic conditions were anesthetized by intraperitoneal injection of pentobarbital (150 mg kg^{-1}). After the onset of adequate anesthesia, the trachea was exposed and a cannula was inserted to the trachea. Bronchoalveolar lavage was performed with 1 ml PBS containing 0.1% BSA and 0.05 mM EDTA and repeated twice. The collected fluid was immediately processed as follows. BALF (300 μl) was cytocentrifuged (Cytospin 4, Thermo Shandon) and stained with DiffQuick (Fisher Scientific) for differential cell counts. On the other hand, cellular BALF (30–50 μl) was stained with trypan blue and the total cell count was manually.

Hypoxic exposure. WT and *Trpa1* KO mice were exposed continuously to hypoxic conditions using a gas mixture of room air and N_2 at flow rate of 1 L min^{-1} in a

transparent plastic chamber. The concentration of O_2 in the chamber was monitored continuously with model JKO-25 (Jikco, Co. Ltd.) and maintained to 15 ± 1.0%. The chamber was opened every 2–3 day for 10–15 min to clean the cages and replenish food and water. The mice were provided *ad libitum* access to food and water. Mice used in this experiment were sacrificed at 8–9 days after hypoxic exposure.

Hemodynamic and ventricular weight measurements. The mice exposed to hypoxic conditions were anesthetized by intraperitoneal injection of pentobarbital (50 mg kg^{-1}). The trachea was exposed and cannulated, and the mice were artificially ventilated at room air. The thoracic cavity was opened, PE-50 polyethylene tubing connected to a pressure transducer (DX-360, Nihon Kohden) was inserted into the right ventricle. RV pressure was fed into a personal computer after analog-to-digital conversion (PowerLab, ADInstrument). For ventricular weight measurement, RV was dissected from LV and septum (S) after removal of the atria. The ventricles were blotted dry and weighed. The ratio of RV weight to LV weight plus S, [RV/(LV + S)], was used as an index of right ventricular hypertrophy.

Lung histology. The pulmonary artery was perfused with PBS followed by 4% paraformaldehyde in PBS. Lungs were distended by injection through the trachea of 4% paraformaldehyde in PBS and excised them. Excised lungs were fixed in 4% paraformaldehyde overnight at 4°C. For frozen sections, fixed tissues were equilibrated with 30% sucrose in PBS for 2 days at 4°C and then embedded in OCT compound (Sakura Finetek). Cryostat sections (20 μm in thickness) were affixed to micro slides (MATSUNAMI), dried at room temperature, fixed in cold acetone for 10 min and then dried at room temperature. Samples were rehydrated in TBS and then were blocked with 1% BSA and 5% NGS in TBS for 1 h at room temperature. Samples were then incubated overnight at 4°C with R-PE-conjugated mouse F4/80-specific antibody (Serotec) or FITC-conjugated mouse GR1-specific antibody (BD Pharmingen). The

fluorescence images were acquired with a confocal laser-scanning microscope as described above (See "Immunohistochemistry of airway-and lung-identified nodose ganglion neurons."). For pulmonary vascular morphometry, the fixed tissues were embedded in paraffin and then stained with hematoxylin and eosin. Images for arterioles were captured with a microscope digital camera system (Nikon), and arterial area was measured using an image analysis program (ImageJ 1.42; NIH). Percent wall thickness was calculated by the following formula: Wall thickness (%) = $area_{ext} - area_{int} / area_{ext} \times 100$, where $area_{ext}$ and $area_{int}$ are the area bounded by external and internal elastic lamina, respectively. For each lung section, > 100 vessels were analyzed in multiple lung sections from three mice.

Statistical analyses. All data are expressed as means ± s.e.m.. We accumulated the data for each condition from at least three independent experiments. We evaluated statistical significance with the Student's t-test for comparisons between two mean values. We carried out multiple comparisons among more than three groups with ANOVA followed by Tukey–Kramer post hoc test. Respiratory parameters were also assessed by ANOVA with repeated measures design. A value of $P < 0.05$ was considered significant.

References

1. Lane, N. *Oxygen: The Molecule that made the World.* (Oxford Univ. Press, Oxford, 2002).
2. Lopez-Barneo, J., Pardal, R. & Ortega-Sáenz, P. Cellular mechanism of oxygen sensing. *Annu. Rev. Physiol.* **63,** 259–287 (2001).
3. Kulkarni, A. C., Kuppusamy, P. & Parinandi, N. Oxygen, the lead actor in the pathophysiologic drama: enactment of the trinity of normoxia, hypoxia, and hyperoxia in disease and therapy. *Antioxid. Redox Signal.* **9,** 1717–1730 (2007).
4. Gonzalez, C., Almaraz, L., Obeso, A. & Rigual, R. Carotid body chemoreceptors: from natural stimuli to sensory discharges. *Physiol. Rev.* **74,** 829–898 (1994).
5. Howe, A., Pack, R. J. & Wise, J. C. Arterial chemoreceptor-like activity in the abdominal vagus of the rat. *J. Physiol. (Lond.)* **320,** 309–318 (1981).
6. Cardenas, H. & Zapata, P. Ventilatory reflexes originated from carotid and extracarotid chemoreceptors in rats. *Am. J. Physiol.* **244,** R119–R125 (1983).
7. De Sanctis, G. T., Green, F. H. & Remmers, J. E. Ventilatory responses to hypoxia and hypercapnia in awake rats pretreated with capsaicin. *J. Appl. Physiol.* **70,** 1168–1174 (1991).
8. Schwenke, D. O., Bolter, C. P. & Cragg, P. A. Are the carotid bodies of the guinea-pig functional? *Comp. Biochem. Physiol., Part A Mol. Integr. Physiol.* **146,** 180–188 (2007).
9. Kubin, L., Alheid, G. F., Zuperku, E. J. & McCrimmon, D. R. Central pathways of pulmonary and lower airway vagal afferents. *J. Appl. Physiol.* **101,** 618–627 (2006).
10. Yu, J., Zhang, J. F. & Fletcher, E. C. Stimulation of breathing by activation of pulmonary peripheral afferents in rabbits. *J. Appl. Physiol*. **85,** 1485–1492 (1998).
11. Adriaensen, D. *et al.* Evidence for a role of neuroepithelial bodies as complex airway sensors: comparison with smooth muscle-associated airway receptors. *J. Appl. Physiol.* **101,** 960–970 (2006).
12. Chou, Y. *et al.* Differential effects of airway afferent nerve subtypes on cough and respiration in anesthetized guinea pigs. *Am. J. Physiol. Regul. Integr. Comp. Physiol.* **295,** R1572–R1584 (2008).
13. Nassenstein, C. *et al.* Expression and function of the ion channel TRPA1 in vagal afferent nerves innervating mouse lungs. *J. Physiol. (Lond.)* **586,** 1595–1604 (2008).
14. Bessac, B. F. *et al.* TRPA1 is a major oxidant sensor in murine airway sensory neurons. *J. Clin. Invest.* **118,** 1899–1910 (2008).
15. Bessac, B. F. & Jordt, S. Breathtaking TRP channels: TRPA1 and TRPV1 in airway chemosensation and reflex control. *Physiology (Bethesda)* **23,** 360–370 (2008).

16. Weir, E. K., López-Barneo, J., Buckler, K. J. & Archer, S. L. Acute oxygen-sensing mechanisms. *N. Engl. J. Med.* **353,** 2042–2055 (2005).
17. López-López, J. R. & Pérez-García, M. T. Oxygen sensitive Kv channels in the carotid body. *Respir. Physiol. Neurobiol.* **157,** 65–74 (2007).
18. Ward, J. P. Oxygen sensors in context. *Biochim. Biophys. Acta.* **1777,** 1–14 (2008).
19. Semenza, G. L. & Wang, G. L. A nuclear factor induced by hypoxia via de novo protein synthesis binds to the human erythropoietin gene enhancer at a site required for transcriptional activation. *Mol. Cell. Biol.* **12,** 5447–5454 (1992).
20. Schofield, C. J. & Ratcliffe, P. J. Oxygen sensing by HIF hydroxylases. *Nat. Rev. Mol. Cell Biol.* **5,** 343–354 (2004).
21. Webb, J., Coleman, M. & Pugh, C. Hypoxia, hypoxia-inducible factors (HIF), HIF hydroxylases and oxygen sensing. *Cell. Mol. Life Sci.* **66,** 3539–3554 (2009).
22. Folz, R. J., Abushamaa, A. M. & Suliman, H. B. Extracellular superoxide dismutase in the airways of transgenic mice reduces inflammation and attenuates lung toxicity following hyperoxia. *J. Clin. Invest.* **103,** 1055–1066 (1999).
23. Clapham, D. E. TRP channels as cellular sensors. *Nature* **426,** 517–524 (2003).
24. Nilius, B. TRP channels in disease. *Biochim. Biophys. Acta.* **1772,** 805–812 (2007).
25. Hara, Y. *et al.* LTRPC2 Ca^{2+}-permeable channel activated by changes in redox status confers susceptibility to cell death. *Mol. Cell* **9,** 163–173 (2002).
26. Yoshida, T. *et al.* Nitric oxide activates TRP channels by cysteine S-nitrosylation. *Nat. Chem. Biol.* **2,** 596–607 (2006).
27. Xu, S. *et al.* TRPC channel activation by extracellular thioredoxin. *Nature* **451,** 69–72 (2008).
28. Perraud, A. *et al.* Accumulation of free ADP-ribose from mitochondria mediates oxidative stress-induced gating of TRPM2 cation channels. *J. Biol. Chem.* **280,** 6138–6148 (2005).
29. Hinman, A., Chuang, H., Bautista, D. M. & Julius, D. TRP channel activation by reversible covalent modification. *Proc. Natl Acad. Sci. USA* **103,** 19564–19568 (2006).
30. Macpherson, L. J. *et al.* Noxious compounds activate TRPA1 ion channels through covalent modification of cysteines. *Nature* **445,** 541–545 (2007).
31. Takahashi, N. *et al.* Molecular characterization of TRPA1 channel activation by cysteine-reactive inflammatory mediators. *Channels (Austin)* **2,** 287–298 (2008).
32. Story, G. M. *et al.* ANKTM1, a TRP-like channel expressed in nociceptive neurons, is activated by cold temperatures. *Cell* **112,** 819–829 (2003).
33. Nagatomo, K. & Kubo, Y. Caffeine activates mouse TRPA1 channels but suppresses human

TRPA1 channels. *Proc. Natl Acad. Sci. USA* **105,** 17373–17378 (2008).

34. Gracheva, E. O. *et al.* Molecular basis of infrared detection by snakes. *Nature* **464,** 1006–1011 (2010).
35. Caterina, M. J. *et al.* The capsaicin receptor: a heat-activated ion channel in the pain pathway. *Nature* **389,** 816–824 (1997).
36. Nagata, K., Duggan, A., Kumar, G. & García-Añoveros, J. Nociceptor and hair cell transducer properties of TRPA1, a channel for pain and hearing. *J. Neurosci.* **25,** 4052–4061 (2005).
37. Kwan, K. Y. *et al.* TRPA1 Contributes to Cold, Mechanical, and Chemical Nociception but Is Not Essential for Hair-Cell Transduction. *Neuron* **50,** 277–289 (2006).
38. Mitchell, G. S. Back to the future: carbon dioxide chemoreceptors in the mammalian brain. *Nat. Neurosci.* **7,** 1288–1290 (2004).
39. Petrus, M. *et al.* A role of TRPA1 in mechanical hyperalgesia is revealed by pharmacological inhibition. *Mol. Pain* **3,** 40 (2007).
40. Aarts, M. *et al.* A key role for TRPM7 channels in anoxic neuronal death. *Cell* **115,** 863–877 (2003).
41. Bayley, J. *et al.* Sdhd and Sdhd/H19 Knockout Mice Do Not Develop Paraganglioma or Pheochromocytoma. *PLoS ONE* **4,** e7987 (2009).
42. Topol, I. A. *et al.* Experimental determination and calculations of redox potential descriptors of compounds directed against retroviral zinc fingers: Implications for rational drug design. *Protein Sci.* **10,** 1434–1445 (2001).
43. Kim, D. & Cavanaugh, E. J. Requirement of a soluble intracellular factor for activation of transient receptor potential A1 by pungent chemicals: role of inorganic polyphosphates. *J. Neurosci.* **27,** 6500–6509 (2007).
44. Webb, J. D., Murányi, A., Pugh, C. W., Ratcliffe, P. J. & Coleman, M. L. MYPT1, the targeting subunit of smooth-muscle myosin phosphatase, is a substrate for the asparaginyl hydroxylase factor inhibiting hypoxia-inducible factor (FIH). *Biochem. J.* **420,** 327–333 (2009).
45. Yu, A. Y. *et al.* Impaired physiological responses to chronic hypoxia in mice partially deficient for hypoxia-inducible factor 1alpha. *J. Clin. Invest.* **103,** 691–696 (1999).
46. Hathout, Y. *et al.* Characterization of intermediates in the oxidation of zinc fingers in human immunodeficiency virus type 1 nucleocapsid protein P7. *Drug Metab. Dispos.* **24,** 1395–1400 (1996).
47. Hu, H. *et al.* Zinc activates damage-sensing TRPA1 ion channels. *Nat. Chem. Biol.* **5,** 183–190 (2009).

48. Nolan, P. C. & Waldrop, T. G. In vivo and in vitro responses of neurons in the ventrolateral medulla to hypoxia. *Brain Res.* **630,** 101–114 (1993).
49. Dinkova-Kostova, A. T. *et al.* Direct evidence that sulfhydryl groups of Keap1 are the sensors regulating induction of phase 2 enzymes that protect against carcinogens and oxidants. *Proc. Natl Acad. Sci. USA* **99,** 11908–11913 (2002).
50. Voss, A. A. *et al.* Identification of hyperreactive cysteines within ryanodine receptor type 1 by mass spectrometry. *J. Biol. Chem.* **279,** 34514–34520 (2004).
51. Feldman, R. G. A systematic study of parameters of afferent vagal stimulation in the anesthetized dog: blood pressure reflexes. *Acta Neuroveg. (Wien)* **25,** 134–143 (1962).
52. Manchanda, S. *et al.* Frequency and volume thresholds for inhibition of inspiratory motor output during mechanical ventilation. *Respir. Physiol.* **105,** 1–16 (1996).
53. Onodera, M., Kuwaki, T., Kumada, M. & Masuda, Y. Determination of ventilatory volume in mice by whole body plethysmography. *Jpn. J. Physiol.* **47,** 317–326 (1997).
54. Nishida, M. *et al.* Amplification of receptor signalling by Ca^{2+} entry-mediated translocation and activation of PLCγ2 in B lymphocytes. *EMBO J.* **22,** 4677–4688 (2003).
55. Okada, T. *et al.* Molecular and functional characterization of a novel mouse transient receptor potential protein homologue TRP7. Ca^{2+}-permeable cation channel that is constitutively activated and enhanced by stimulation of G protein-coupled receptor. *J. Biol. Chem.* **274,** 27359–27370 (1999).
56. Ho, S. N. *et al.* Site-directed mutagenesis by overlap extension using the polymerase chain reaction. *Gene* **77,** 51–59 (1989).
57. Cockman, M. E. *et al.* Posttranslational hydroxylation of ankyrin repeats in IkappaB proteins by the hypoxia-inducible factor (HIF) asparaginyl hydroxylase, factor inhibiting HIF (FIH). *Proc. Natl Acad. Sci. USA* **103,** 14767–14772 (2006).
58. Metzen, E. *et al.* Nitric oxide impairs normoxic degradation of HIF-1alpha by inhibition of prolyl hydroxylases. *Mol. Biol. Cell* **14,** 3470–3481 (2003).
59. Klein, A., Flügel, D. & Kietzmann, T. Transcriptional regulation of serine/threonine kinase-15 (STK15) expression by hypoxia and HIF-1. *Mol. Biol. Cell* **19,** 3667–3675 (2008).
60. Lee, S. *et al.* Neuronal apoptosis linked to EglN3 prolyl hydroxylase and familial pheochromocytoma genes: developmental culling and cancer. *Cancer Cell* **8,** 155–167 (2005).
61. Shi, M. & Liu, Y. H. Traditional Morita–Baylis–Hillman reaction of aldehydes with methyl vinyl ketone co-catalyzed by triphenylphosphine and nitrophenol. *Org. Biomol. Chem.* **4,** 1468–1470 (2006).

62. Yi, H. W., Park, H. W., Song, Y. S. & Lee, K. J. Reaction of the Morita–Baylis–Hillman acetates of 2-azidobenzaldehydes with triethyl phosphite: synthesis of 1-diethylphosphono-1,2-dihydroquinolines and 3-acetoxymethylquinolines. *Synthesis* 1953–1960 (2006).
63. Pachamuthu, K. & Vankar, Y. D. Palladium catalysed region and stereoselective reduction of Baylis-Hillman coupling products derived allylic acetates. *Tetrahedron Lett.* **39,** 5439–5442 (1998).
64. Cockman, M. E. *et al.* Proteomics-based identification of novel factor inhibiting hypoxia-inducible factor (FIH) substrates indicates widespread asparaginyl hydroxylation of ankyrin repeat domain-containing proteins. *Mol. Cell Proteomics* **8,** 535–546 (2008).
65. Ling, G. *et al.* Renal sympathetic nerve activity in mice: comparison between mice and rats and between normal and endothelin-1 deficient mice. *Brain Res.* **808,** 238–249 (1998).
66. Toyama, S., Sakurai, T., Tatsumi, K. & Kuwaki, T. Attenuated phrenic long-term facilitation in orexin neuron-ablated mice. *Respir. Physiol. Neurobiol.* **168,** 295–302 (2009).
67. Deng, B. *et al.* Contribution of orexin in hypercapnic chemoreflex: evidence from genetic and pharmacological disruption and supplementation studies in mice. *J. Appl. Physiol.* **103,** 1772–1779 (2007).
68. Terada, J. *et al.* Ventilatory long-term facilitation in mice can be observed during both sleep and wake periods and depends on orexin. *J. Appl. Physiol.* **104,** 499–507 (2008).
69. Epstein, R. A., Epstein, M. A., Haddad, G. G. & Mellins, R. B. Practical implementation of the barometric method for measurement of tidal volume. *J. Appl. Physiol.* **49,** 1107–1115 (1980).

General Conclusion

The current studies identified the physiological role and activation mechanism of redox-sensitive TRP channels

Nitric oxide activates TRP channels by cysteine S-nitrosylation

This study demonstrates a novel activation mechanism mediated by direct oxidative cysteine modifications in TRP channels. TRPC1, C4, C5, V1, V3 and V4 of TRPC and TRPV families, commonly categorized as receptor-activated channels and thermosensor channels, show prominent responses to nitric oxide (NO) and free cysteine-selective reactive disulfides to elicit Ca^{2+} entry in HEK293 cells. Chemical labeling and functional studies of cysteine mutants, as well as membrane sidedness of reactive disulfide action, indicate that the nitrosylation/modification site Cys553 accessible from the cytoplasm and Cys558 are essential for the marked sensitivity of TRPC5. Importantly, the responsive TRPs harbor conserved cysteines on the same N-terminal side of the putative 'pore'-forming region.

The study provides evidence that the modification site is the structural determinant for 'NO sensor' function of TRP channels that mediate crosstalk between NO and Ca^{2+} signaling in native systems. Moreover, in the S5-S6 linker, it is suggested that at least the 'pore'-flanking region harboring the modification site is accessible from the cytoplasm, despite the common prediction that S5-S6 linkers of TRPs are extracellularly disposed like those of other cation-permeable channels such as K^+ channels. Thus, the present investigation represents a significant advance in conceptual understanding of structural bases of the physiological 'sensor' function of TRP channels as well as an architecture of the interface between 'gate' and 'pore' universal among cation-permeable channels.

Molecular characterization of TRPA1 channel activation by cysteine-reactive inflammatory mediators

TRPA1 is a member of the transient receptor potential (TRP) cation channel family, and is predominantly expressed in nociceptive neurons. Ths study shows that a variety of 'endogenous' inflammatory mediators (15-deoxy-$\Delta^{12,14}$-prostaglandin J_2 (15d-PGJ_2), nitric oxide (NO), hydrogen peroxide (H_2O_2), and protons (H^+)) activate human TRPA1 heterologously expressed in HEK cells. Functional characterization of site-directed cysteine mutants of TRPA1 in combination with labeling experiments using biotinylated 15d-PGJ_2 demonstrate that modifications of cytoplasmic N-terminal cysteines (Cys421 and Cys621) are responsible for the activation of TRPA1 by 15d-PGJ_2. In TRPA1 responses to other cysteine-reactive inflammatory mediators, such as NO and H_2O_2, the extents of impairment by respective cysteine mutations differ from those in TRPA1 responses to 15d-PGJ_2. Interestingly, the Cys421 mutation critically impairs the TRPA1 response to H^+ as well. These findings suggest that TRPA1 channels are targeted by an array of inflammatory mediators to elicit inflammatory pain in the nervous system.

TRPA1 senses O_2 availability in non-carotid body chemoreceptors

This study identifies TRPA1 channel as a novel sensor for molecular oxygen (O_2). TRPA1 channels are activated upon hyperoxia by O_2 via its prominent sensitivity to cysteine-mediated oxidation, and also upon hypoxia via relief from inhibition by O_2-dependent prolyl hydroxylases. Each represents a previously unrecognized activation mechanism in ion channels. Our *in vivo* studies using *Trpa1*-deficient mice show that hyperoxia- and hypoxia-induced vagal afferent nerve activities and their consequent ventilatory responses are severely impaired. Also, pulmonary inflammation and hypertension are abnormally induced in normoxia and are aggravated in hyperoxia and hypoxia, respectively. Thus, TRPA1 expressed in non-carotid body vagal

chemoreceptors detects changes in O_2 availability and regulates O_2 supply *in vivo*.

In aerobic organisms, O_2 intake is tightly controlled in order to secure energy production while minimizing the risk of oxidative damage. Mammals' respiratory systems have evolved to respond to changes in O_2 availability via the carotid body and other chemoreceptors. However, the molecular target of O_2 action and the molecular mechanisms underlying O_2 sensing in chemoreceptors are still elusive. Our work clearly answers these issues, and represents an outstanding advance in conceptual understanding of biology of sensing and adaptation.

List of Publications

1. Yoshida, T., Inoue, R., Morii, T., **Takahashi, N.**, Yamamoto, S., Hara, Y., Tominaga, M., Shimizu, S., Sato, Y. & Mori, Y. Nitric oxide activates TRP channels by cysteine S-nitrosylation. ***Nature Chem. Biol.*** 2, 596–607 (2006).
2. Yamamoto, S., Shimizu, S., Kiyonaka, S., **Takahashi, N.**, Wajima, T., Hara, Y., Negoro, T., Hiroi, T., Kiuchi, Y., Okada, T., Kaneko, S., Lange, I., Fleig, A., Penner, R., Nishi, M., Takeshima, H. & Mori, Y. TRPM2-mediated Ca^{2+} influx induces chemokine production in monocytes that aggravates inflammatory neutrophil infiltration. ***Nature Med.*** 14, 738–747 (2008).
3. **Takahashi, N.**, Mizuno, Y., Kozai, D., Yamamoto, S., Kiyonaka, S., Shibata, T., Uchida, K. & Mori, Y. Molecular characterization of TRPA1 channel activation by cysteine-reactive inflammatory mediators. ***Channels (Austin)*** 2, 287–298 (2008).
4. Bogeski, I., Kummerow, C., Al-Ansary, D., Schwarz, E. C., Koehler, R., Kozai, D., **Takahashi, N.**, Peinelt, C., Griesemer, D., Bozem, M., Mori, Y., Hoth, M. & Niemeyer, B. A. Differential redox regulation of ORAI ion channels: a mechanism to tune cellular calcium signaling. ***Science Signal.*** 3, ra24 (2010).
5. Yamamoto, S., **Takahashi, N.** & Mori, Y. Chemical physiology of oxidative stress-activated TRPM2 and TRPC5 channels. ***Prog. Biophys. Mol. Biol.*** in press.

List of Japanese Publications

1. 清中茂樹, 加藤賢太, **高橋重成**, 正木隆男, 森泰生. カルシウムシグナル制御チャネルの作用化合物と創薬 Novel Ca^{2+} modulators in drug discovery. *医学のあゆみ* 223, 479–183 (2007).
2. **高橋重成**, 秋山智志, 水野雄介, 井上隆司, 森泰生. TRPC チャネルによる血管トーヌスの調節 TRPC channel regulate the vascular tonus. *医学のあゆみ* 223, 1136–1140 (2007).
3. 山本伸一郎, **高橋重成**, 清中茂樹, 森泰生. 環境応答を担うイオンチャネル～活性化学種により活性化される TRP チャネルの分子機能 Ion channels responsible for environmental response: Molecular function of TRP channels activated by reactive chemical species. *蛋白質 核酸 酵素* 54, 212–223 (2009).
4. **高橋重成**, 山本伸一郎, 森泰生. 酸化ストレス作動性 TRP チャネルの化学生理学 Chemical physiology of oxidative stress-activated TRP channels. *実験医学* 27, 196–204 (2009).
5. **高橋重成** TRP チャネル. ***Medical Tribune ことばのカルテ*** 11 月 5 日号 (2009).
6. 沼田朋大, 香西大輔, **高橋重成**, 加藤賢太, 瓜生幸嗣, 山本伸一郎, 金子雄, 眞本達生, 森泰生. TRP チャネルの構造と多様な機能. *生化学* 81, 962–983 (2009).
7. 清中茂樹, **高橋重成**, 香西大輔, 森泰生. 化学物質の感覚分子生物学～TRP チャネルはどのように物質を感知し脳へ伝えるか. *化学* 64, 27–33 (2009).